PB82-103771

Testing and Analysis of a Wet-Dry Crossflow Cooling Tower, Volume I Test Program and Results

Tennessee Valley Authority
Chattanooga

Prepared for

Industrial Environmental Research Lab.
Research Triangle Park, NC

Jul 81

U.S. Department of Commerce
National Technical Information Service
NTIS

EPA
TVA

United States
Environmental Protection
Agency

Industrial Environmental Research
Laboratory
Research Triangle Park NC 27711

EPA-600/7-81-106a
July 1981

PB82-103771

Tennessee Valley
Authority
Office of Power

Energy Demonstrations
and Technology
Chattanooga TN 37401

TVA/OP/EDT-81/47a

Testing and Analysis of a Wet-Dry Crossflow Cooling Tower
Volume I:
Test Program and Results

Interagency
Energy/Environment
R&D Program Report

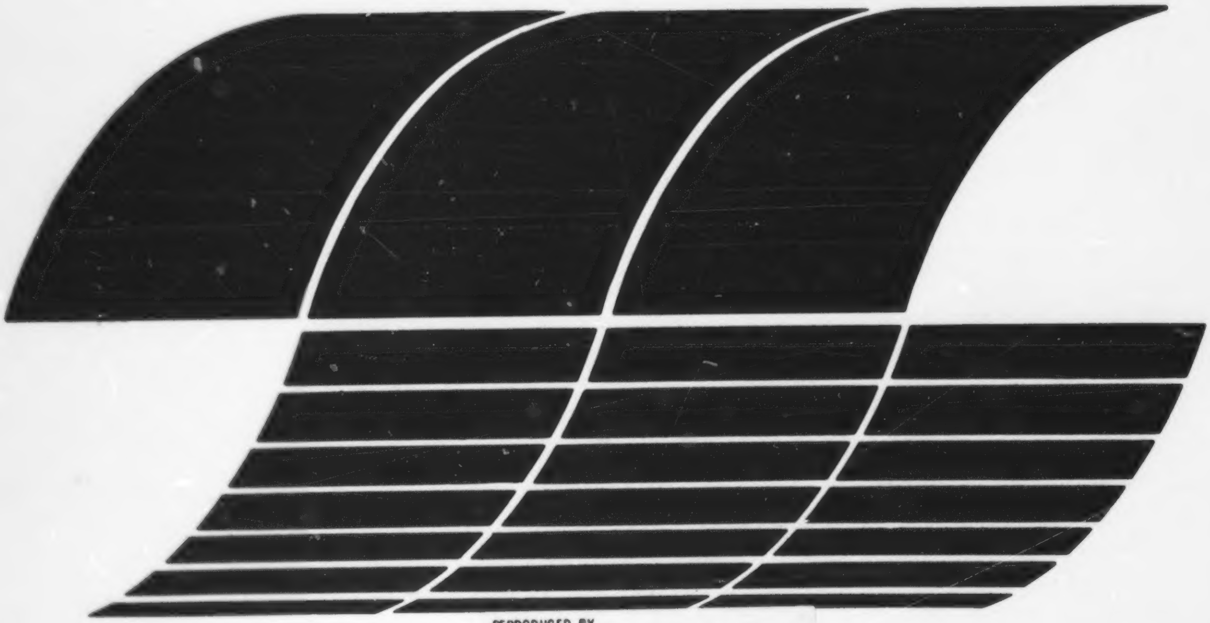

REPRODUCED BY
NATIONAL TECHNICAL
INFORMATION SERVICE
U.S. DEPARTMENT OF COMMERCE
SPRINGFIELD, VA 22161

RESEARCH REPORTING SERIES

Research reports of the Office of Research and Development, U.S. Environmental Protection Agency, have been grouped into nine series. These nine broad categories were established to facilitate further development and application of environmental technology. Elimination of traditional grouping was consciously planned to foster technology transfer and a maximum interface in related fields. The nine series are:

1. Environmental Health Effects Research
2. Environmental Protection Technology
3. Ecological Research
4. Environmental Monitoring
5. Socioeconomic Environmental Studies
6. Scientific and Technical Assessment Reports (STAR)
7. Interagency Energy-Environment Research and Development
8. "Special" Reports
9. Miscellaneous Reports

This report has been assigned to the INTERAGENCY ENERGY-ENVIRONMENT RESEARCH AND DEVELOPMENT series. Reports in this series result from the effort funded under the 17-agency Federal Energy/Environment Research and Development Program. These studies relate to EPA's mission to protect the public health and welfare from adverse effects of pollutants associated with energy systems. The goal of the Program is to assure the rapid development of domestic energy supplies in an environmentally-compatible manner by providing the necessary environmental data and control technology. Investigations include analyses of the transport of energy-related pollutants and their health and ecological effects; assessments of, and development of, control technologies for energy systems; and integrated assessments of a wide range of energy-related environmental issues.

EPA REVIEW NOTICE

This report has been reviewed by the participating Federal Agencies, and approved for publication. Approval does not signify that the contents necessarily reflect the views and policies of the Government, nor does mention of trade names or commercial products constitute endorsement or recommendation for use.

This document is available to the public through the National Technical Information Service, Springfield, Virginia 22161.

TECHNICAL REPORT DATA

(Please read Instructions on the reverse before completing)

1. REPORT NO. EPA-600/7-81-106a
2.
3. RECIPIENT'S ACCESSION NO. PB82 10377 1
4. TITLE AND SUBTITLE Testing and Analysis of a Wet/Dry Crossflow Cooling Tower; Volume I. Test Program and Results
5. REPORT DATE July 1981
6. PERFORMING ORGANIZATION CODE
7. AUTHOR(S) D. L. Ayers, M. R. Hogan, A. E. Hribar, and R. A. Luceta
8. PERFORMING ORGANIZATION REPORT NO. TVA/OP/EDT - 81/47a
9. PERFORMING ORGANIZATION NAME AND ADDRESS

Westinghouse Electric Corporation
1310 Beulah Road
Pittsburgh, Pennsylvania 15235

10. PROGRAM ELEMENT NO. 1NE624A
11. CONTRACT/GRANT NO. EPA IAG-D8-E721-BE
12. SPONSORING AGENCY NAME AND ADDRESS

EPA, Office of Research and Development
Industrial Environmental Research Laboratory
Research Triangle Park, NC 27711

13. TYPE OF REPORT AND PERIOD COVERED Task Final; 7/77-5/81
14. SPONSORING AGENCY CODE EPA/600/13
15. SUPPLEMENTARY NOTES IERL-RTP project officer is Theodore G. Brna; TVA project director is H. B. Flora, II (Div. of Energy Demonstrations and Technology, Chattanooga, TN 37401).
16. ABSTRACT

The report discusses the test program and performance analysis of a single-cell mechanical-draft wet/dry cooling tower in Cliffside, NC. Objectives of the program were to obtain performance data and results on mass transfer, heat transfer, fluid flow, plume formation, and acoustic characteristics for comparison with models/theories. Correlations are presented for the wet-fill mass transfer coefficient, wet-fill water loss, Colburn j-factor for the finned tubes, and fan efficiency in terms of one or more of the following: water loading in the tubes, air loading over the fins, log mean humidity difference, outlet water temperature, Reynolds number, and airflow rate. Acoustic data were fitted to a series of curves for each of the eight octave bands. Attempts to model plume data failed. The report also describes the test facility, test procedures, instrumentation, data acquisition, and data reduction.

17. KEY WORDS AND DOCUMENT ANALYSIS

a. DESCRIPTORS		b. IDENTIFIERS/OPEN ENDED TERMS	c. COSATI Field/Group	
Pollution	Fluid Flow	Pollution Control	13B	20D
Cooling Towers		Stationary Sources	13A, 07A, 13I	
Tests	Plumes		14B	21B
Analyzing	Acoustics			20A
Mass Transfer			14G	
Heat Transfer			20M	

18. DISTRIBUTION STATEMENT Release to Public
19. SECURITY CLASS *(This Report)* Unclassified
20. SECURITY CLASS *(This page)* Unclassified
21. NO. OF PAGES 186
22. PRICE

EPA Form 2220-1 (9-73)

TESTING AND ANALYSIS OF A WET-DRY CROSSFLOW COOLING TOWER,
VOLUME I: TEST PROGRAM & RESULTS

by

D. L. Ayers, M. R. Hogan, A. E. Hribar, R. A. Lucheta
Westinghouse Electric Corporation
Research & Development Center
1310 Beulah Road
Pittsburgh PA 15235

TVA Contract No. TV46267
TVA Project Director: Hollis B. Flora II

Tennessee Valley Authority
Division of Energy Demonstrations and Technology
Chattanooga, Tennessee 37401

EPA Interagency Agreement No. D8-E721-BE
Program Element No. INE624A

EPA Project Officer: Theodore G. Brna

Industrial Environmental Research Laboratory
Office of Environmental Engineering and Technology
Research Triangle Park, NC 27711

Prepared for

U.S. ENVIRONMENTAL PROTECTION AGENCY
Office of Research and Development
Washington, DC 20460

i.a

DISCLAIMER

This report was prepared as an account of work sponsored by the United States Government. Neither the United States nor the Tennessee Valley Authority, nor any of their employees, makes any warranty, express or implied, or assumes any legal liability or responsibility for the accuracy, completeness, or usefulness of any information, apparatus, product, or process disclosed, or represents that its use would not infringe privately owned rights. Reference herein to any specific commercial product, process, or service by trade name, mark, manufacturer, or otherwise, does not necessarily constitute or imply its endorsement, recommendation, or favoring by the United States Government or any agency thereof. The views and opinions of authors expressed herein do not necessarily state or reflect those of the United States Government or any agency thereof.

TESTING AND ANALYSIS OF A WET-DRY CROSSFLOW COOLING TOWER,

TVA Contract No. TV46267
and
Interagency Agreement EPA-IAG-D8-E721-BE

ABSTRACT

This program was initiated with the objective of measuring and analyzing mass transfer, heat transfer, fluid flow, plume formation and acoustic characteristics of a wet/dry crossflow cooling tower, under contract from the Tennessee Valley Authority.

The test apparatus was a fully instrumented mechanical draft cooling tower constructed by Westinghouse Electric Corporation at the Cliffside Plant of Duke Power Company, Cliffside, North Carolina. Data were acquired at the test site by personnel from Westinghouse Power Generation Services Division and analyzed by Westinghouse Research and Development Center.

Results of the analysis of test data are generally in the form of correlations or predictive computer codes. Data on mass transfer coefficient, water loss, heat exchanger air-side convective heat transfer coefficient, fan system efficiency, acoustic propagation and plume formation are presented.

This report also describes the facility itself, its operational procedure, instrumentation, data acquisition techniques and data reduction procedures.

TABLE OF CONTENTS

VOLUME I

Page

Abstract iii

List of Illustrations. ix

List of Tables xii

1.0 INTRODUCTION. 1

2.0 CONCLUSIONS 6

2.1 Thermal and Flow Tests 6

2.2 Acoustics Tests. 9

2.3 Plume Tests. 10

3.0 RECOMMENDATIONS 11

3.1 Thermal and Flow Tests 11

3.2 Plume Tests. 12

4.0 THERMAL PERFORMANCE TESTS 13

4.1 Thermal and Flow Instrumentation 15

4.1.1 Instrument Calibration Procedures 22

4.2 Data Acquisition and Transfer. 23

4.3 Thermal and Flow Data Reduction. 31

4.3.1 Tower Heat and Mass Transfer. 31

4.3.1.1 Wet Fill Heat and Mass Transfer Coefficients 38

4.3.1.1.1 Computation of Ka 38

4.3.1.1.2 Calculation of Grid Size. . 45

4.3.1.2 Heat Exchanger Heat Transfer Analysis. 47

4.3.1.3 Heat Exchanger Air-Side Heat Transfer Coefficient Computation. 53

4.3.1.4 Airflow Rate Analysis and Computation. 54

4.3.1.5 Water Flow Rate Analysis and Computation 60

4.3.2 Data Reduction Computer Code. 67

4.3.2.1 Data Reduction Main Program Functions. 67

(Continued)

Table of Contents (cont'd) Page

4.4 Analysis of Thermal and Flow Data. 69
4.4.1 Correlation Forms 69
4.4.2 Statistical Analysis of Data. 75
4.4.3 Linear Regression 77
4.5 Results of Correlations. 80
4.5.1 Mass Transfer Coefficient Ka. 80
4.5.2 Rate of Water Loss Due to Evaporation (ΔL/L). . 87
4.5.3 Dry Heat Exchanger Air-Side Convective Heat Transfer Coefficient H. 91
4.5.4 Fan Efficiency. 95
4.6 Nomenclature 109
4.7 References 116
5.0 ACOUSTICS TESTS 117
5.1 Description of Acoustic Instrumentation. 117
5.1.1 Data Acquisition Equipment. 117
5.1.2 Data Analysis Equipment 123
5.2 Acoustic Data Acquisition Techniques 123
5.3 Acoustic Data Reduction Techniques 127
5.4 Analysis of Data 127
5.4.1 Experimental Design 129
5.4.2 Observed Noise Levels 131
5.4.3 Statistical Model 131
5.4.4 Examination of Model Fit. 135
5.5 Noise Prediction Computer Code 139
5.5.1 Program Code Modifications. 139
5.5.1.1 Atmospheric Absorption 141
5.5.2 Program Code Operation. 144
5.6 Discussion of Results. 146
5.6.1 Experimental Data 146
5.6.2 Regression Analysis 147
5.6.3 Noise Prediction Code 148
5.6.3.1 Ground Absorption. 148
5.6.3.2 Wind and Temperature Fluctuations. . . 150

(Continued)

Table of Contents (cont'd)

Page

- 5.7 Acknowledgements 150
- 5.8 Acoustics References 150
- 5.9 Accustics Nomenclature 151

6.0 PLUME TESTS 153

- 6.1 Plume Instrumentation. 153
- 6.2 Plume Data Acquisition Technique at the Cliffside Site 159
  - 6.2.1 Data Handling at Westinghouse Fluid Systems Laboratory. 161
  - 6.2.2 Data Handling at Westinghouse R&D Center. . . . 161
- 6.3 Plume Modeling 164
- 6.4 Analysis of Plume Data 165
- 6.5 Discussion of Results. 166
  - 6.5.1 Validation of the Rubin Model 166
  - 6.5.2 Compilation of Plume Data 167
  - 6.5.3 Possible Further Studies. 167
- 6.6 References 167

7.0 ACKNOWLEDGEMENTS. 169

VOLUME II

List of Illustrations. vii

List of Tables xi

APPENDICES 1

- A. Description of Tower Test Facility. 1
  - A.1 Introduction 1
  - A.2 Tower Construction 1
  - A.3 Water System 11
  - A.4 Air Supply 11
  - A.5 Controls 13
- B. Cooling Tower Startup, Operating and Shutdown Procedures 15

(Continued)

Table of Contents (cont'd)

Page

B.1 Startup Procedures 15

B.2 Shutdown Procedure 18

B.3 Operation Procedure. 19

C. Data Reduction Program. 23

D. Data Correlation Computer Codes 117

D.1 Input Data Files 117

D.2 Ka Correlation Code. 119

D.3 Water Loss Correlation Code. 122

D.4 Heat Exchanger Air-Side Heat Transfer Coefficient Correlation Code 123

D.5 Fan Efficiency Correlation Code. 124

E. Cooling Tower and Background Noise Data 179

F. Noise Prediction Computer Model Documentation 185

F.1 Program Structure. 185

F.2 Summary of Programs. 185

F.3 Input Data Format. 187

F.4 Sample Output Listings 191

G. Noise Prediction Computer Code. 195

H. Basic Plume and Cooling Tower Data. 207

I. Rubin's Program and Input Data. 251

J. Comparison of Computed and Observed Plume Parameters. . 265

LIST OF ILLUSTRATIONS

VOLUME I

Figure No.	Title	Page
1.0-1	Side View of Tower Showing Location of Dew Cells, Thermocouples, and Velocity Probes	2
1.0-2	Schematic of One-Half the Cooling Tower Cell, Showing Water Flow Control and Measurement System	4
4.1.1	Mercury Manometer Used to Calibrate the Ellison Annubar Water Flow Meter	14
4.1.2	Ellison Annubar Water Flow Meter in its Insulated and Heated Housing	14
4.1-3	Photograph of the Kiel Probe Rake at the Fan Stack Inlet	16
4.1-4	Photograph of the Wafer Switch Control for Kiel Probe Pressures (See Figure 4.1-6 for Schematic)	16
4.1-5	Electromanometer Used for Pressure Measurement	18
4.1-6	Schematic Diagram of the Fan Stack Air Velocity Measuring System's Probe/Wafer Switch/Purge Air/Pressure Transducer System	19
4.1-7	Fluke Model 2240B Digital Data Acquisition System	18
4.3-1	Wet Fill Heat and Mass Transfer Control Volume	30
4.3-2	An Illustration of the Two-Dimensional Representation of the Wet Fill and its Grid Structure	40
4.3-3	Typical Wet Fill Grid and Nomenclature Employed in Defining the Temperature of the Grid i,j	42
4.3-4	Error in Mass Transfer Coefficient as a Function of Computation Time and the Experimental Multiplication Factor	48
4.3-5	Tower Heat Exchanger Tube and Fin Geometry, and Nomenclature Employed in the Heat Transfer Analysis	49
4.3-6	Stack Velocity as a Function of Distance Across the Stack at the Velocity Pressure Probe Station	56
4.3-7	Fan-Stack Model and Nomenclature Employed for the Calculation of Air Flow Rate from the Fan Curve	58

(Continued)

List of Illustrations (cont'd)

Figure No.	Title	Page
4.3-8	Schematic of Dry Heat Exchanger Hydraulic System with the Manometer Employed to Measure the Frictional Pressure Drop	62
4.3-9	Dry Heat Exchanger Water Flow Rate Calibration. The Pressure Drop-Water Density Ratio is Shown as a Function of Water Flow Rate. Also Indicated is the Least Squares Curve Used to Represent the Calibration in the Data Reduction	64
4.3-10	Heat Exchanger Pressure Transducer Voltage as a Function of Dry Heat Exchanger Water Flow Rate. Also Shown is the Second Order Least Squares Polynomial used to Represent the Calibration in the Data Reduction Program	66
4.5.4-1	Airflow System Efficiency as a Function of Airflow Rate	94
4.5.4-2	Airflow System Efficiency as a Function of Airflow Rate for a Rotational Speed of 60 RPM	96
4.5.4-3	Airflow System Efficiency as a Function of Airflow Rate for a Rotational Speed of 90 RPM	98
4.5.4-4	Airflow System Efficiency as a Function of Airflow Rate for a Rotational Speed of 101 RPM	99
4.5.4-5	Airflow System Efficiency as a Function of Airflow Rate for a Rotational Speed of 113 RPM	100
4.5.4-6	Airflow System Efficiency as a Function of Airflow Rate for a Rotational Speed of 119 RPM	101
4.5.4-7	(a) Fan Pressure Rise and System Characteristic as a Function of Volumetric Flow Rate. Each Fan Curve Represents a Unique Pitch (λ).	102
	(b) Fan Efficiency for Three Blade Angles as a Function of Volumetric Flow Rate. Also Shown is Anticipated Fan Efficiency Behavior While Coupled to the System Characteristic Shown in Figure 6-7a.	102
4.5.4-8	Airflow System Efficiency as a Function of Airflow Rate for an 8-Degree Blade Pitch	104
4.5.4-9	Airflow System Efficiency as a Function of Airflow Rate for a 10-Degree Blade Pitch	105
4.5.4-10	Airflow System Efficiency as a Function of Airflow Rate for a 12-Degree Blade Pitch	106

(Continued)

List of Illustrations (cont'd)

Figure No.	Title	Page
4.5.4-11	Airflow System Efficiency as a Function of Airflow Rate for a 14-Degree Blade Pitch	107
4.5.4-12	Airflow System Efficiency as a Function of Airflow Rate for a 16-Degree Blade Pitch	108
4.5.4-13	Airflow System Efficiency and Approximating Straight Line as a Function of Volumetric Flow Rate	110
5.1-1	Data Acquisition Equipment	118
5.1-2	Frequency Response Calibration of the B&K 4145 Microphone. Upper Curve - Free-Field Normal Incidence Response; Lower Curve - Pressure Response	120
5.1-3	Free-Field Corrections for the B&K 4145 Microphone with Protective Grid as a Function of Incidence Angle	121
5.1-4	Free-Field Response Corrections for the B&K 4145 Microphone When Used with the B&K UA 0207 Windscreen	122
5.1-5	Measured Frequency Response at 15 ips of the Stellavox SP-7 Recording Channels	119
5.1-6	Data Reduction Equipment	124
5.2-1	Ground Level Measurement Locations	126
5.5-1	Source-Receiver Geometry	141
6.1-1	(a) Tethersonde Instrument Package	154
	(b) Tethersonde Balloon in Flight	154
6.1-2	Sample Theodolite Data	158

VOLUME II

Figure No.	Title	Page
A-1	Aerial View of the Cliffside Experimental Cooling Tower	2
A-2	Photograph of the Cliffside Tower Showing the Control House	2
A-3	Schematic of Hot Water Supply and Cold Water Return Systems for the Tower Test Facility	3
A-4	View of Tower Showing Precast Side Wall Construction	4
A-5	View of Dry Heat Exchangers on the Tower Inlet Face	4
A-6	Photograph of the Wet Fill Elements in Their Wire Mesh Spacer Grid	6

(Continued)

List of Illustrations (cont'd)

Figure No.	Title	Page
A-7	View of Inlet Fill Elements Being Installed	7
A-8	View of the Rear of the Fill Section Showing the Drift Eliminator Assembly	8
A-9	Distribution Nozzles in the Hot Water Basin at the Top of the Tower	8
A-10	Fan Deck and a Portion of the Fan Stack	9
A-11	View of the Hot Water Distribution Header at the Top of the Tower	9
A-12	Tower Hot Water Supply Piping	10
A-13	Tower Hot Water Circulating Pump	10
A-14	Tower Hot Water Supply Pump with Bypass Line	12
A-15	Tower Air Circulating Fan	12
A-16	View into the Bottom of Fan Stack, Showing the Fan Drive Assembly	14
A-17	Motor Controls for the Fan Drive System	14
F-1	Flow Diagram for Main Program TOWER	184
F-2	Flow Diagram for Subroutine ABSORB	186
F-3	Flow Diagram for Subroutine GRND	187
F-4	Flow Diagram for Subroutine SOURCE	188
F-5	Flow Diagram for Subroutine TITLE	188
I-1	Format of Data Prepared for Rubin's Program	250

LIST OF TABLES

VOLUME I

Table No.	Title	Page
4.1-1	Locations of Thermocouples, Dewcells and Thermometers	20
4.2-1	Sample of Raw Tower Data from a Dry Heat Exchanger Test	24
4.2-2	Delineation of Input Paper Tape Data by Channel for Thermal and Flow Data	28
4.4-1	Thermal and Flow Test Grid	70
4.5.1-1	Mass Transfer Coefficient Correlation Data	82
4.5.2-1	Water Loss Correlation Data	88
4.5.2-2	Comparison of All Wet and Winter Wet Correlations of Water Loss $\Delta L/L$	90
4.5.3-1	Dry Heat Exchanger Heat Transfer Coefficient Correlation Data	92
5.1-1	Measurement Equipment Models	118
5.1-2	Data Reduction Equipment Models	124
5.4-1	Independent Variables and Corrected Noise Levels	128
5.4-2	Fitted Coefficients for Surviving Model Terms	132
5.4-3	Comparison of Measured (Y) and Predicted ($\hat{Y}$) Noise Levels* with Standard Error (S)	134
5.4-4	Estimates of Standard Deviation	140
6.2.1-1	Sample Data, as Received	162

VOLUME II

C-1	Sample Input Listing for Nonplume Tests	26
C-2	Delineation of Input Paper Tape Data by Channel	28
C-3	Tower Diffuser Throat Static and Velocity Pressure Data	30

(Continued)

List of Tables (cont'd)

Table No.	Title	Page
C-4	Listing of the Tower Data Reduction Computer Code	30
C-5	Sample Output Listing	110
D-1	Examples of Punched Card Output from the Data Reduction Program (Appendix C) Used as Input to Correlation Programs	126
D-2	Listing of the Mass Transfer Coefficient Correlation Computer Code	127
D-3	Sample Output from the Mass Transfer Coefficient Correlation Code	136
D-4	Listing of the Water Loss Correlation Computer Code	141
D-5	Sample Output from the Water Loss Correlation Code	152
D-6	Listing of the Colburn j Factor Correlation Computer Code	157
D-7	Sample Output from the Colburn j Factor Correlation Code.	161
D-8	Listing of the Fan System Efficiency Correlation Computer Code	167
D-9	Sample Output from the Fan System Efficiency Correlation Code	169
E-1	Measured Octave Band Noise Levels, dB*	180
E-2	Measured Overall Noise Levels, dB*	183
F-1	Sample Output from Program Tower	190
H-1	Sample of Raw Data File for Plume Tests	208
I-1	The Rubin Plume Prediction Computer Code	252
J-1	Comparison of Predicted and Observed Plume Characteristics	269

TESTING AND ANALYSIS
OF A WET-DRY CROSSFLOW COOLING TOWER,
VOLUME I: TEST PROGRAM & RESULTS

D. L. Ayers, M. R. Hogan, A. E. Hribar, and R. A. Lucheta
Heat Transfer and Fluid Dynamics

SECTION 1.0

INTRODUCTION

In 1973-1974 Westinghouse Electric Corporation designed and constructed a fully-instrumented wet/dry counterflow cooling tower with the aim of using the facility to acquire tower performance data while operating under typical power plant conditions. The tower facility was located at the Cliffside plant of Duke Power Company and acted as an adjunct to the cooling tower system which had previously serviced this plant.

Subsequently the tower test facility was purchased by the Tennessee Valley Authority under contract number TV46267. The aim of TVA was to use the tower test facility to obtain operating performance data in order to better understand cooling tower dynamics and to verify tower performance parameters in a cooling tower design computer code also obtained from Westinghouse under the contract. Under the terms of this contract Westinghouse Power Generation Services Division was to operate the test facility to obtain raw data while Westinghouse Research Laboratories were to reduce and analyze the data. The purpose of this report is to document the cooling tower data acquisition, reduction and analysis.

Dwg. 7722A97

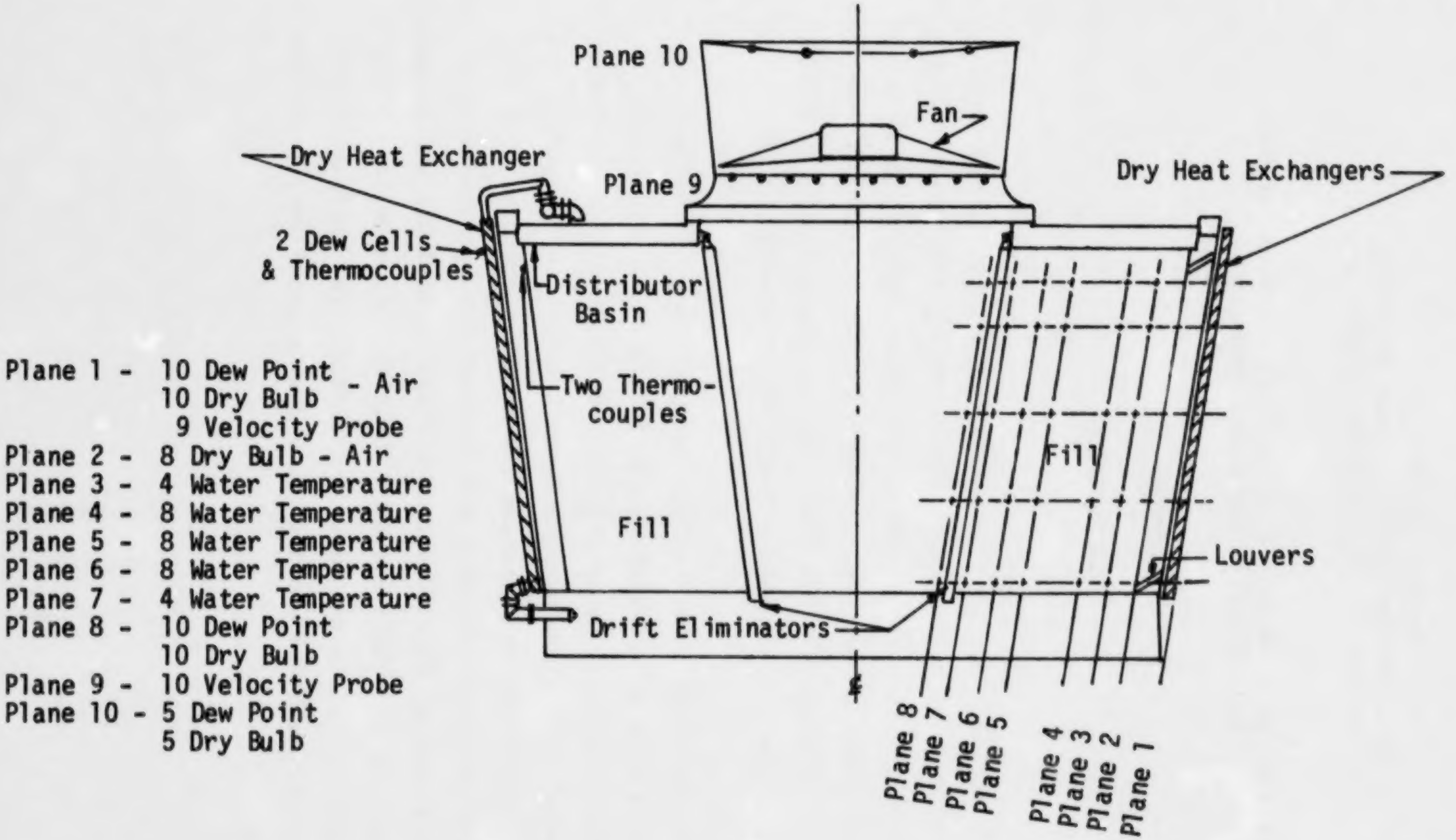
Plane 10
Fan
Dry Heat Exchanger
Plane 9
Dry Heat Exchangers
2 Dew Cells & Thermocouples
Distributor Basin
Two Thermocouples
Fill
Fill
Louvers
Drift Eliminators
℄
Plane 8
Plane 7
Plane 6
Plane 5
Plane 4
Plane 3
Plane 2
Plane 1

Plane 1 - 10 Dew Point - Air
10 Dry Bulb
9 Velocity Probe
Plane 2 - 8 Dry Bulb - Air
Plane 3 - 4 Water Temperature
Plane 4 - 8 Water Temperature
Plane 5 - 8 Water Temperature
Plane 6 - 8 Water Temperature
Plane 7 - 4 Water Temperature
Plane 8 - 10 Dew Point
10 Dry Bulb
Plane 9 - 10 Velocity Probe
Plane 10 - 5 Dew Point
5 Dry Bulb

Figure 1.0-1 Side View of Tower Showing Location of Dew Cells, Thermocouples, and Velocity Probes.

The cooling tower test facility was equipped to acquire data on airflow rate and distribution, water flow rate and distribution, fan speed and power, air pressure, air dry bulb and dew point temperatures and water temperatures. Figure 1.0-1 shows schematically the location of the instrumentation used to measure air properties in the test facility. Velocity probes were located in inlet and discharge planes to measure the distribution of airflow and total airflow. As explained later, these probes could not be used as intended. Also, due to the adverse environment, air dry bulb and dew point temperatures could not be measured in the fill volume, but were measured in the fill inlet and discharge planes, with considerable care taken to shield sensors from flowing water. Airflow was induced by a variable speed, variable pitch axial fan within the stack at the top of the tower. Figure 1.0-2 shows the water flow control and measurement system. Total water flow was measured with an Ellison Annubar flow meter, and the water was balanced between the two sides of the tower by remote control valves. Flow was balanced by equalizing water level in the two distributor basins at the top of the tower, and the flow into each basin could also be measured, each basin having been calibrated for water flow versus water depth in the basin. For the measurement of water flow through dry heat exchangers, the static pressure difference between top header and bottom header was used, since this pressure difference is a function of the square of the water velocity in the exchanger tubes.

From the acquired data thermodynamic and flow parameters such as mass transfer coefficient, water loss, dry heat exchanger heat transfer coefficient and fan efficiency may be reduced. Further, by operating the tower under a wide variety of conditions (weather, water inlet temperature, airflow rate, water flow rate, fan speed and fan blade pitch) it is possible to ascertain how the thermodynamic and flow parameters vary with these independent variables, by way of data correlations.

Dwg. 7722A98

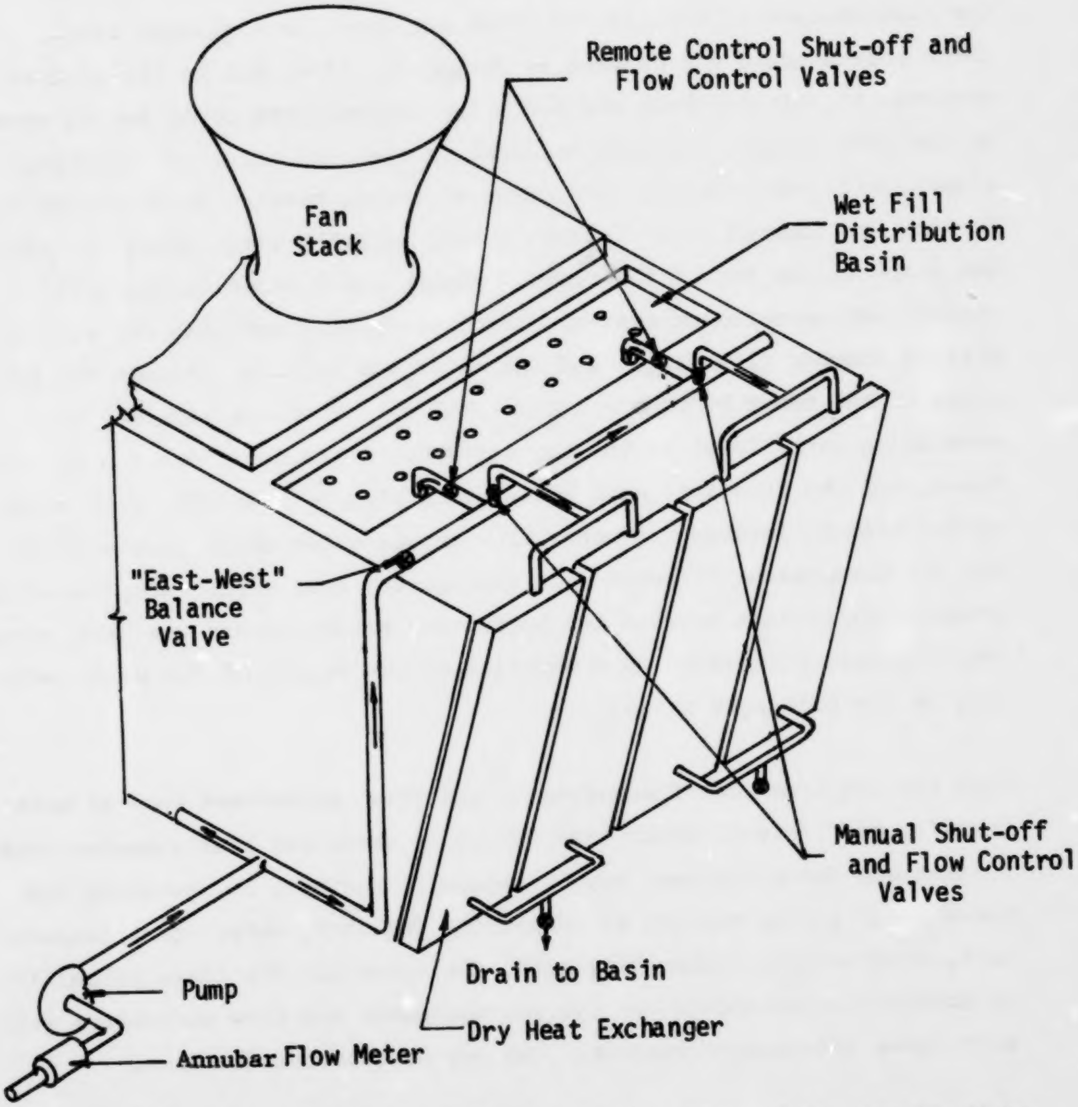
Remote Control Shut-off and
Flow Control Valves
Fan
Stack
Wet Fill
Distribution
Basin
"East-West"
Balance
Valve
Manual Shut-off
and Flow Control
Valves
Drain to Basin
Pump
Dry Heat Exchanger
Annubar Flow Meter

Figure 1.0-2 Schematic of One-Half The Cooling Tower Cell, Showing Water Flow Control and Measurement System.

In addition to the thermodynamic and flow instrumentation previously installed at the facility, instrumentation necessary to acquire acoustic and plume data were installed. The acoustics and plume data were also analyzed to determine their sensitivity to the tower independent parameters.

This report contains details of the tower instrumentation, techniques used to acquire test data, the data reduction procedure, analyses of data and discussion of results. The appendices contain a detailed description of the test facility, the data reduction computer program, computer programs used to analyze reduced data, plume data and a mathematical model for plume formation.

Section 4.0 of this report contains details of thermal and flow tests, while Sections 5.0 and 6.0 cover acoustics and plume tests, respectively. Since each section represents disparate technologies, each contains its own set of nomenclature and references, where necessary.

SECTION 2.0

CONCLUSIONS

The cooling tower test program as delineated in TVA contract TV46267 was completed and all significant test results are presented in this report. Based on the findings of this program the following conclusions may be drawn.

2.1 THERMAL AND FLOW TESTS

1. While all scheduled tests were performed, out of a total of 2760 runs made, only 1399 runs were recoverable by the analyst. The unrecoverable data were caused by instrument error, operator error, faulty instruments in inaccessible areas of the tower, data logging equipment failure and the generally hostile environment in the tower. The recovered data were sufficient to obtain adequate correlations of data for fill mass transfer coefficient, percent water loss, dry heat exchanger air-side heat transfer coefficient and fan system efficiency.

2. The mass transfer coefficient data are best correlated by the equation:

$$Ka = .2615\, L^{.875}\, G^{.683}\, T^{-1.392} \tag{2.1-1}$$

where Ka is mass transfer coefficient per unit volume of fill (lbm/hr-ft^3), L is water loading (lbm/hr-ft^2), G is air loading (lbm/hr-ft^2) and T is average outlet water temperature. Use of this correlation in tower design is iterative because of the use of average exit water temperature. This correlation was obtained by using all wet fill test data points where water loading was 10,000 lbm/hr-ft^2 or less, a total of 498 data points. For this correlation the coefficient of multiple determination, R^2, was .961, so that the multiple correlation coefficient R is .980, a reasonably good fit. All other attempts to correlate Ka with L, G and other representative system temperatures or with other limits on L or G resulted in smaller multiple correlation coefficients (see Table 4.5.1-1) and, thus, Equation (2.1-1) should be used in tower designs having fill elements like those in this tower (see Appendix A for a description of the fill). It should be noted that Equation (2.1-1) predicts a degradation in Ka with increasing water exit temperature and, thus, tower performance should suffer correspondingly with increasing ambient temperature.

A slightly less accurate correlation which ignores temperature effects:

$$Ka = .00029\ L^{.830}\ G^{.838} \qquad (2.1\text{-}2)$$

may be used as a first estimate in utilizing Equation (2.1-1) or for preliminary work. Equation (2.1-2) was also obtained using all wet fill test data with water loading less than 10,000 lbm/hr-ft^2, but with no water temperature dependency. The multiple correlation coefficient here is .969.

3. Percent water loss may be computed from the correlation:

$$\Delta L/L = 367.8\ L^{-.767}\ G^{.396}\ \Delta\omega^{.457} \qquad (2.1\text{-}3)$$

where L and G are as before and $\Delta L/L$ is percent water loss and $\Delta\omega$ is the log-mean specific humidity difference as defined in Equation (4.4.1-8). Again this correlation requires iterative solution in tower design. The coefficient of multiple correlation R is .961 for Equation (2.1-3). This equation was obtained by linear regression using only wet fill test data taken in the spring. Comparable correlations, restricted to other seasons or combining all wet test data, were inferior to Equation (2.1-3) for various reasons, including smaller values of R.

For less accurate work the equation:

$$\Delta L/L = 488.8\ L^{-.724}\ G^{.467}\ \Delta\omega^{.800} \qquad (2.1\text{-}4)$$

may be used, where $\Delta\omega$ is the specific humidity difference between air saturated at the inlet water temperature and air at the inlet of the tower fill. The multiple correlation coefficient R is .918 for Equation (2.1-4). This equation resulted from correlating all wet fill test data, with no seasonal or water loading limitations.

4. The correlation that best fits the dry heat exchanger air-side heat transfer coefficient data, in the form of Colburn j factor, is:

$$j = .2853\ Re^{-.5335} \qquad (2.1\text{-}5)$$

However, the data scatter here is quite large and caution in using this equation is urged (see Section 4.5). The correlation coefficient for Equation (2.1-5) is -.606, which is quite poor. Section 4.5 presents another correlation (Run 2, Table 4.5.3-1) where the correlation coefficient was -.783, a significant improvement. As stated there, however, the coefficient and exponent in the correlation are grossly different from those found in the literature for comparable heat transfer surface. Thus we caution the reader in using any dry heat transfer surface correlations in Section 4.5.

5. Fan system efficiency is defined as

$$\eta_f = \frac{\alpha Q \Delta P}{E} \qquad (2.1\text{-}6)$$

where η_f is efficiency, Q is airflow through the fan in ft^3/min, ΔP is fan pressure rise in inches of water, E is electrical input to the fan motor in kilowatts and α is the appropriate units conversion factor to make η_f dimensionless. This airflow system efficiency includes the losses inherent in the drive motor and gear box, as well as the fan itself. It was found that fan system efficiency correlates quite simply with total airflow rate by

$$\eta_f = -1.004\times10^{-2} + 2.4\times10^{-7} Q \qquad (2.1\text{-}7)$$

where the units of flow Q are ft^3/minute. The correlation coefficient for Equation (2.1-7) is .887.

6. Of all thermal and flow data collected, airflow rate is most suspect. The probe system built into the fan stack inlet to measure velocity pressure distribution across the fan inlet did not work properly due to water plugging of pressure lines. An air-water energy balance was used to deduce air mass flow rate. Thus the energy balance could not be used, as originally intended, to cull out deviant mass transfer and water loss data sets.

2.2 ACOUSTICS TESTS

1. Empirically fitted statistical model equations for the octave band noise levels at the fan stack discharge and in front of the louvered face of the tower were successfully developed from the measured noise levels.

2. The model equations give the noise levels as a function of the fan blade pitch, fan speed, total water flow rate and percent of water flow passing through the heat exchangers. The equations are valid over the range of the measured data discussed in Section 5.0.

3. The noise prediction code accounts for the tower operating variables, the tower size, atmospheric absorption, ground attenuation and fan stack directivity.

4. The noise prediction code predicts linear, A-weighted and octave band noise levels.

5. The ground absorption calculation assumes that the terrain is flat and the ground cover is essentially uniform between the tower and receiver. The code is set up assuming a grass-covered surface—it can be readily changed to accommodate other types of cover.

6. The noise prediction model has been verified only in the near field. The high background noise level at the test site precluded making measurements which could be used for verification of the far-field predictions.

2.3 PLUME TESTS

1. The apparatus described in Section 6.0 seems capable of gathering atmospheric boundary layer data, with the exception that the wind direction measurements fluctuate widely.

2. The plume dispersion model evaluated in this report is unsatisfactory.

SECTION 3.0

RECOMMENDATIONS

Based upon the work conducted in this program and discussed in detail in the body of this report, the following recommendations are made.

3.1 THERMAL AND FLOW TESTS

1. In future experimental programs of this nature, it is recommended that all instrumentation and data acquisition be directly linked and the data automatically logged, with man removed from the loop. Although this costs more at the outset, the time and expense saved in not having to rectify human error will more than offset equipment cost.

2. In future experimental programs of this nature it is recommended that the data reduction capability be located at the test site and the data reduced when available so that problems in data logging may be pinpointed and corrected immediately when they occur. This will tend to reduce the need for costly retest and subsequent program delays. In this program logged data were mailed to a remote facility for reduction and data logging errors that developed were not discovered until they had spoiled many subsequent test runs.

3. It is recommended that all suggested correlation equations be used for the design of cooling towers of the kind used here, except for the dry heat exchanger air-side heat transfer coefficient (Colburn j factor) correlation. In the design of finned-tube heat exchangers like those in the Cliffside wet/dry tower, it is recommended that the designer obtain air-side heat transfer coefficients from the exchanger manufacturer or, if such data are not available, that Reference 8 of Section 4.0 be used

or, as a last resort, that the data be obtained in another experiment conducted in a more controllable environment. The designer is warned that the recommended correlations are valid only for the same or similar equipment.

4. It is recommended in future wet fill cooling tower testing that pitot tubes not be used to measure air velocities downstream of the fill. The sensing system tubing cannot be maintained free of liquid water, the presence of which renders acquired data meaningless. It is recommended that some other means, not sensitive to the accumulation of water, be used to measure air velocity.

3.2 PLUME TESTS

1. The mathematical model for plume dispersion evaluated in this report should not be used.

2. In planning further field studies of cooling tower plumes, it would be desirable to seek a wider range of atmospheric conditions than were available during this study, which is limited to mostly stable, early morning hours in the spring. Also, in planning plume studies for wet/dry cooling towers, a program should be set up to study the conditions necessary to eliminate the plume, and this study should be independent of the plume trajectory study.

SECTION 4.0

THERMAL PERFORMANCE TESTS

The cooling tower test facility described in Appendix A was operated from December 1977 to November 1978 to obtain data on thermal, acoustic and plume performance. The nearly one-year test period provided test data under a variety of weather conditions, hopefully representative of the wide swings in ambient dry bulb and dew point temperatures that such a tower would see in a typical year. In this section the thermal performance is described. The acoustics results are presented in Section 5.0 and plume studies are given in Section 6.0.

The tower test facility has the capability of acquiring thermal data leading to the deduction of wet fill mass transfer coefficient, water loss rate, dry heat exchanger air-side heat transfer coefficient and fan performance. The tower is also equipped to measure airflow distribution at the inlet (dry heat exchanger) face and at the outlet (drift eliminator discharge) face of the energy transfer portion of the tower. During tests it was found that the air velocity measuring instrumentation (Kiel probes) were inadequate to accurately measure the airflow and so plans to study airflow distribution were abandoned early in the program.

So that the reader may properly understand the tests performed and their significance, this section includes a description of thermal and flow instrumentation, data acquisition techniques, data reduction procedures and a thorough analysis of the reduced data.

Dwg. 7697A65

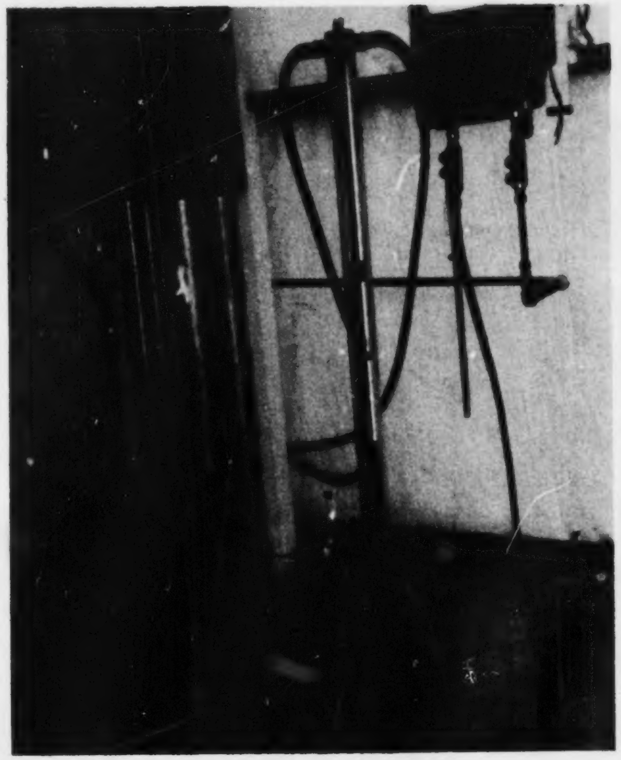

Figure 4.1-1. Mercury Manometer Used to Calibrate the Ellison Annubar Water Flow Meter.

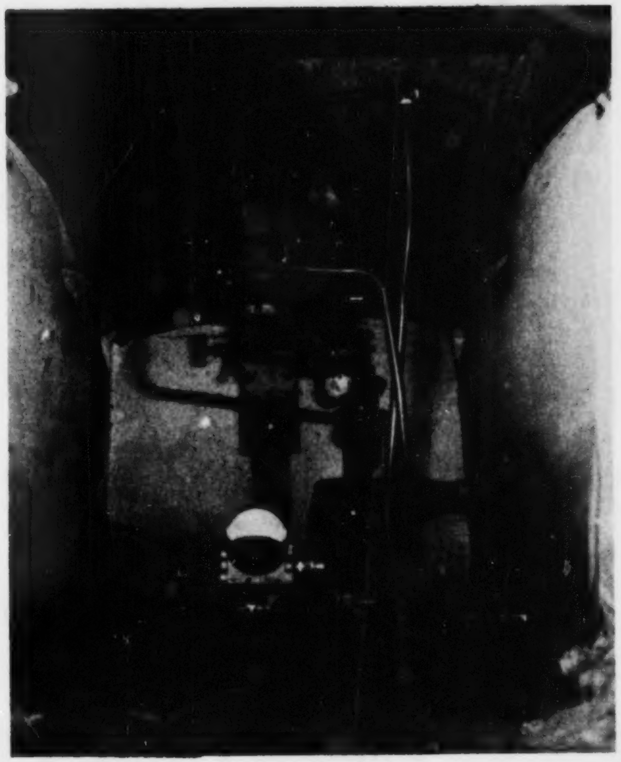

Figure 4.1-2. Ellison Annubar Water Flow Meter in its Insulated and Heated Housing.

4.1 THERMAL AND FLOW INSTRUMENTATION

Total flow of water to the tower was measured with an Ellison Annubar flow meter. This instrument outputs a pressure signal which is related to total water flow. This pressure was measured in two ways. The first was via a Taylor Instrument electronic flow meter housed in an insulated and thermostatically-controlled instrument box adjacent to the inlet piping containing the sensor. The 10 to 50 ma signal from the electronic flow meter was automatically logged by the Fluke model 2240B data logger located in the control trailer. The second measurement was made with a 50-inch "U" tube manometer with a 2.95 specific gravity fluid. This manometer was located in the control shed (see Appendix A) adjacent to the inlet flow pipe. Leads from the sensor to the instruments were heat taped and insulated. The manometer was used to calibrate the electronic flow meter and was used as a backup instrument in case of failure of the electronic instrument. The manometer and electronic flow meter are shown in Figures 4.1-1 and 4.1-2, respectively.

Water flow to either side of the tower was balanced by maintaining the same water depth in both basins above the wet fill. For wet/dry testing, where part of the water flow in each side was diverted to the dry heat exchangers, the flow split was first balanced in the wet fill basins. Then portions of the water were diverted to each dry heat exchanger, adjustments being made to this diversion until the wet fill basins showed identical, lower water depths. The volumetric flow of water through the dry exchangers was measured with a Statham model PM230 strain gage differential pressure transducer connected between the upper and lower headers of the exchangers. A second "U" tube manometer was used to calibrate this transducer and as a backup instrument. Calibration of this flow was obtained by diverting all flow to the dry exchangers and then using the total water flow instrument, the Ellison Annubar, as the primary instrument for water flow in the exchangers.

Dwg. 7697A66

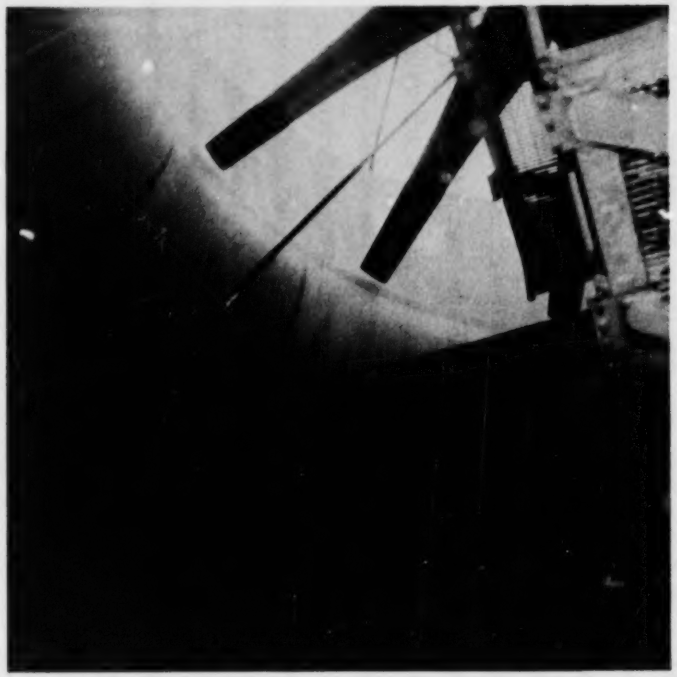

Figure 4.1-3. Photograph of the Kiel Probe Rake at the Fan Stack Inlet.

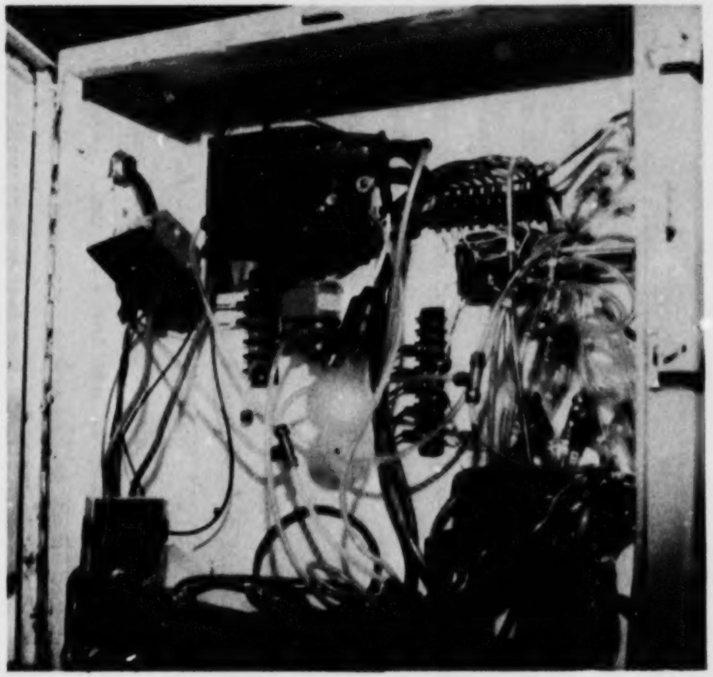

Figure 4.1-4. Photograph of the Wafer Switch Control for Kiel Probe Pressures (See Figure 4.1-6 for Schematic).

The total airflow measuring system consisted of two 17-feet-long pressure rakes mounted on the intake of the fan, as shown in the upper center left of Figure 4.1-3. Each rake held five Kiel probes which were connected by tygon tubing, wrapped in heat tape and insulated in a conduit, to an electrically-operated fluid wafer switch, shown in Figure 4.1-4. The tygon leads were connected to a single pressure transducer through the wafer switch which was stepped from one pressure port to the next by a signal from manual controls in the control trailer where the data logging equipment was located. The transducer output was displayed on a Datametrics model 1014A electromanometer located in the control trailer, shown in Figure 4.1-5. To maintain the tygon lines clear of condensate and sediment, a second stepped fluid wafer switch was connected between the tubing and a 9 psig air supply. For 10 seconds prior to a pressure being measured through the first wafer switch, the second switch opened and allowed the supply air to clear the tygon line of contaminants. When the 10 second purge had ended the second wafer switch closed to isolate the sensor probe from the purge air and the first wafer switch opened to connect the probe to the sensing transducer. A 10 second settling time was allowed before the transducer pressure signal was logged. Figure 4.1-6 is a schematic diagram of the probe/wafer switch/purge air system.

Most temperature measurements in this system were obtained with copper-constantan thermocouples, while air moisture content was measured with Foxboro model 2711TG dewcells. A thermocouple in the wet fill had its junction located at the throat of a small plastic water-collecting funnel to isolate the junction from the airstream. Thermocouples used to measure air dry bulb temperature were located in short sections of plastic piping whose axis was aligned with the direction of airflow. The piping contained a baffle system which intercepted and removed water droplets before they could impinge on the junction. It was very important that the airstream did not impinge on the wet fill water junctions and that water droplets did not collect on the airstream dry bulb

Dwg. 7697A67

Figure 4.1-5. Electromanometer Used for Pressure Measurement.

Figure 4.1-7. Fluke Model 2240B Digital Data Acquisition System.

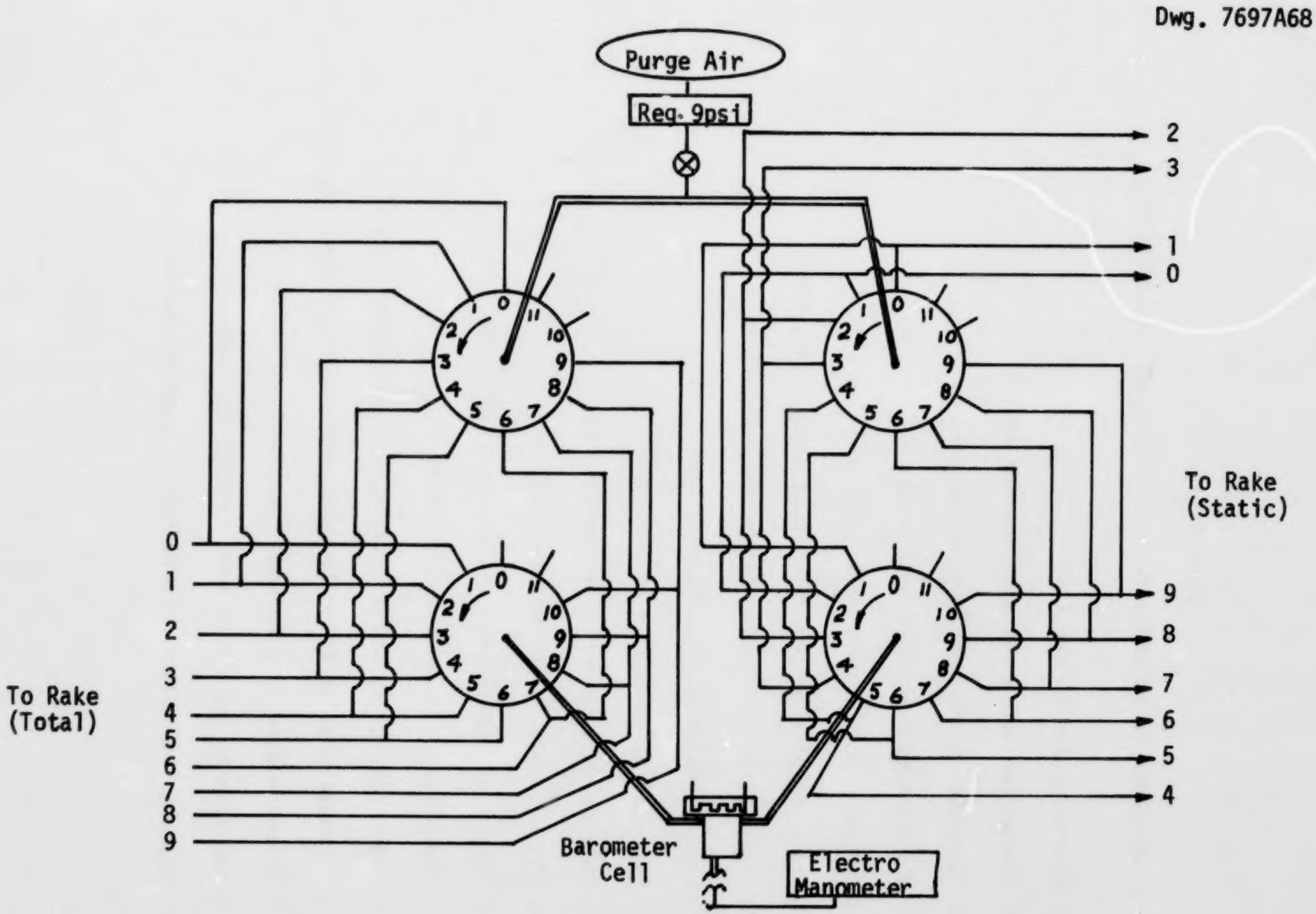
Dwg. 7697A68
Purge Air
Reg. 9psi
2
3
1
0
To Rake
(Static)
9
8
7
6
5
4
To Rake
(Total)
0
1
2
3
4
5
6
7
8
9
Barometer
Cell
Electro
Manometer
0
1
2
3
4
5
6
7
8
9
10
11

Figure 4.1-6. Schematic Diagram of the Fan Stack Air Velocity Measuring System's Probe/Wafer Switch/Purge Air/Pressure Transducer System.

TABLE 4.1-1

LOCATIONS OF THERMOCOUPLES, DEWCELLS AND THERMOMETERS

32 Thermocouples in the fill

10 Thermocouples on the west heat exchanger

10 Dewcells on the west heat exchanger

2 Thermocouples on east heat exchanger

2 Dewcells on the east heat exchanger

10 Thermocouples at the drift eliminator exit, west

10 Dewcells at the drift eliminator exit, west

5 Thermocouples at discharge of fan stack

5 Dewcells at discharge of fan stack

1 Thermocouple in hot water inlet pipe

1 Thermocouple in hot water basin

2 Thermocouples in heat exchanger outlet, west

1 Thermocouple in cold water return

10 Thermocouples at inlet louvers, air discharge from HX

2 Thermocouples at inlet louvers, air discharge from HX, east

2 Thermocouples on pole near test trailer for ambient

2 Dewcells on pole near test trailer for ambient

2 Mercury bulb thermometers, one at each manometer

junctions as both perturbations produce significant error in the measured temperature. A few temperature measurements were made with mercury bulb thermometers. Table 4.1-1 gives the number and location of thermocouples, dewcells and thermometers. The thermocouples and dewcells were connected directly to a Fluke model 2240B data logger located in the control trailer and shown in Figure 4.1-7. Thermometer readings were hand typed on the data logger tape when all automatically-acquired data had been logged (see Section 4.2).

Fan motor current and supply voltage were monitored in the control shed on an ammeter and voltmeter, respectively. A 20:1 current transformer and 35:1 potential transformer reduced the current and voltage to 1.8 amperes and 120 volts, respectively, thus allowing the use of an Esterline Angus model AW, 0 to 1000 watt, recording, two-element A.C. wattmeter. The wattmeter was located in the control trailer. Values taken from the current, voltage, and wattage indicating instruments were hand tabulated, then typed onto the data tape after automated data logging was complete.

Fan speed was measured with a proximity sensor, amplifier, and a Veeder Root electronic counter. The proximity sensor was triggered once per revolution of the fan and the counter integrated those triggers for 60 seconds. Values from the speed counter were tabulated and then typed onto the data tape.

The primary measuring instrument was a Fluke 2240B data logger. The microprocessor controlled data logger was programmed through front panel push button switches to execute an exact measurement routine. The Fluke instrument measures voltage to 1 microvolt (1μv) and temperature to one-tenth degree (.1°) Celsius or Fahrenheit. Measurements are displayed on light-emitting diode front panel digits, printed copy, and through a teletype on punched paper tape. An internal digital linearization module permits temperature to be recorded directly in degrees. The final system configuration allowed 120 channels of analog data to be input to the data logger.

4.1.1 Instrument Calibration Procedures

Gross flow calibration is discussed in Section 4.1. The Ellison Annubar was calibrated by the manufacturer. The Datametrics electronic manometer and Fluke data acquisition systems were calibrated by their manufacturers at the time of delivery. Fluke specifies "system accuracy" (includes all instrument errors such as A/D error, scanner error, power supply internal warm-up, etc.) at:

90 days (20° to 30°C) ±.01% RDG + .005% RNG + 3 μV (slow speed)

1 year (15°C to 35°C) ±.02% RDG + .01% RNG + 5 μV (slow speed).

Reference stability is ±.003%/°C and ±.003%/hr.

The temperature and scaling option when used with the high resolution A/D converter produces a system specification of .1°F resolution. For type T (copper-constantan) thermocouples operating in the temperature range of 32°F to 750°F worst case resolution is .1°F, NBS nonconformity is .1°F, 90-day system accuracy is .6°F, and one-year system accuracy is .8°F. No attempt was made to recalibrate the data acquisition system.

The Datametrics Electromanometer was calibrated daily using an internal reference for range and zero. Manufacturer's specifications indicate linearity: ±.01% F.S., zero coefficient: ±5PPM/°F, sensitivity coefficient: ±30PPM/°F. These specifications apply only to the 1014-A power supply and signal conditioner.. The "barocell" is calibrated at 10 TORR F.S. Worst case linearity (from the barocell calibration report) is .01% at 1 mm Hg. System accuracy is therefore ±.0002 mm Hg.

Dew cells were calibrated by the manufacturer. No attempt at recalibration was made during the test.

Fan motor current and supply voltage were measured on standard analog meters. These meters are accurate to ±2% F.S. No calibration was attempted. Fan power was measured on an Esterline-Angus wattmeter which was calibrated at the factory. Stated accuracy is ±1% F.S. over the temperature +20° to 120°F.

The fan speed was measured on a digital electronic counter which used power line frequency for a reference. Since power line stability is better than .05% and digital resolution is 1 RPM, fan speed error was less than ±1 RPM.

4.2 DATA ACQUISITION AND TRANSFER

The procedures used to start up, shut down and run the tower test facility are quite detailed. They are not truly germaine to data acquisition but in the event the test facility is ever used again, they would be of great value. Therefore the startup and shutdown procedures are listed in Appendix B. Likewise, the detailed procedure used to run the facility during data acquisition is presented there.

When the facility operators had ascertained that the proper test conditions were set, the actual procedure for acquiring thermal and flow data was initiated by taking the data on fan stack pressures. The wafer switches which connected the Kiel probe signals to their pressure transducer were stepped through 11 positions, each time waiting 10 seconds for the decay of pressure line transients. The output was displayed on the electromanometer and entered into the Fluke data logger. One channel of the 11 was the null signal from the transducer, one was a static pressure in the fan stack entrance and the remainder were velocity pressures (total minus static pressure) from each of nine Kiel probes.

After logging air velocity data the data logger was allowed to sequence through the automated acquisition of temperature and water flow pressure drop data, a total of 110 channels. Finally, when the automated sequence was complete, facility operators hand-typed 18 channels of data

TABLE 4.2-1

SAMPLE OF RAW TOWER DATA FROM A DRY HEAT EXCHANGER TEST

```
032212
119:08:50:22

  322121
  0 - 0.001 V
119:08:50:32

  322121
  0 + 1.525 V
119:08:50:42

  322121
  0 + 1.762 V
119:08:50:56

  322121
  0 + 5.172 V
119:08:51:06

  322121
  0 + 2.348 V
119:08:51:12

  322121
  0 + 2.030 V
119:08:51:17

  322121
  0 + 1.532 V
119:08:51:22

  322121
  0 + 1.542 V
119:08:51:32

  322121
  0 + 2.277 V
119:08:51:37

  322121
  0 + 2.362 V
119:08:51:44
```

(Continued)

Table 4.2-1 (cont'd)

```
   322121
   0 + 2.175 V
 119:08:51:52

   322121
  10 +  81.4 F    11 + 104.1 F    12 + 102.3 F    13 + 105.1 F
  14 +  60.3 F    15 +  61.4 F    16 + 105.6 F    17 + 104.3 F
  18 +  86.0 F    19 + 107.4 F    20 + 117.7 F    21 + 104.3 F
  22    OL    F   23 + 105.9 F    24 + 104.0 F    25 +  60.8 F
  26 +  60.9 F    27 +  50.0 F    28 +  50.9 F    29 +  61.4 F
  30 +  61.1 F    31 +  61.4 F    32 +  61.2 F    33 +  82.0 F
  34 +  81.8 F    35 + 104.6 F    36 + 107.8 F    37 +  15.6 F
  38 + 103.2 F    39 + 115.3 F    40 + 117.0 F    41 + 105.4 F
  42 + 104.6 F    43 + 103.6 F    44 + 104.4 F    45 +  68.1 F
  46 +  67.6 F    47 +  69.6 F    48 +  69.6 F    49 +  78.2 F
  50 +  68.8 F    51 +  76.6 F    52 +  67.1 F    53 +  77.5 F
  54 +  70.4 F    55 +  77.6 F    56 +  69.2 F    57 +  69.3 F



  58 +  66.9 F    59 +  66.9 F    60 +  69.0 F    61 +  62.5 F
  62 +  67.2 F    63 +  67.0 F    64 +  67.9 F    65 +  59.4 F
  66 +  66.2 F    67 +  66.6 F    68 +  67.2 F    69 +  69.7 F
  70 +  68.6 F    71 +  69.9 F    72 +  70.2 F    73 +  65.8 F
  74 +  77.9 F    75 +  65.8 F    76 +  67.7 F    77 +  78.7 F
  78 +  77.8 F    79 +  77.5 F    80 +  78.3 F    81 +  77.8 F
  82 +  74.0 F    83 +  72.2 F    84 +  78.0 F    85 +  77.5 F
  86 +  76.4 F    87 +  55.5 F    88 + 112.8 F    89 + 111.6 F
  90 + 107.1 F    91 + 110.0 F    92    BT    F   93 + 104.1 F
  94 +  78.3 F    95 +  78.7 F    96 +  77.4 F    97 +  75.7 F
  98 +  77.1 F    99 +  74.9 F   100 +  78.0 F   101 +  77.7 F
 102 +  80.0 F   103 +  79.0 F   104 +  74.2 F   105 +  58.3 F
 106 + 106.9 F   107 + 108.6 F   108 +  67.3 F   109 +  67.3 F
 110 + 103.9 F   111 + 104.1 F   112 +  50.0 F   113 +  63.9 F
 114 +  75.0 F   115 +  74.9 F   116 +  63.2 F   117    BT    F
 118 +  1.98MV
 119:08:54:43

   322121
 118 +  1.64MV  118 +  1.83MV  118 +  1.92MV  118 +  1.73MV
 118 +  1.82MV  118 +  1.84MV  118 +  1.79MV  118 +  1.85MV
 118 +  1.94MV  118 +  1.70MV  118 +  1.80MV  118 +  1.97MV
 118 +  2.04MV  118 +  2.14MV  118 +  2.02MV  118 +  1.92MV
 118 +  1.76MV  118 +  1.99MV  118 +  1.91MV  118 +  2.07MV
```

(Continued)

Table 4.2-1 (cont'd)

```
119:08:55:16

  322121
119 + 42.57MV  119 + 41.52MV  119 + 42.54MV  119 + 44.53MV
119 + 43.03MV  119 + 44.22MV  119 + 39.54MV  119 + 43.37MV
119 + 44.35MV  119 + 44.03MV  119 + 45.99MV  119 + 43.80MV
119 + 46.22MV  119 + 46.91MV  119 + 44.39MV  119 + 43.72MV
119 + 42.69MV  119 + 42.30MV  119 + 44.67MV  119 + 43.16MV
120 4090.  121 44.0  122 44.0  123 43.0  124 36.5  125 36.0
126 35.5  127 7.2  128 5.5  129 65.0  130 2.95  131 15.0
132 15.0  133 60.0  134 127.  135 12.  136 .200  137 30.22
119:08:57:29
```

which had been read from isolated instruments. This sequence was followed for five sets of data at every set of test conditions.

Table 4.2-1 is a listing of a typical run. The figure 322121 which appears throughout the data is the test number; the first digit indicating this was a dry heat exchanger test, the second indicating it was run in the spring, the third, fourth and fifth digits indicating test conditions (water flow rate, airflow rate) and the last digit indicating this is the first of five runs under these conditions. Also scattered throughout the data are the characters 119:xx:yy:zz, where 119 indicates data was acquired on the 119th day of 1978 and xx:yy:zz is the time of day in hours, minutes and seconds. As for other entries in the sample data, Table 4.2-2 lists their definitions. Note that channel 118, the output from the pressure transducer between the top and the bottom of the dry heat exchanger, and channel 119, the output from the Ellison Annubar flow meter, are logged 20 times so that they may be averaged. The data for channels 120 through 137 were hand-typed, the data having been previously logged manually from separate individual instruments. When all five runs at a given set of conditions had been logged, a duplicate punched paper tape was made to insure its availability when the master punched tape was forwarded by mail to Westinghouse Fluid Systems Laboratory (WFSL) for analysis.

Before describing the reduction and correlation of data, mention should be made of the condition of the raw data as received by the analyst and how it was processed. Recall that thermal and flow data were acquired at the test site using a combination of automated acquisition and hand-typed input of visual readings of instruments. The data for a given run were transferred to the analyst on punched paper tape. The control characters generated by the data acquisition equipment were not compatible with the computer (Purdue University CDC6500) used to reduce the raw data. Consequently, each raw data tape received from the tower site had to be processed by a minicomputer (PDP-8E) which read raw tapes, sensed control characters and produced a new data tape with CDC-compatible control characters. The translated tapes were then used with the

TABLE 4.2-2

DELINEATION OF INPUT PAPER TAPE DATA BY CHANNEL FOR THERMAL AND FLOW DATA

Channel	Description
0	11 repetitions of time, run ID, and fan stack Kiel probe pressure transducer output. The first grouping contains the transducer's zero, Group 2 and 3 are velocity pressures, 4 is a static pressure, and the remaining are velocity pressures.
10	Tower basin cold water return temperature
11-13	Heat exchanger air inlet dewcell temperature
14-15	Heat exchanger inlet air temperature
16-17	Heat exchanger inlet air dewcell temperature
18	Tower hot water inlet temperature
19-21	Heat exchanger inlet air dewcell temperature
22	Not used
23-24	Heat exchanger inlet air dewcell temperature
25-32	Heat exchanger inlet air temperature
33-34	Heat exchanger outlet water temperature
35-44	Wet fill outlet air dewcell temperature
45-57	Fill water temperature
58-59	Ambient air temperature
60-76	Fill water temperature
77-86	Wet fill outlet air temperature

(Continued)

Table 4.2-2 (cont'd)

Channel	Description
88	Not used
89-93	Stack exit air dewcell temperature
94-98	Stack exit air temperature
99-105	Fill inlet air temperature
106-107	Ambient air dewcell temperature
108-109	Fill water temperature
110-117	Not used
118	Dry heat exchanger pressure drop transducer
119	Annubar element transducer
120	Tower voltage (v)
122-126	Tower pump amperage (a)
127	Annubar manometer column rise above datum (in)
128	Annubar manometer column fall below datum (in)
129	Annubar manometer ambient temperature (°F)
130	Manometer fluid specific gravity
131	Dry heat exchanger manometer column fall below datum (in)
132	Dry heat exchanger manometer column rise above datum (in)
133	Dry heat exchanger manometer temperature (°F)
134	Fan rotational speed (rpm)
135	Fan pitch (degrees)
136	Fan power (reading x 700 = kw)
137	Barometric pressure (in Hg)

Dwg. 7697A69

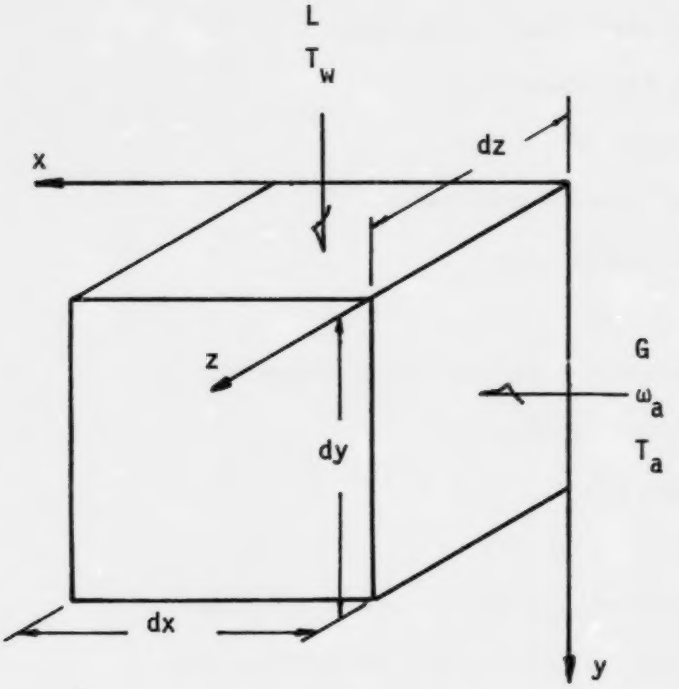
L
T_w
x
dz
z
dy
G
ω_a
T_a
dx
y

Figure 4.3-1. Wet Fill Heat and Mass Transfer Control Volume.

reduction program described in Section 4.3. The reduction program produced both paper output and punched cards containing reduced data. These data cards were segregated and sorted as to test type (wet, wet/dry, dry, fan, short fill) and test number so that ultimate correlations could be obtained without unnecessarily handling extraneous data. As for the condition of the raw data, it left a lot to be desired from the standpoint of completeness and usability. In particular, a run contained 137 pieces of test data, the first 119 coming from automated acquisition and the remaining 18 from hand-fed data. The last 18 pieces were generally so inconsistent that each had to be scanned by the analyst and, in almost all cases, corrected because of some obvious error. This could be done because each test point was repeated five times and visual scanning showed that, perhaps in one run, the data in question was incorrect, possibly due to digit transposition or dropping of a digit. In many cases, the data were so inconsistent from run to run that it all had to be thrown out. In many cases, one or two runs out of five were deleted because of the very large number of incorrect or missing pieces of data in each set. As a consequence, although the test schedule (Section 4.4) shows that a total of 2760 separate runs were to be made, only 1399 or 51 percent were recoverable by the analyst.

4.3 THERMAL AND FLOW DATA REDUCTION

4.3.1 Tower Heat and Mass Transfer

Consider the control volume in Figure 4.3-1. Water enters the top of the volume at L lbm/hr-ft^2 and some temperature, T_w. Air with specific humidity ω_a and temperature T_a enters from the side with a mass velocity of G. The energy entering the control volume is

$$E_i = LT_wCp_wdxdz + Gh_adzdy \qquad (4.3\text{-}1)$$

Using a first order Taylor series to estimate the energy out of the control volume yields,

$$E_o = Cp_w \left(L + \frac{\partial L}{\partial y} dy\right)\left(T_w + \frac{\partial T_w}{\partial y} dy\right) dxdz$$

$$+ \left(Gh_a + \frac{\partial h_a}{\partial x} dx\right) dydz \qquad (4.3\text{-}2)$$

and steady state requires that

$$E_o - E_i = 0 \quad . \qquad (4.3\text{-}3)$$

Substitution of (4.3-1) and (4.3-2) in (4-3.3) gives

$$Cp_w L \frac{\partial T_w}{\partial y} = -\left[G \frac{\partial h_a}{\partial x} + Cp_w T_w \frac{\partial L}{\partial y}\right] \qquad (4.3\text{-}4)$$

where second order terms have been dropped. The last term on the right-hand side of (4.3-4) is usually neglected. This can be justified by first recalling the definition of moist air specific enthalpy,

$$h_a = Cp_a T_a + \omega_a h_v \quad . \qquad (4.3\text{-}5)$$

Differentiation yields,

$$\frac{\partial h_a}{\partial x} = Cp_a \frac{\partial T_a}{\partial x} + h_v \frac{\partial \omega_a}{\partial x} \quad . \qquad (4.3\text{-}6)$$

The $\partial Cp_a/\partial x$ and $\partial h_v/\partial x$ terms have been neglected since they are very small relative to the other terms in (4.3-6). From conservation of mass it is known that,

$$\frac{\partial L}{\partial y} = G \frac{\partial \omega_a}{\partial x} \quad . \qquad (4.3\text{-}7)$$

Substitution of (4.3-6) and (4.3-7) into the right-hand side of (4.3-4) results in,

$$G \frac{\partial h_a}{\partial x} + Cp_w T_w \frac{\partial L}{\partial y} = G \left[Cp_a \frac{\partial T_a}{\partial x} + \frac{\partial \omega_a}{\partial x} (h_v + Cp_w T_w)\right] . \qquad (4.3\text{-}8)$$

Since the water vapor specific enthalpy is at least an order of magnitude greater than the specific enthalpy of the water, $Cp_w T_w$ can be dropped from (4.3-8). With this simplification it becomes

$$G \frac{\partial h_a}{\partial x} + Cp_w T_w \frac{\partial L}{\partial y} \simeq G \left[Cp_a \frac{\partial T_a}{\partial x} + h_v \frac{\partial \omega_a}{\partial x}\right] . \qquad (4.3\text{-}9)$$

It can be seen that the right-hand side of (4.3-9) is the space derivative of the air specific enthalpy [refer to (4.3-6)]. Equation (4.3-9) can, therefore, be rewritten as,

$$G \frac{\partial h_a}{\partial x} + Cp_w T_w \frac{\partial L}{\partial y} \simeq G \frac{\partial h_a}{\partial x} . \qquad (4.3\text{-}10)$$

Replacement of the right-hand side of (4.3-4) with that of (4.3-10) yields the desired simplified result.

$$Cp_w L \frac{\partial T_w}{\partial y} = -G \frac{\partial h_a}{\partial x} . \qquad (4.3\text{-}11)$$

To get an expression for the mass transfer coefficient or tower transfer units in terms of measurable variables consider a deformable control volume whose surface corresponds to that of a water droplet. Conservation of energy requires

$$\frac{\partial U_w}{\partial t} = q \qquad (4.3\text{-}12)$$

where U_w is the water's internal energy. Using the chain rule of differentiation on (4.3-12) yields the more useful expression,

$$\frac{\partial U_w}{\partial t} = \frac{\partial U_w}{\partial y}\frac{dy}{dt} \quad . \tag{4.3-13}$$

Recall that

$$U_w = m_w Cp_w (T_w - T_{ref}) \tag{4.3-14}$$

where T_{ref} is some reference temperature. Substituting (4.3-14) in (4.3-13) and performing the required differentiation results in.

$$\frac{\partial U_w}{\partial t} = [Cp_w (T_w - T_{ref}) \frac{\partial m_w}{\partial y} + m_w Cp_w \frac{\partial T_w}{\partial y}] \frac{dy}{dt} \quad . \tag{4.3-15}$$

Usually the water loss term $(\partial m_w/\partial y)$ is neglected since it is small relative to the other terms. This can be seen by casting (4.3-15) into a different form. First, note that

$$\frac{\partial m_w}{\partial y} = -m_a \frac{\partial \omega_a}{\partial x} \quad . \tag{4.3-16}$$

Using

$$m_a = \frac{G}{L} m_w \tag{4.3-17}$$

in (4.3-16), and that result in (4.3-15) gives the desired expression,

$$\frac{\partial U_w}{\partial t} = m_w Cp_w \frac{\partial T_w}{\partial y} [1 - \frac{(T_w - T_{ref}) \frac{G}{L} \frac{\partial \omega_a}{\partial x}}{\frac{\partial T_w}{\partial y}}] \frac{dy}{dt} \, . \tag{4.3-18}$$

An order of magnitude analysis on the second term within the braces in (4.3-18) shows it to be on the order of .05. Hence, it can be dropped from (4.3-18),

$$\frac{\partial U_w}{\partial t} = m_w Cp_w \frac{\partial T_w}{\partial y} \frac{dy}{dt} \quad . \qquad (4.3\text{-}19)$$

Equation (4.3-19) can be made more useful by realizing that,

$$V_w = \frac{dy}{dt} \qquad (4.3\text{-}20)$$

and, as a result, (4.3-19) can be written as,

$$\frac{\partial U_w}{\partial t} = m_w Cp_w V_w \frac{\partial T_w}{\partial y} \quad . \qquad (4.3\text{-}21)$$

As a means of eliminating the need for details of the water droplets (4.3-21) can be put into a per unit volume basis. Substitution of the result into (4.3-12) yields,

$$\frac{m_w}{\forall} Cp_w V_w \frac{\partial T_w}{\partial y} = q''' \quad . \qquad (4.3\text{-}22)$$

Now since

$$L = \rho_w V_w = \frac{m_w}{\forall} V_w \quad , \qquad (4.3\text{-}23)$$

(4.3-22) can be rewritten as,

$$q''' = Cp_w L \frac{\partial T_w}{\partial y} \quad . \qquad (4.3\text{-}24)$$

The expression for q''' must account for both sensible and evaporative heat transfer. A Newtonian type of expression is commonly assumed,

$$q''' = Kg \cdot a \cdot (T_a - T_w) + Ka\,(\omega_a - \omega_w)\, h_{fg} \qquad (4.3\text{-}25)$$

where a is the droplet surface area per unit volume, Kg the sensible heat transfer coefficient, and K the mass transfer coefficient. Note that the water droplet temperature is assumed uniform. The subscript w on ω and T indicates conditions at the air-water interface, assumed saturated.

Heat and mass transfer may be related under certain conditions. This presumes the heat and mass transfer to be related in the following fashion,

$$Kg = Le^{n} Cp_{ma} K \tag{4.3-26}$$

where Le^n is the Lewis number to some power (approximately two-thirds for turbulent flows). For water vapor-air mixtures at moderate temperatures the Lewis number is approximately unity; as a result, (4.3-26) can be approximately written as

$$Kg = Cp_{ma} K \ . \tag{4.3-27}$$

Substitution of (4.3-27) into (4.3-25) yields

$$q''' = Ka \left[Cp_{ma} (T_a - T_w) + (\omega_a - \omega_w) h_{fg} \right] \ . \tag{4.3-28}$$

Substituting

$$Cp_{ma} = Cp_a + \omega Cp_{wv} \tag{4.3-29}$$

in (4.3-28) and expanding yields,

$$\begin{aligned} q''' = Ka \, [&(Cp_a T_a + \omega Cp_{wv} T_a + \omega_a h_{fg}) \\ &- (Cp_a T_w + \omega Cp_{wv} T_w + \omega_w h_{fg})] \ . \end{aligned} \tag{4.3-30}$$

The ω which appears in (4.3-30), and originally in (4.3-29), is the result of applying the heat and mass transfer analogy. It is a property which describes the transport process across the boundary layer. It is not clear whether the freestream (ω_a), interfacial (ω_w), film $(\omega_w+\omega_a)/2$, or any other fraction between the freestream and interfacial specific humidity is the characteristic specific humidity. A common, and usually satisfactory estimate is the film specific humidity,

$$\omega = \frac{\omega_w + \omega_a}{2} \ . \tag{4.3-31}$$

If (4.3-31) is used in (4.3-30) and the result rearranged, one finds that,

$$\begin{aligned} q''' &= Ka\ [Cp_a T_a + \omega_a Cp_{wv} T_a + \omega_a h_{fg}] \\ &\quad -Ka\ [Cp_a T_w + \omega_w Cp_{wv} T_w + \omega_w h_{fg}] \\ &\quad +\frac{1}{2}\ Cp_{wv}\ [T_a + T_w][\omega_w - \omega_a]\ Ka \ . \end{aligned} \tag{4.3-32}$$

The first two bracketed terms on the right-hand side of (4.3-32) are the air freestream and interfacial enthalpy, respectively. As a result,

$$q''' = Ka\ [h_a - h_w][1 + \varepsilon] \tag{4.3-33}$$

where

$$\varepsilon = \frac{\frac{1}{2}\ Cp_{wv}\ [T_a + T_w][\omega_w - \omega_a]}{h_a - h_w} \ . \tag{4.3-34}$$

ε is dominated by the difference in specific humidities. An order of magnitude analysis of (4.3-34) indicates ε to be on the order of .03. As a result, ε can be neglected relative to unity, and, consequently, Equation (4.3-33) simplifies to,

$$q''' = Ka\,[h_a - h_w] \quad . \tag{4.3-35}$$

Substitution of (4.3-35) into (4.3-24) yields the expression for the tower mass transfer coefficient,

$$LCp_w \frac{\partial T_w}{\partial y} = Ka\,(h_a - h_w) \quad . \tag{4.3-36}$$

The number of transfer units (NTU) can be calculated from,

$$NTU = \int_o^Y \frac{Kady}{L} \quad . \tag{4.3-37}$$

If Ka is assumed constant throughout the tower, then

$$NTU = \frac{KaY}{L} \quad . \tag{4.3-38}$$

Since the functional relationship between Ka (or NTU) and T_w, h_a, h_w is unknown, Equations (4.3-11) and (4.3-36) must be solved implicitly for Ka. The data obtained from the tower provides the lacking process information so that Ka may be determined.

4.3.1.1 Wet Fill Heat and Mass Transfer Computation

4.3.1.1.1 Computation of Ka

Since neither the air nor the water thermodynamic process is known analytically in the wet fill, it is necessary to start in one corner of a two-dimensional representation of the fill, where the air and water states are known, and numerically march across the tower. The tower is first divided into small rectangles. A Ka is then assumed. Inlet air enthalpy and water temperature are known. An average water temperature, air enthalpy, and a saturated air enthalpy corresponding to the average water temperature is estimated. Equation (4.3-36) is solved for the vertical water temperature gradient. That result is used in (4.3-11) to calculate the air specific enthalpy gradient (with respect to the air streamwise coordinate). Knowledge of the water temperature and air enthalpy gradients enables the outlet states from the rectangle to be computed, as well as new averages. With the new averages available, the solution of (4.3-36) and (4.3-11) is repeated. The solution is considered complete when the water exit temperatures of two iterations are essentially identical. The entire procedure is repeated for each grid. After all of the grids have been solved, an average fill water outlet temperature is computed and compared to the actual recorded outlet temperature. If they are not within the desired accuracy a new Ka is assumed, a solution for all grid points obtained, and a new average outlet water temperature acquired. This new temperature is compared to the experimentally acquired value, hopefully with less error than the first. If necessary, the process is repeated until the calculated value is sufficiently close to the actual temperature. The Ka which enables convergence to occur is the sought-after value. In the remainder of this section the numerical technique will be developed mathematically.

Consider Figure 4.3-2. Since the air and water flow rates, as well as their properties, are assumed uniform across their respective inlets, the wet fill can be considered two dimensional. Consider now a Taylor expansion about some point (x,y)

$$f\,(x + \Delta x, y) \;=\; f\,(x,y) + \frac{\partial f\,(x,y)}{\partial x}\,\Delta x + \varepsilon\,(\Delta x^2) \qquad (4.3\text{-}39)$$

where ε is the remainder of the Taylor expansion. It represents an error which is of Δx^2 order. (4.3-39) can be rearranged to,

$$\frac{\partial f\,(x,y)}{\partial x} = \frac{f\,(x + \Delta x, y) - f\,(x,y)}{\Delta x} - \varepsilon\;. \qquad (4.3\text{-}40)$$

Dwg. 7697A70

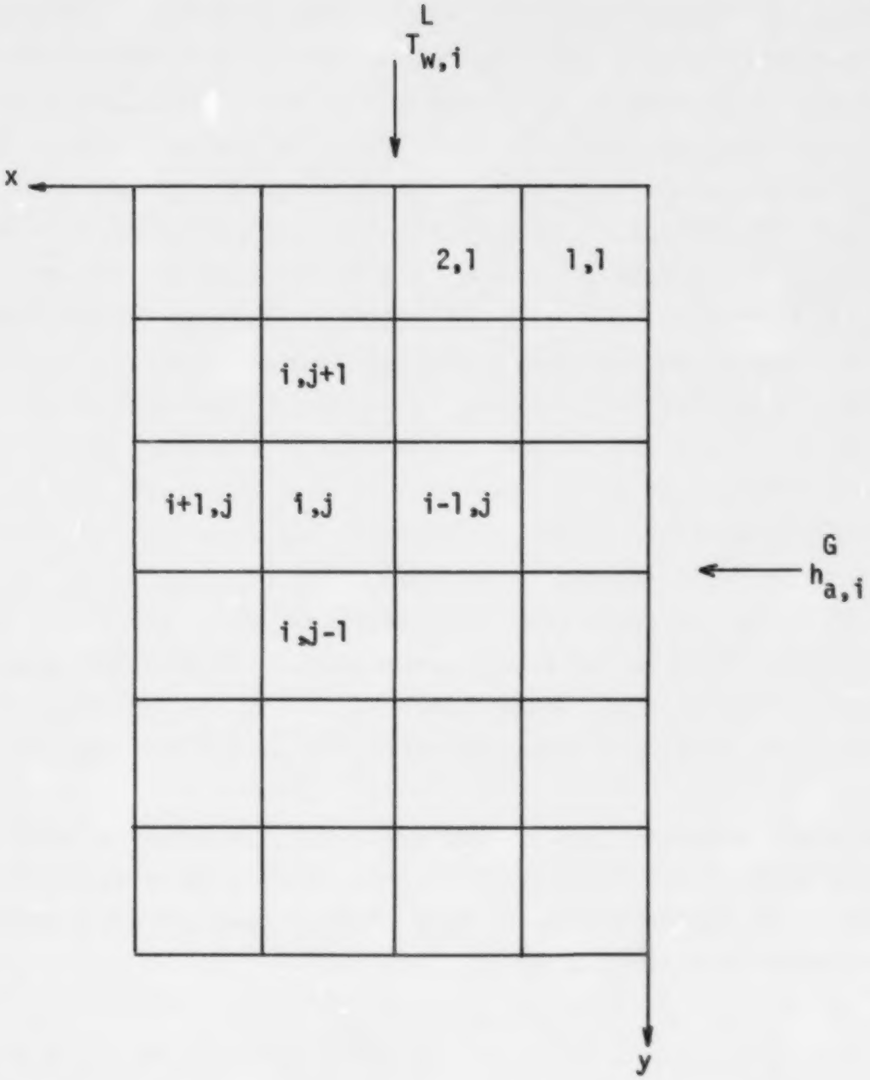
L
$T_{w,i}$
x
2,1
1,1
i,j+1
i+1,j
i,j
i-1,j
G
$h_{a,i}$
i,j-1
y

Figure 4.3-2. An Illustration of the Two-Dimensional Representation of the Wet Fill and its Grid Structure.

It can be seen in (4.3-40) that a derivative can be approximated by a ratio of finite differences within an error of order Δ^2. To use this result (4.3-36) must first be solved for the water temperature gradient,

$$\frac{\partial T_w}{\partial y} = \frac{Ka\ (h_{a,i,j} - h_{w,i,j})}{LCp_w} \qquad (4.3\text{-}41)$$

and then (4.3-40) applied to the result,

$$T_w\ (x, y + \Delta y) = \frac{\partial T_w}{\partial y}\ \Delta y + T_w(x,y) \qquad (4.3\text{-}42)$$

Similarly for (4.3-11),

$$\frac{\partial h_a}{\partial x} = -\frac{Cp_w L \frac{\partial T_w}{\partial y}}{G} \qquad (4.3\text{-}43)$$

$$h_a\ (x + \Delta x, y) = \frac{\partial h_a}{\partial x}\ \Delta x + h_a\ (x,y)\ . \qquad (4.3\text{-}44)$$

$h_a - h_w$, the driving potential for mass transfer, is a function of the spatial coordinates. Since the finite difference technique jumps from one point to another Δ away, the driving potential must be representative of conditions between points. Consider, for example, Figure 4.3-3. Assume for the sake of argument that the integration process is proceeding from coordinates (x_i, y_j) to $(x_i, y_j + \Delta y)$ across element i,j. Conditions are known at $(x_i, y_j + \Delta y)$ after the solution is complete. Conditions within the element, however, are unknown. The properties of element i,j are best approximated by some average of the boundary values. In this work the driving potential appropriate for element i,j was taken to be the difference in average enthalpies, computed as follows:

Dwg. 7697A71

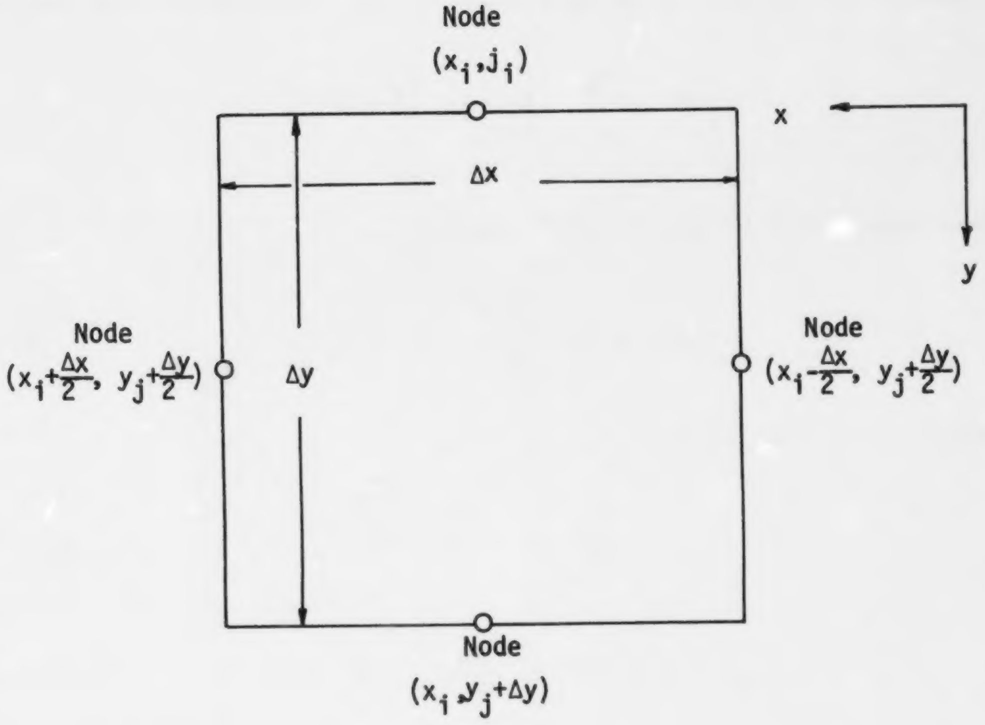
Node
(x_i, j_i)
x
y
Δx
Δy
Node
$(x_i+\frac{\Delta x}{2}, y_j+\frac{\Delta y}{2})$
Node
$(x_i-\frac{\Delta x}{2}, y_j+\frac{\Delta y}{2})$
Node
$(x_i, y_j+\Delta y)$

Figure 4.3-3. Typical Wet Fill Grid and Nomenclature Employed in Defining the Temperature of the Grid i,j.

$$h_{a,i,j} = \frac{h_a\ (x_i - \frac{\Delta x}{2},\ y_j + \frac{\Delta y}{2}) + h_a\ (x_i + \frac{\Delta x}{2},\ y_j + \frac{\Delta y}{2})}{2} \qquad (4.3\text{-}45)$$

$$T_{w,i,j} = \frac{T_w\ (x_i, y_j + \Delta y) + T_w\ (x_i, y_j)}{2} \qquad (4.3\text{-}46)$$

$$h_w = h_{w,i,j} = f\ (T_{w,i,j}) \qquad (4.3\text{-}47)$$

Equations (4.3-41) through (4.3-47) constitute the set of equations which must be solved for each element. The integration starts with element (1,1) [Figure 4.3-2] and proceeds downward until all elements in that column are used. It then continues with the top of the next column, (2,1), and works its way down again. The only restriction on the step-by-step progression through the tower is provided by the boundary conditions. The upper and right-hand side edge of each element must have T_w and h_a, respectively, specified for a solution to be possible. The following steps were followed in calculating Ka:

1. Ka is assumed based on experience.
2. The boundary values for T_w and h_a are set. ($T_w = T_{w,in}$ on $y = 0$ and $h_a = h_{a,in}$ on $x = 0$).
3. Start grid solution: $i = 1$, $j = 1$.
4. An estimate of $T_w\ (x_i, y_j + \Delta y)$ and $h_a\ (x_i + \Delta x/2,\ y_j + \Delta y/2)$ is assumed (refer to Figure 4.3-3).
5. Based on $T_w\ (x_i, y_j + \Delta y)$, $h_w\ (x_i, y_j + \Delta y)$ is calculated from (4.3-46).
6. $h_{a,i,j}$ is calculated from (4.3-45).
7. Equation (4.3-41) is evaluated for $\partial T_{w,i,j}/\partial y$.
8. Equation (4.3-42) is calculated for a refined value of the exit water temperature, $T'_w\ (x_i, y_j + \Delta y)$
9. $\partial h_{a,i,j}/\partial x$ is calculated from (4.3-43).

10. (4.3-44) is evaluated for a refined version of the exit air enthalpy, $h'_a\ (x_i+\Delta x/2,\ y_j+\Delta y/2)$.

11. A check is made as to whether

$$\left|\ T_w\ (x_i,y_j+\Delta y) - T'_w\ (x_i,y_j+\Delta y)\ \right| < .001$$

or (4.3-48)

$$\left|\ \frac{T_w\ (x_i,y_j+\Delta y) - T'_w\ (x_i,y_j+\Delta y)}{T_w\ (x_i,y_j+\Delta y) - T_w\ (x_i,y_j)}\ \right| < .00001$$

Three actions can result from (4.3-48).

(a) True. Convergence has been obtained, the grid solution is complete. Let

$$T_w\ (x_i,y_j+\Delta y) \;=\; T'_w\ (x_i,y_j+\Delta y)$$

$$h_a\ (x_i + \frac{\Delta x}{2},\ y_j + \frac{\Delta y}{2}) \;=\; h'_a\ (x_i + \frac{\Delta x}{2},\ y_j + \frac{\Delta y}{2}) \qquad (4.3\text{-}49)$$

$$T_w\ (x_i,y_{j+1}) \;=\; T_w\ (x_i,y_j+\Delta y)$$

$$h_a\ (x_{i+1} - \frac{\Delta x}{2},\ y_j + \frac{\Delta y}{2}) \;=\; h_a\ (x_i + \frac{\Delta x}{2},\ y_j + \frac{\Delta y}{2})$$

Increment j if possible. If not, then increment i and re-index j to 1 (i.e., start again at top of next downstream column.) Repeat steps 4 through 11.

(b) False. Convergence has not been achieved yet. A better estimate[1] of $T_w\ (x_i,y_j+\Delta y)$ and $h_a\ (x_i+ x/2,y_j+\Delta y/2)$ is made. Steps 5 through 11 are repeated.

(c) True. Convergence has been achieved at all grid points. If M is the maximum number of i increments and N the maximum j, then the average fill outlet water temperature is calculated from

$$T'_{w,o,avg} = \frac{1}{M} \sum_{i=1}^{M} T_w (x_i, y_N) \qquad (4.3\text{-}49)$$

If

$$|T'_{w,o,avg} - T_{w,o,avg}| < .01 \qquad (4.3\text{-}50)$$

or

$$\left| \frac{T'_{w,o,avg} - T_{w,o,avg}}{T_{w,o,avg}} \right| < .0001$$

where $T_{w,o,avg}$ is the actual water temperature obtained by experiment*, then the assumed version of Ka is considered correct and the tower solution complete. If (4.3-50) is false, then a better estimate of Ka is performed and steps 2 through 11 repeated. The Secant method[2] is employed in obtaining the correct Ka for a given $T_{w,o,avg}$.

4.3.1.1.2 Calculation of Grid Size

Since this data reduction program was to be used a great many times, it was important that the grid size be no finer than necessary for the desired accuracy in Ka. This section presents the technique utilized in calculating the grid size. In following the derivation, first consider Figure 4.3-2 and the following approximation for the water temperature gradient,

$$\frac{\partial T_w(x_1, y_1)}{\partial y} = \frac{T_w(x_1, y_1) - T_w(x_1, y_2)}{\Delta y} - \varepsilon\ (\Delta y) \qquad (4.3\text{-}51)$$

---

*The fill outlet water temperature was acquired by averaging the bottom fill thermocouples, whereas the inlet water temperature was taken to be the measured distribution basin temperature. Air-side inlet conditions were computed from the average of the fill inlet dry-bulb and dewcell temperatures, from which specific enthalpy can be calculated.

where ε is the truncation error (or order Δy), and x_1, y_1, y_2 arbitrary vertical coordinates. (4.3-51) can be obtained from a Taylor's expansion, e.g., solve (4.3-39) for ∂f/∂x. Using (4.3-36) in (4.3-51) to eliminate the temperature gradient yields,

$$\frac{T_w(x_1,y_1) - T_w(x_1,y_2)}{\Delta y} - \varepsilon(\Delta y) = \frac{Ka[h_a(x_1,y_1) - h_w(x_1,y_1)]}{LCp_w} \qquad (4.3\text{-}52)$$

Solving for ε (Δy),

$$\varepsilon(\Delta y) = \frac{T_w(x_1,y_1) - T_w(x_1,y_2)}{\Delta y} - \frac{Ka[h_a(x_1,y_1) - h_w(x_1,y_1)]}{LCp_w} \qquad (4.3\text{-}53)$$

For the error to be zero, the following must be true,

$$\frac{T_w(x_1,y_1) - T_w(x_1,y_2)}{\Delta y} = \frac{Ka[h_a(x_1,y_1) - h_w(x_1,y_1)]}{LCp_w} \qquad (4.3\text{-}54)$$

or since Δy = Y/N,

$$N = \frac{KaY\,[h_a(x_1,y_1) - h_w(x_1,y_1)]}{LCp_w\,[T_w(x_1,y_1) - T_w(x_1,y_2)]} \qquad (4.3\text{-}55)$$

The number of air streamwise divisions (M) can be calculated in a similar fashion,

$$M = \left[\frac{T_w(x_1,y_1) - T_w(x_1,y_2)}{h_a(x_2,y_1) - h_a(x_1,y_1)}\right]\frac{LCp_w dN}{GY} \qquad (4.3\text{-}56)$$

To allow for more flexibility (4.3-55) was multiplied by an experimental multiplication factor Xmf,

$$N = \frac{Xmf \cdot K \cdot a \cdot Y \, [h_a(x_1,y_1) - h_w(x_1,y_1)]}{LCp_w \, [T_w(x_1,y_1) - T_w(x_1,y_2)]} \qquad (4.3\text{-}57)$$

Figure 4.3-4 shows the effect of Xmf on computation time and accuracy. Note that the error in the figure is dimensional and relative to a Ka calculated for Xmf = 2.0, a value for which subsequent increases produced only small and random perturbations to Ka. Clearly the accuracy improves very little for Xmf > 1, and at great expense. All data reduction for this work was performed with Xmf = 1, considered to be a good tradeoff between accuracy (approximately 2 percent) and run time (about 7 seconds). For each set of data both M and N were calculated. To evaluate N, Ka was estimated from

$$Ka = \frac{1188.0 \, L^{.599} G^{.438}}{T_{w,i}^{\;2.04}} \qquad (4.3\text{-}58)$$

which is an expression developed in previous years by the Fluid Systems Laboratory. $h_w(x_1,y_1)$ [Equation (4.3-57)] was based on inlet water conditions, $h_a(x_1,y_1)$ on fill inlet conditions, $h_a(x_2,y_1)$ on the air state at the fill outlet, and the water temperature difference in the denominator of (4.3-57) and numerator of (4.3-56) were taken to be the difference in the inlet water temperature and the average of the first array of fill thermocouples. M and N were calculated for each Ka. In this way accuracy as well as good utilization of computer time was maintained.

4.3.1.2 Heat Exchanger Heat Transfer Analysis

This section presents the heat transfer analysis utilized to determine the heat exchanger air-side heat transfer coefficient from the tower test data. Figure 4.3-5 should be referred to for tube and fin nomenclature.

The total heat transfer rate from the tower heat exchanger can be calculated from

Curve 717153A

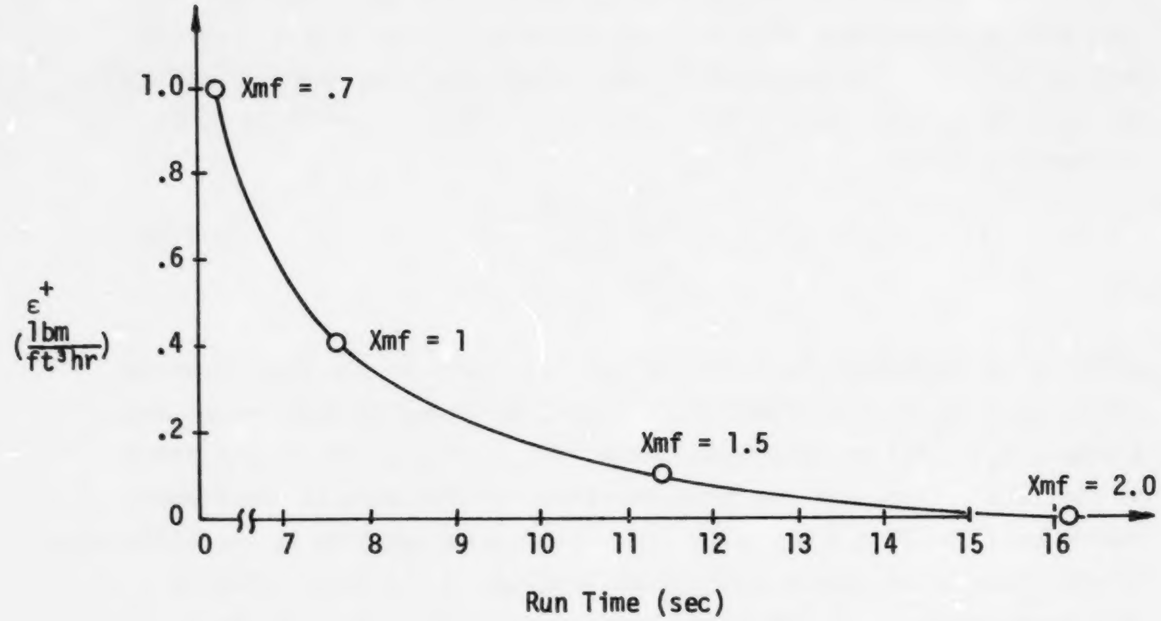

Figure 4.3-4. Error in Mass Transfer Coefficient as a Function of Computation Time and the Experimental Multiplication Factor.

$\varepsilon^+ =$ Ka (Xmf = 2.0) - Ka (Xmf)

Dwg. 7697A72

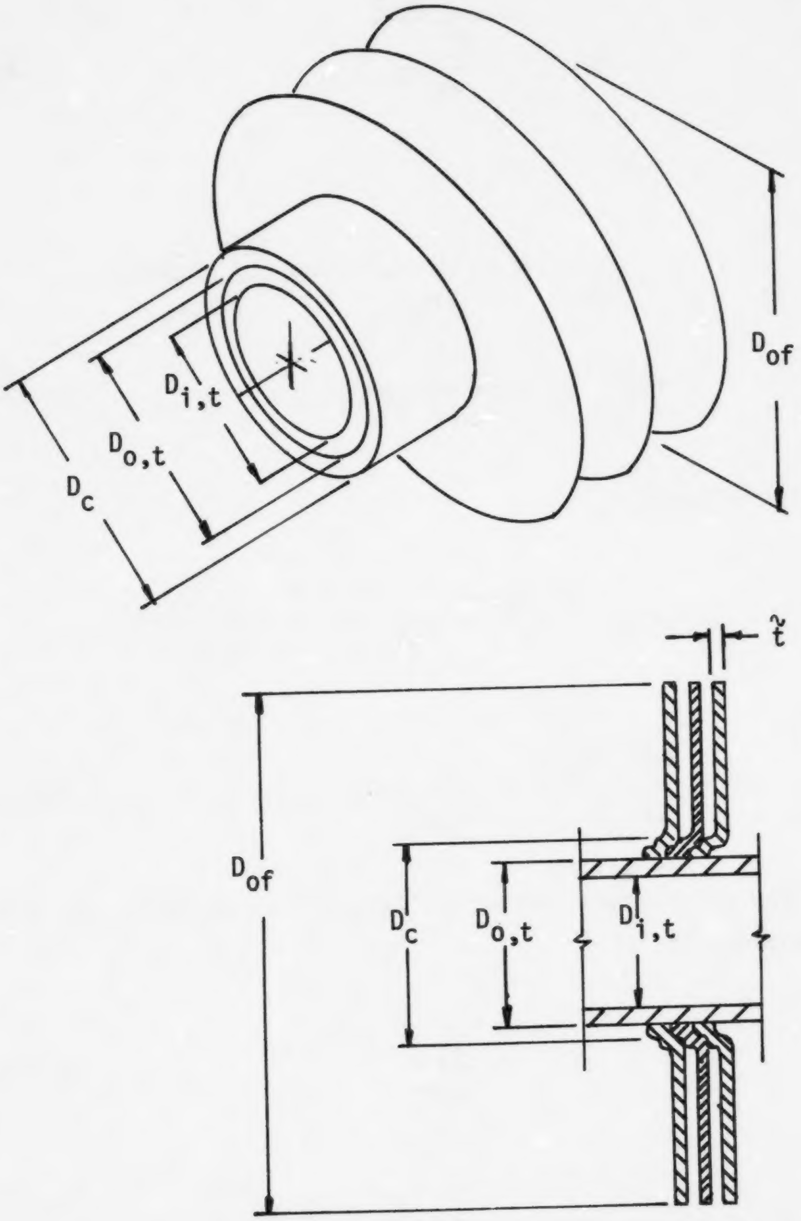
D_of
D_i,t
D_o,t
D_c
t̃
D_of
D_c
D_o,t
D_i,t

Figure 4.3-5. Tower Heat Exchanger Tube and Fin Geometry, and Nomenclature Employed in the Heat Transfer Analysis.

$$q = \frac{F \cdot \Delta T_{\ell mtd}}{\sum_{i=1}^{N} R_i} \tag{4.3-59}$$

where

$$\sum_{i=1}^{N} R_i = \frac{1}{H_w A_{i,t}} + \frac{\ell n[D_{o,t}/D_{i,t}]}{2\pi k_t \tilde{L}_t} + \frac{\ell n[D_c/D_{o,t}]}{2\pi k_f \tilde{L}_t}$$

$$+ \frac{1}{H_c A_{o,t}} + \frac{1}{(A_{co} + \eta A_f)H_a} \quad . \tag{4.3-60}$$

Solving for the unknown H_a,

$$H_a = \{ (A_{co} + \eta A_f) \left(\frac{F\Delta T_{\ell mtd}}{q} - \frac{1}{H_w A_{i,t}} - \frac{\ell n[D_{o,t}/D_{i,t}]}{2\pi k_t \tilde{L}_t} \right.$$

$$\left. - \frac{\ell n[D_c/D_{o,t}]}{2\pi k_f \tilde{L}_t} - \frac{1}{H_c A_{o,t}} \right) \}^{-1} \tag{4.3-61}$$

F, the crossflow temperature correction factor, can be calculated from the work of Bowman, et. al.^{3},

$$F = \frac{r_{cf}}{r_{ccf}} \tag{4.3-62}$$

where

$$r_{ccf} = \frac{p - \tilde{q}}{\ell n \left[\frac{1-\tilde{q}}{1-p}\right]} \tag{4.3-63}$$

and

$$p = \frac{T_{w,i} - T_{w,o}}{T_{w,i} - T_{a,i}}$$

$$\tilde{q} = \frac{T_{a,o} - T_{a,i}}{T_{w,i} - T_{a,i}} \qquad (4.3\text{-}64)$$

and

$$r_{cf} = \sum_{m=0}^{\infty} \sum_{n=0}^{\infty} (-1)^{m+n} \frac{(m+n)!}{m!(n+1)!n!(m+1)!} \left(\frac{p}{r_{cf}}\right)^{m} \left(\frac{\tilde{q}}{r_{cf}}\right)^{n} . \qquad (4.3\text{-}65)$$

The solution of (4.3-65) for r_{cf} is necessarily numerical but once it is determined, F can be easily calculated from (4.3-62) in conjunction with (4.3-63) and (4.3-64).

$\Delta T_{\ell mtd}$, the driving potential for heat transfer, is determined from,

$$\Delta T_{\ell mtd} = \frac{(T_{w,i} - T_{a,o}) - (T_{w,o} - T_{a,i})}{\ell n \left[\frac{T_{w,i} - T_{a,o}}{T_{w,o} - T_{a,i}}\right]} \qquad (4.3\text{-}66)$$

The fin efficiency, η, can be calculated from the work of Gardner[4],

$$\eta = \frac{2}{U_b\,[1 - (U_e/U_b)^2]} \left[\frac{I_1(U_b) - \beta K_1(U_b)}{I_o(U_b) + \beta K_o(U_b)} \right] \qquad (4.3\text{-}67)$$

where I_o and I_1 are zeroth and first order modified Bessel functions of the first kind, K_o and K_1 zeroth and first order modified Bessel functions of the second kind, and

$$\beta = \frac{I_1(U_e)}{K_1(U_e)} \qquad (4.3\text{-}68)$$

$$U_b = \left[\frac{D_{o,f} - D_c}{2}\right] \left[\frac{2H_a}{k_f \tilde{t}}\right]^{1/2} \left[\frac{D_{o,f}}{D_c} - 1\right]^{-1} \qquad (4.3\text{-}69)$$

$$U_e = U_b \left[\frac{D_{o,f}}{D_c}\right] \qquad (4.3\text{-}70)$$

Eckels[5] provides a means of estimating the collar-to-tube-surface contact resistance,

$$H_c = 4.51 \times 10^5 \left\{ \frac{\tilde{t}}{\left[\frac{1}{N_f \tilde{t}} - 1\right]^2 D_{o,t}} \right\}^{.6422} \qquad (4.3\text{-}71)$$

Since the water-side heat transfer coefficient is also unknown, it too must be estimated. The following expression from Sieder and Tate[6] was used to estimate the water-side film coefficient,

$$H_w = .027 \left[\frac{k_w}{D_i}\right] Re_d^{.8}\, Pr_w^{1/3} \left[\frac{\mu_w}{\mu_{w,wall}}\right]^{.14} \qquad (4.3\text{-}72)$$

All water properties in (4.3-72) are evaluated at the freestream or bulk temperature, except for $\mu_{w,wall}$ which is evaluated at the tube wall. The bulk water temperature was considered to be the arithmetic average of the inlet and outlet temperature ($T_{w,avg}$). The wall temperature was found from,

$$T_{w,wall} = \frac{T_{w,avg} R_o + T_{a,avg} R_1}{R_o + R_1} \qquad (4.3\text{-}73)$$

where $T_{a,avg}$ is the arithmetic average of the air inlet and outlet temperature, R_1, the first term on the right-hand side of (4.3-60), and R_o, the sum of the remaining terms on the right-hand side of (4.3-60). q, the heat transfer rate from the water to the air, is known from,

$$q = \dot{m}_a Cp_a \left(T_{a,i} - T_{a,o}\right) \qquad (4.3\text{-}74)$$

where $\dot{m}_a$, $T_{a,i}$, and $T_{a,o}$ are measured values.

With Equations (4.3-62) through (4.3-74), the air-side heat transfer coefficient can be calculated from (4.3-61). Since the fin efficiency [Equation (4.3-67)] via (4.3-69), and the water-side film coefficient [Equation (4.3-72)] via (4.3-73) are functions of the air-side heat transfer coefficient, the solution of Equation (4.3-61) is iterative with respect to itself, (4.3-67) and (4.3-72).

4.3.1.3 Heat Exchanger Air-Side Heat Transfer Coefficient Computation

The calculation of the air-side heat transfer coefficient is complicated by the fact that it is a function of the fin efficiency (a function of the air-side heat transfer coefficient) and the water-side film coefficient (a function of the tube wall temperature and thus a function of the air-side film coefficient). Nevertheless, the computation is relatively straightforward. The procedure is as follows:

1. All air properties are computed at the average air temperature.
2. The heat exchanger heat transfer rate is calculated from (4.3-74).
3. An average wall temperature and air-side film coefficient is assumed.
4. Fin efficiency (4.3-67), water-side heat transfer coefficient (4.3-72), and the log mean temperature difference (4.3-66) are calculated.
5. The cross-flow correction factor (4.3-62) is calculated. [Equation (4.3-65) is solved numerically with the Secant method[2].)

6. A refined estimate of the air-side heat transfer coefficient is computed via (4.3-61). Although the air-side heat transfer coefficient is, in effect, a function of itself, the dependency is very weak. As a result, only two iterations on wall temperature (steps 3-6) are usually necessary to obtain closure. For this work, three iterations were used to insure a high degree of computational accuracy.

7. After the required three iterations, the Stanton, Nusselt, Reynolds, etc. numbers are computed for later correlation.

4.3.1.4 Airflow Rate Analysis and Computation

The tower air flow rate was calculated from velocity pressure measurements at the throat of the stack, conservation of energy considerations, and from a static pressure measurement at the fan inlet. The objective was to supplant the velocity pressure data if it was determined to be unreliable. This can occur because water is often ingested by the probes as a result of the stack environment. If the water is not purged from the signal-conveying tubing , it will drastically alter the sensed pressure. Initially the purging system was unreliable and the alternative energy conservation technique for calculating air flow rates was employed. After the purging system was operating satisfactorily the velocity pressure measurements were utilized, with the other methods held as backups.

As noted in Section 3.0, ten pairs of Kiel and static pressure probes were installed across the throat of the stack. They were circuited such that velocity pressure was sensed in nine of them, while the remaining one was set up for a static pressure measurement. The velocity was calculated from the velocity pressure measurement according to the following relationship,

$$V = \sqrt{\frac{2P_v}{\rho}} \qquad (4.3\text{-}75)$$

Figure 4.3-6 is a graph of four velocity data sets taken a few moments apart under steady state conditions. It illustrates two important points. First, any water trapped in the signal tubing can be readily discerned by the resulting anomolous velocities, e.g., data points near the stack wall and centerline. Second, it illustrates the problem of determining the air flow rate by this method. Under ideal conditions all of the velocity pressure measurements would be free of error and a simple radial integration of the velocity profile would yield an air flow rate. This, however, is not the case in this wet environment. Despite purging before each measurement, erratic readings did occur periodically in a given traverse. In almost all instances the bad reading was confined to one probe station, though the particular station was random. As a result, the air flow rate was calculated by averaging the measured velocities. Even though this is not as rigorous as an integral technique, it tended to dampen the effect of one erroneous reading rather than amplifying it, as would radial integration.

The second method of determining air flow rate, used for the first tests during which time the purging system was being perfected, was based on conservation of energy. Considering the tower as a control volume, conservation of energy requires that,

$$\dot{m}_a (h_{a,o} - h_{a,i}) = \dot{m}_w (T_{w,i} - T_{w,o}) \; . \tag{4.3-76}$$

Solving for the air mass flow rate yields the desired final result,

$$\dot{m}_a = \frac{\dot{m}_w (T_{w,i} - T_{w,o})}{(h_{a,o} - h_{a,i})} \tag{4.3-77}$$

This technique is considered viable because of the very good accuracy obtainable in measuring water flow rate and the inlet and outlet air states. Contrarywise, utilization of this method precluded the use of energy conservation in checking the quality of the data.

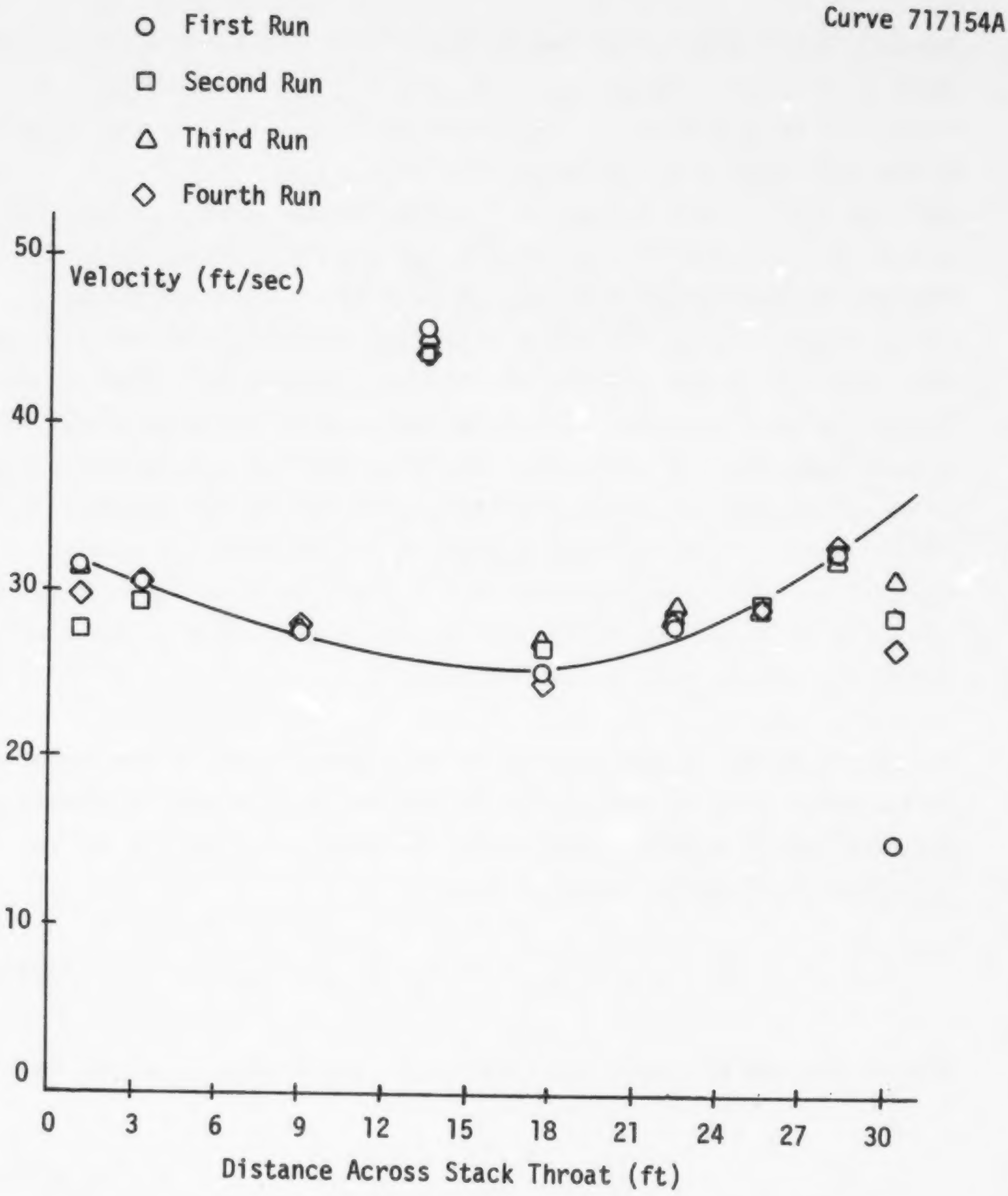

Figure 4.3-6. Stack Velocity as a Function of Distance Across the Stack at the Velocity Pressure Probe Station.

The third method by which air flow rate was calculated uses the fan inlet static pressure, a diffuser loss model, and the available fan curve. It was retained only as a limited check, and was never used in the heat and mass transfer calculations. The method of solution is based on obtaining the fan pressure rise, via diffuser loss calculations, and then obtaining the air flow rate for the given pressure rise from the manufacturer's fan curves.

Shown in Figure 4.3-7 is an illustration of the fan stack system. Note that the station at the fan inlet will be denoted by subscript (i), the fan outlet by (o), and the stack discharge by (e). Conservation of energy and momentum from the fan outlet to the stack discharge yields,

$$P_e = P_o + \frac{1}{2}\rho_o V^2_{s,o} \left[1 - \left(\frac{\tilde{r}_o}{\tilde{r}_e}\right)^2\right] + \frac{1}{2}\rho_o V^2_{a,o} \left[1 - \left(\frac{\tilde{A}_o}{\tilde{A}_e}\right)^2\right] - \frac{1}{2} K\ell\, \rho_o\, V^2_{a,o} \tag{4.3-78}$$

where the subscripts (s) and (a) denote the swirl and axial velocity component, respectively. $K\ell$ is the stack loss coefficient and P_e is atmospheric pressure. The static pressure rise across the fan is,

$$\Delta Pr = P_o - P_i \tag{4.3-79}$$

or upon substitution of (4.3-79) in (4.3-78),

$$\Delta Pr = P_e + \frac{1}{2}K\ell\rho_o V^2_{a,o} - \frac{1}{2}\rho_o V^2_{s,o} \left[1 - \left(\frac{\tilde{r}_o}{\tilde{r}_e}\right)^2\right] - \frac{1}{2}\rho_o V^2_{a,o} \left[1 - \left(\frac{\tilde{A}_o}{\tilde{A}_e}\right)^2\right] - P_i \tag{4.3-80}$$

Dwg. 7697A73

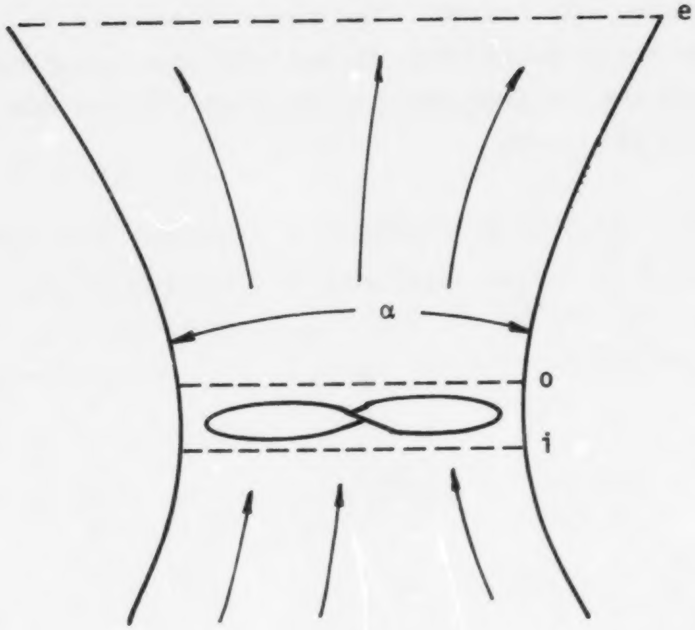

Figure 4.3-7. Fan-Stack Model and Nomenclature Employed for the Calculation of Air Flow Rate From the Fan Curve.

Assume the fan inlet flow to be axial,

$$V_{s,o} = \frac{\Delta P_r}{\rho_o \tilde{\omega} \bar{r}} \qquad (4.3\text{-}81)$$

where $\bar{r}$ is the mean radius and can be calculated from,

$$\bar{r} = \left[\frac{1 + (\tilde{r}_{hub}/\tilde{r}_{tip})^2}{2} \right]^{1/2} \qquad (4.3\text{-}82)$$

Substituting (4.3-81) in (4.3-80), and then applying the definition of volume flow rate to $V_{a,o}$ in (4.3-80) results in,

$$\Delta Pr = P_e - P_i + \frac{\rho_o K\ell Q^2}{2\tilde{A}_o^2} - \frac{\Delta Pr^2}{2\rho_o \tilde{\omega}^2 \bar{r}^2} \left[1 - \left(\frac{\tilde{r}_o}{\tilde{r}_e}\right)^2\right]$$

$$- \frac{\rho_o Q^2}{2\tilde{A}_o^2} \left[1 - \left(\frac{\tilde{A}_o}{\tilde{A}_e}\right)^2\right] . \qquad (4.3\text{-}83)$$

Idel'Chik[7] presents correlations for calculating $K\ell$ for common diffuser geometries. For a conical diffuser, such as is the case here,

$$K\ell = 3.2 \left(\tan \frac{\alpha}{2}\right]^{5/4} \left[1 - \frac{\tilde{A}_o}{\tilde{A}_e}\right]^2 + \frac{\lambda}{8 \sin \frac{\alpha}{2}} \left[1 - \left(\frac{\tilde{A}_o}{\tilde{A}_e}\right)^2\right] . \qquad (4.3\text{-}84)$$

where α is the diffuser included angle, and λ the wall friction coefficient. λ was calculated from smooth wall correlations based on the axial Reynolds number.

The fan curve can be represented by

$$Q - f(\Delta Pr, \theta, \tilde{\omega}) = 0 \qquad (4.3\text{-}85)$$

where θ is the blade angle and ω the rotational speed. Equation (4.3-85) existed in subroutine form and could reproduce the manufacturer's data. The different operating rotational speeds were taken into account by the fan scaling laws.

Written in a more generalized form, (4.3-83) becomes

$$\Delta Pr - f(\Delta Pr, Q, y_i) = 0 \qquad (4.3\text{-}86)$$

where f is a generalized function and y_i represents the known parameters in (4.3-83). Equations (4.3-85) and (4.3-86) represent a system of non-linear algebraic equations which were solved via the Secant method[2] for determining the roots of an equation.

4.3.1.5 Water Flow Rate Analysis and Computation

Since the flow to the tower was divided into two equal streams, half to each cell, and each stream could be diverted to its respective heat exchanger in any amount, at least two streams had to be monitored during tests. Total flow to the tower was measured by an Annubar flow meter whereas the flow diverted through the dry heat exchanger was determined from its known flow versus pressure drop characteristics.

The Annubar is a device which is constructed in such a way that a given flow rate generates a known pressure drop across two pressure taps. For this work the signal was measured by both a manometer and a pressure transducer. If the manometer measurement was being used, then the total water flow rate was calculated from

$$\tilde{Q} = C \sqrt{\frac{\rho_w}{\rho_{w,60}}} \sqrt{\gamma} \qquad (4.3\text{-}87)$$

where C = 18962.615 gal-$lb_f^{1/2}$/in-min (a constant which is a result of the calibration, the particular pipe diameter in use, and the Annubar design), ρ_w is the metered water density, $\rho_{w,60}$ is the density of water at 60°F, and γ the Annubar element differential pressure in lb_f/in^2. γ was calculated from

$$\gamma = \frac{\rho_{w,39.2}}{1728} \left[\frac{\rho_{mf}}{\rho_{w,39.2}} - \frac{\rho_w}{\rho_{w,39.2}}\right] \bar{\gamma} g \qquad (4.3\text{-}88)$$

where $\bar{\gamma}$ is the manometer column height, ρ_{mf} the density of the manometer fluid, $\rho_{w,39.2}$ the density of water at 39.2°F (4°C). The reason that two different standard water densities are used is due to the different standards followed by the Annubar manufacturer (60°F) and the manometer fluid manufacturers (4°C) in defining specific gravity. Equations (4.3-87) and (4.3-88) could be rewritten more simply in terms of specific gravity ($\rho/\rho_{w,std}$) but could be misapplied if one did not realize that two different standard water densities were employed.

To calculate the water flow rate from the pressure transducer output it must be noted that its output was in percent of full scale, and full scale was defined as the transducer output (proportional to the Annubar differential pressure [γ]) at a flow rate of 25,468 gpm. With Equation (4.3-87) it can be written that,

$$\tilde{Q}_{fs} = C \sqrt{\frac{\rho_{w,fs}}{\rho_{w,60}}} \sqrt{\gamma_{fs}} \qquad (4.3\text{-}89)$$

or

Dwg. 7697A74

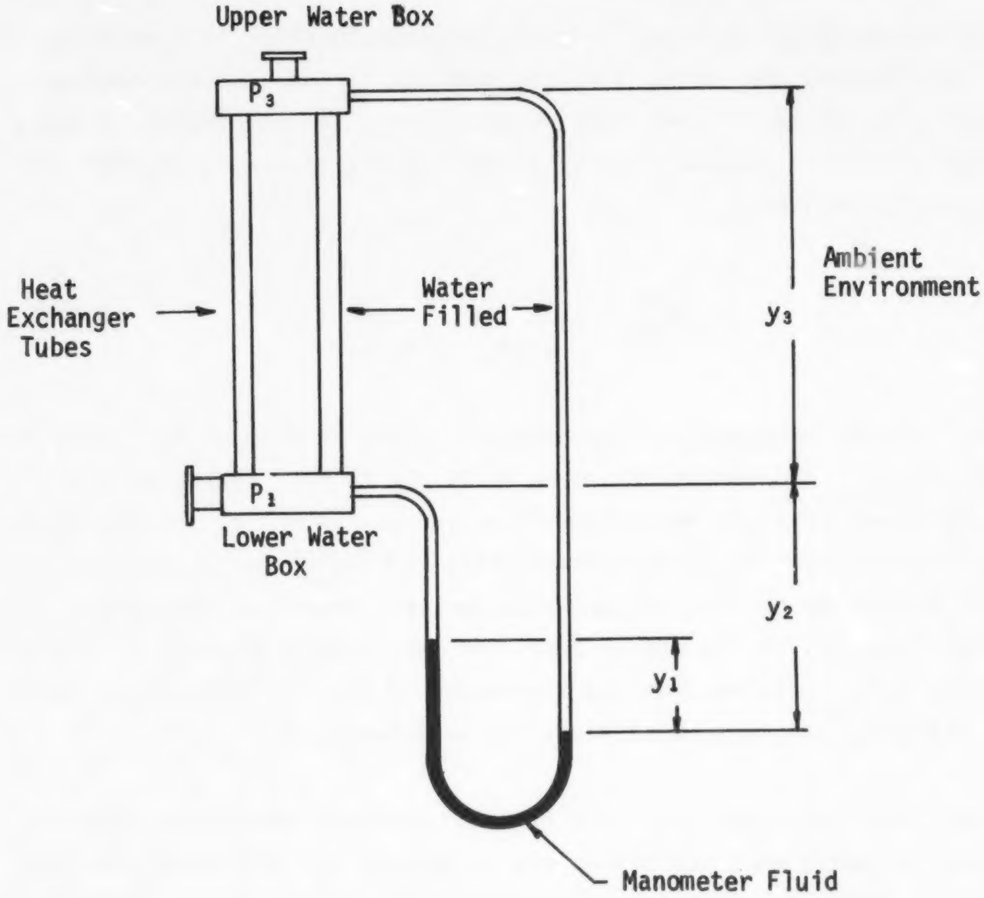
Upper Water Box
P_3
Heat Exchanger Tubes
Water Filled
Ambient Environment
y_3
P_1
Lower Water Box
y_2
y_1
Manometer Fluid

Figure 4.3-8. Schematic of Dry Heat Exchanger Hydraulic System with the Manometer Employed to Measure the Frictional Pressure Drop.

$$C = \tilde{Q}_{fs} \left[\frac{\rho_{w,fs}}{\rho_{w,60}}\right]^{-1/2} \gamma_{fs}^{-1/2} \qquad (4.3\text{-}90)$$

Substitution of C in (4.3-87) with (4.3-90) yields,

$$\tilde{Q} = \tilde{Q}_{fs} \sqrt{\frac{\rho_w}{\rho_{w,fs}}} \sqrt{\frac{\gamma}{\gamma_{fs}}} \qquad (4.3\text{-}91)$$

or since the measurement is recorded as percent of full scale, P_{fs},

$$\tilde{Q} = \tilde{Q}_{fs} \sqrt{\frac{\rho_w}{\rho_{w,fs}}} \sqrt{\frac{P_{fs}}{100}} \qquad (4.3\text{-}92)$$

The water flow rate was calculated from the manometer measurement (i.e., Equation [4.3-87]) for all tests in which it was available. The pressure transducer measurement (i.e., Equation [4.3-92]) was utilized as a backup only. As a continuing check, the difference between the two flow rate computational measurement techniques was always computed and printed for each run. Usually the difference was less than 3 percent.

By knowing the frictional pressure drop through the dry heat exchanger as a function of water flow rate, the amount of water diverted to it could be determined. In other words, the dry heat exchanger was used much in the same way as an orifice plate except the calibration was initially unknown. Consider the equation for viscous pressure losses between the upper and lower water boxes shown in Figure 4.3-8,

$$P_3 - P_1 = \Delta P_{htx}$$

$$\Delta P_{htx} = \left[\frac{\rho_w Q^2}{2\tilde{A}^2 g_c} \frac{y_3}{D} f + \frac{1}{2} Ke\rho_w \frac{Q^2}{\tilde{A}^2 g_c} + \frac{1}{2} Ko\rho_w \frac{Q^2}{\tilde{A}^2 g_c} \right] \qquad (4.3\text{-}93)$$

Curve 717155A

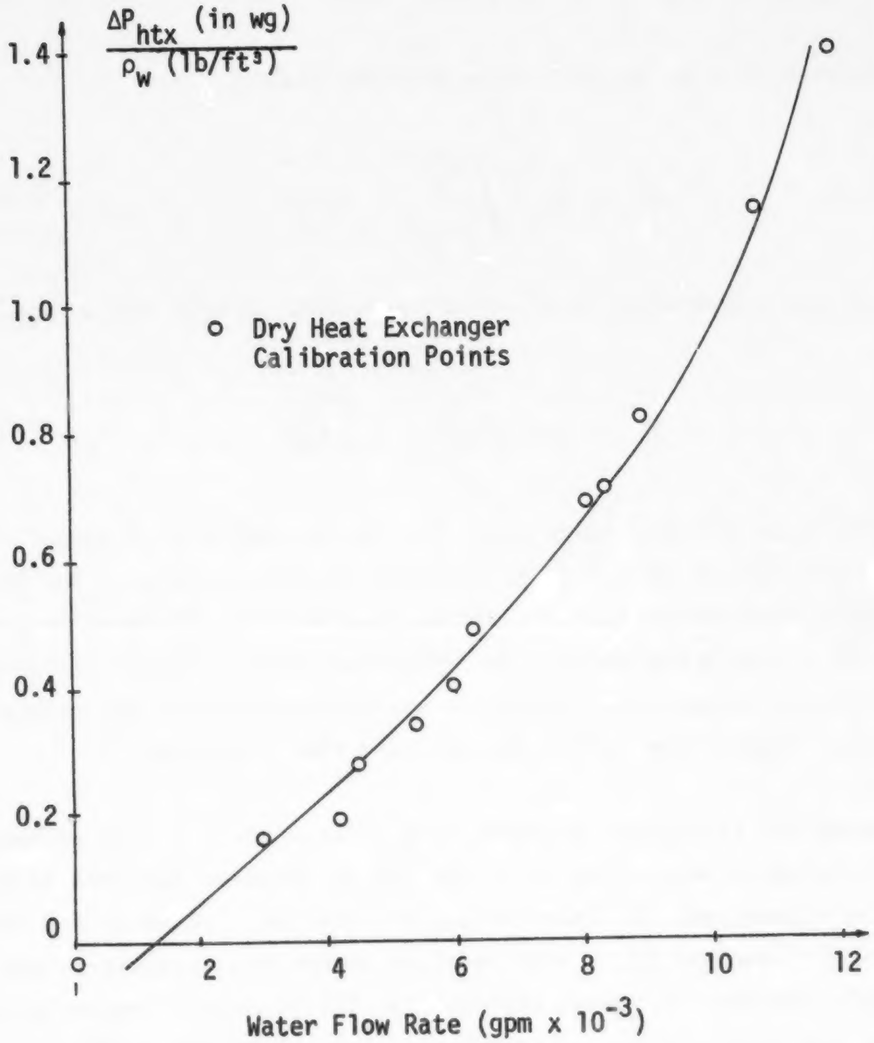

Figure 4.3-9. Dry Heat Exchanger Water Flow Rate Calibration. The Pressure Drop-Water Density Ratio is Shown as a Function of Water Flow Rate. Also Indicated is the Least Squares Curve Used to Represent the Calibration in the Data Reduction.

Ke and Ko are entrance and exit loss coefficients respectively, $\tilde{A}$ is the total tube cross-sectional area, y_3 the heat exchanger tube length, D the diameter, Q the total water flow rate through the dry heat exchanger, and f the Moody friction factor. (4.3-93) can be rewritten as

$$\frac{\Delta P_{htx}}{\rho_w} = f(Q) \qquad (4.3\text{-}94)$$

Since the friction factor and the loss coefficients are functions of the Reynolds number, and subsequently a function of temperature via the fluid properties, Equation (4.3-94) is only an approximation since $\Delta P_{htx}/\rho_w$ is shown only as a function of flow rate. However, for the relatively narrow temperature range encountered by the heat exchanger water, Equation (4.3-94) is only negligibly in error.

Calibration of the heat exchanger was accomplished by diverting all the tower flow through the dry heat exchanger. In this way the Annubar monitored the flow rate while the dry heat exchanger pressure drop was noted.

For computational purposes Equation (4.3-94) was rearranged and cast into second order polynomial form,

$$Q = C_1 + C_2 \frac{\Delta P_{htx}}{\rho_w} + C_3 \left(\frac{\Delta P_{htx}}{\rho_w}\right)^2 \qquad (4.3\text{-}95)$$

where C_1, C_2, and C_3 are constants determined from a least squares analysis. Figure 4.3-9 shows the heat exchanger calibration and the least squares curve.

The dry heat exchanger pressure drop (ΔP_{htx}) was measured with both a manometer and a pressure transducer. Figure 4.3-8 shows the heat

Curve 717156A

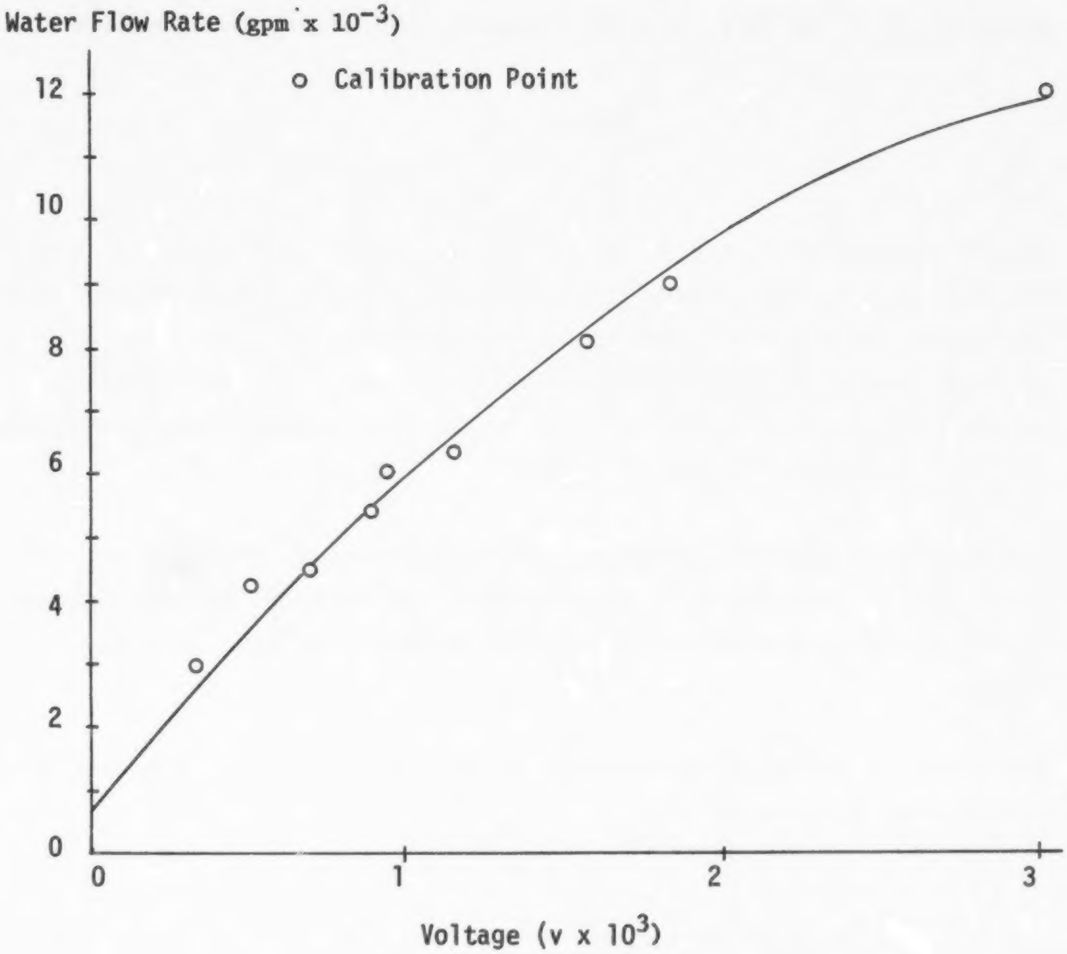

Figure 4.3-10. Heat Exchanger Pressure Transducer Voltage as a Function of Dry Heat Exchanger Water Flow Rate. Also Shown is the Second Order Least Squares Polynomial Used to Represent the Calibration in the Data Reduction Program.

exchanger and manometer system. From Figure 4.3-8 it can be shown that the heat exchanger pressure drop can be calculated from,

$$\Delta P_{htx} = [\rho_w(T_{htx}) - \rho_w(T_{amb})]\ gy_3 + [\rho_{mf}(T_{amb}) - \rho_w(T_{amb})]\ gy_1 \qquad (4.3\text{-}96)$$

where the density dependence on temperature is indicated by the parenthesis. Note that the first term in braces on the right-hand side of (4.3-96) is the hydrostatic correction for the difference in heat exchanger and manometer tubing fluid density, resulting from different temperatures. Although inclusion of this correction is rigorously correct, its effect on the flow rate was very small.

The pressure transducer was connected in parallel with the manometer. Its output was calibrated against the Annubar. Figure 4.3-10 presents the calibration and the least squares quadratic polynomial employed in the computations. The manometer measurement was used in the data reduction for all runs in which it was available.

4.3.2 Data Reduction Computer Code

This section is intended to be a brief overview of the data reduction program. The interested reader is referred to the program listing (Appendix C) which contains sufficient comment cards to be self-explanatory. A sample input and output can also be found in Appendix C. Most of the calculations are performed within subroutines; as a result the main program is composed almost entirely of call statements and the routing logic. A brief description of the nine main program fundamental units or functions follows.

4.3.2.1 Data Reduction Main Program Functions

A. Set Geometry and Program Parameters - Here the geometry of the fan, fill, heat exchanger, instrumentation, etc. are set. Various options such as preference for manometer or transducer sensed pressure drop for flow calculation, solution convergence maximum errors, etc. may be selected.

B. Read Input - A subroutine which decodes the Fluke and manually-typed data is called (refer to Appendix C for additional information). All of the input is passed to the main program via common blocks. The six-digit run identifier is also decoded.

C. Water Flow Rate Determination - Water flow rate to the wet fill and/or dry heat exchanger is calculated. This calculation depends on the first digit of the six-digit run identifier. If it indicates a wet/dry test, then the logic knows there must be an accounting of two water streams. If it is all wet or all dry, then the program must account for only one water stream.

D. Air and Water State Determination - All of the necessary state properties of the air and water streams are calculated at every point of interest, i.e., tower inlet, fill inlet and outlet, stack outlet, distribution basin, heat exchanger inlet and outlet, fill outlet, etc.

E. Airflow Rate Computation - As described in previous sections, the airflow rate could be calculated by several methods. This section of the program computes the airflow rate by the three methods and then utilizes the one selected by the program option for the heat and mass transfer calculations.

F. Wet Fill Calculations - The tower mass transfer coefficient and number of transfer units are calculated. Note that this portion of the program is not entered if the run identifier indicates a dry test.

G. Dry Heat Exchanger Calculations - This portion of the program is activated if the run identifier indicates a wet/dry or a dry test. All pertinent properties of the dry heat exchanger such as air-side heat transfer coefficient, Reynolds number, etc. are calculated.

H. Fan Calculations - Fan-motor-gear train efficiency as well as the dimensionless pressure and flow coefficient are computed.

I. Output - This final program function relies entirely on the type of test being reduced. It was designed to glean the maximum amount of information from a given test for additional study at a later date. A good example is a

> wet/dry test. Clearly wet/dry type output is warranted but, in addition, the fan calculations are also outputted despite it not being a fan test. As another example, consider a plume test. Not only was plume data printed (and punched for later retrieval) but wet, dry (if available on this particular test), and fan data were also retrieved.

4.4 ANALYSIS OF THERMAL AND FLOW DATA

The main purpose of the entire cooling tower test program was to obtain performance data which would allow interpretations of how critical tower performance parameters are affected by operating conditions. The test program had been set up so that the ranges of these operating conditions spanned those that one typically finds in an operating tower. By operating the tower over a one-year time period it was hoped that weather-dependent conditions would also undergo typical annual swings.

To insure statistical significance of the data, a large number of tests were scheduled in blocks throughout the year. Table 4.4-1 lists these test blocks and the ranges of significant operating variables for each block. As was noted previously, only 1399 or 51 percent of these runs ultimately reached a final reduced state.

4.4.1 Correlation Forms

There are four tower characteristics which can be obtained from the reduced thermal and flow data: mass transfer coefficient per unit volume Ka, water loss $\Delta L/L$, dry heat exchanger air-side heat transfer coefficient H and fan drive efficiency η_f, each of which is a function of various tower independent parameters such as water loading L and air loading G.

For the fill-averaged mass transfer coefficient, a correlation of the form:

TABLE 4.4-1

THERMAL AND FLOW TEST GRID

Block	Test Type*	Season **	No. of Runs	Range of L (#/hr-ft^2)	Range of G (#/hr-ft^2)	Fan Angle (deg)	%Wet	%Dry	Dry GPM Each Side
1	1	1	60	3750-7500	2575-5150	0	100	0	0
2	1	1	60	3750-7500	2575-5150	0	100	0	0
3	1	1	60	3750-7500	2575-5150	0	100	0	0
4	1	1	60	3750-7500	2575-5150	0	100	0	0
5	1	7	60	3750-7500	2575-5150	0	100	0	0
6	1	2	60	3750-7500	2575-5150	0	100	0	0
7	1	2	60	3750-7500	2575-5150	0	100	0	0
8	1	2	60	3750-7500	2575-5150	0	100	0	0
9	1	3	60	3750-7500	2575-5150	0	100	0	0
10	1	3	60	3750-7500	2575-5150	0	100	0	0
11	1	3	60	3750-7500	2575-5150	0	100	0	0
12	1	3	60	3750-7500	2575-5150	0	100	0	0
13	7	3	60	4500-9000	2575-5150	0	100	0	0
14	7	3	60	4500-9000	2575-5150	0	100	0	0
15	7	3	60	4500-9000	2575-5150	0	100	0	0
16	7	3	60	5600-11200	2575-5150	0	100	0	0
17	7	3	60	5600-11200	2575-5150	0	100	0	0
18	7	3	60	5600-11200	2575-5150	0	100	0	0

*Types of Tests:
1 = all wet, 18 feet air travel
2 = wet/dry
3 = dry
4 = fan
5 = plume
6 = acoustics
7 = all wet, 14 and 10 feet air travel

**Season
1 = winter
2 = spring
3 = summer
4 = fall

(Continued)

Table 4.4-1 (cont'd)

Block	Test Type*	Season **	No. of Runs	Range of L (#/hr-ft^2)	Range of G (#/hr-ft^2)	Fan Angle (deg)	%Wet	%Dry	Dry GPM Each Side
19	2	1	135	250-3750	2575-5150	0	10-50	50-90	3000-5400
20	2	1	135	250-3750	2575-5150	0	10-50	50-90	3000-5400
21	2	1	135	250-3750	2575-5150	0	10-50	50-90	3000-5400
22	2	1	135	250-3750	2575-5150	0	10-50	50-90	3000-5400
23	3	2	90	0	2570-5150	0	0	100	6000-12000
24	3	2	90	0	2570-5150	0	0	100	6000-12000
25	3	2	90	0	2570-5150	0	0	100	6000-12000
26	3	3	90	0	2570-5150	0	0	100	6000-12000
27	3	3	90	0	2570-5150	0	0	100	6000-12000
28	3	3	90	0	2570-5150	0	0	100	6000-12000
29	4	2	120	3750-7500	2570-5150	0	100	0	0
30	4	2	120	3750-7500	2570-5150	+2	100	0	0
31	4	2	120	3750-7500	2570-5150	-2	100	0	0
32	4	2	120	3750-7500	2570-5150	+4	100	0	0
33	4	2	120	3750-7500	2570-5150	-4	100	0	0

$$Ka = C_o L^a G^b T^c \qquad (4.4.1\text{-}1)$$

was used as equations of this form are the most commonly found in the cooling tower mass transfer literature and physical arguments can be made for the exponential dependence on L and G. Addition of the temperature dependency T^c was examined in light of some past experience in the literature which shows that mass transfer coefficient is a weak function of water film temperature, perhaps due to the temperature dependency of water transport properties. Correlations with and without temperature effects were obtained.

Water loss, which can be expressed as a fraction of water inlet flow rate ($\Delta\dot{m}/\dot{m}$) and thus as $\Delta L/L$, must be a function of the tower fill mass transfer coefficient. Locally, within the fill, the rate of water loss $\dot{m}$ from the liquid phase into the vapor phase within a volume (dx)(dy)(dz) can be expressed as

$$d\dot{m} = Ka\ (\omega_w - \omega_a)\ dx\ dy\ dz \qquad (4.4.1\text{-}2)$$

and over the entire fill:

$$\dot{m} = \int\int\int Ka\ (\omega_w - \omega_a)\ dx\ dy\ dz \qquad (4.4.1\text{-}3)$$

where Ka here is a distributed value, Ka <x,y,z>. We are unable to determine the distributed Ka and would have great difficulty in using it if it could be determined. We thus, as shown in Section 4.3, determined an average value over the entire fill volume. Using this value of volume-averaged Ka we may write Equation (4.4.1-3) as

$$\dot{m} = Ka \int\int\int (\omega_w - \omega_a)\ dx\ dy\ dz \qquad (4.4.1\text{-}4)$$

Dividing this equation by fill width and depth Z and X we have:

$$\frac{\dot{m}}{XZ} = L = Ka \int\int\int (\omega_w - \omega_a) \frac{dx}{X} dy \frac{dz}{Z} \qquad (4.4.1\text{-}5)$$

Further, multiplying the right-hand side by Y and dividing both sides by L we have

$$\frac{\Delta L}{L} = \frac{Ka\ Y}{L} \int\int\int (\omega_w - \omega_a) \frac{dx}{X} \frac{dy}{Y} \frac{dz}{Z} \qquad (4.4.1\text{-}6)$$

Equation (4.4.1-6) indicates that the fractional water loss should be a function of the number of transfer units NTU, or Ka itself, and a fill-volume-averaged humidity difference between the water surface and the air free stream. In this experimental apparatus we were not instrumented to measure ω within the fill so the integration indicated in Equation (4.4.1-5) was not possible. We only knew values at the fill extrema (top, bottom, front and rear). Since we know Ka can be correlated by $C_o L^a G^b$, we have attempted to correlate $\Delta L/L$ with the form

$$\Delta L/L = C_1 L^d G^e \Delta\omega^f \qquad (4.4.1\text{-}7)$$

where $\Delta\omega$ is humidity difference based upon some combination of known extrema states, one combination being the log-mean value across the fill:

$$\Delta\omega_{\ell m} = \frac{\Delta\omega_1 - \Delta\omega_2}{\ell n \frac{\Delta\omega_1}{\Delta\omega_2}} \qquad (4.4.1\text{-}8)$$

This is the same approach which is used in expressing temperature difference in counterflow and crossflow heat exchangers. Further, from prior arguments we would like to see $d = a-1$, $e = b$, $f = 1$ and $C_1 = C_o Y$.

As for the dry heat exchanger air-side heat transer coefficient H, the most common method of reporting these heat transfer coefficient data is in terms of the dimensionless parameters, Nusselt number ($H\ell/k$), Prandtl number ($\mu c/k$) and Reynolds number ($V\ell\rho/\mu$). Specifically, heat transfer texts, e.g., References 1 and 2, report heat transfer coefficient data in the form of the Colburn "j-factor", (Nu/Re Pr) $Pr^{2/3}$, as a function of Reynolds number. Reference 1, especially, presents the heat transfer coefficient for externally-finned (circular fins) tubing in this manner for many geometries. The data reported by Reference 1 are linear curves on log-log plots, so one would expect correlations of the form

$$j = \left(\frac{Nu}{Re\ Pr}\right) Pr^{2/3} = C_2 R_e^n \qquad (4.4.1\text{-}9)$$

to fit our data. In order to compare our data with that of Reference 1, their convention in expressing characteristic length ℓ (for Nusselt and Reynolds numbers) was adopted here. Reference 1 defines ℓ as the volume of air space in the heat exchanger divided by the air-side heat transfer surface area in that volume. Their reason for adopting this convention is that data for heat exchangers of disparate types may be handled with a common characteristic length.

Fan efficiency data presented some severe problems in attempts to correlate data (see Section 4.5.4). Parameters such as fan blade pitch angle, speed and water loading should have some effect on the fan's operating point, and thus fan efficiency. However, the simplest of correlations, linear variation in fan drive efficiency with volumetric flow rate, was found to fit the data best. The fan efficiency is reported here in the form:

$$\eta_f = C_3 + C_4\ Q \qquad (4.4.1\text{-}10)$$

4.4.2 Statistical Analysis of Data

In many instances there were several methods available for correlation of a given set of test data, and some means was necessary to determine which method produced the best fit or least error. The standard error of estimate, similar to standard deviation, was used to evaluate the validity of competing correlations. The correlation coefficient was used to examine the degree to which candidate independent variables correlate with the dependent variable.

To show how these parameters were used in evaluating each correlation, let us use the expression for mass transfer coefficient:

$$Ka = C_o L^a G^b T^c \qquad (4.4.2\text{-}1)$$

For each set of tower test data there are N subsets of corresponding variables Ka_i, L_i, G_i and T_i and a corresponding Ka_i^* from Equation (4.4.2-1). Since Ka_i is not, and should not be, a constant (since it varies with L, G and T, all of which varied from run to run) it is not feasible to perform an analysis on the variation $|Ka_i - Ka_i^*|$ or $|Ka_i - \overline{Ka}_i|$. Rather, for each data point Ka_i, a ratio $\phi_i = Ka_i/Ka_i^*$ was formed after the correlation, Equation (4.4.2-1), was obtained. If the data correlated perfectly, then $\phi_i = 1.0$, $i = 1,2,3...N$. With the set of ϕ_i, a population mean, $\overline{\phi} = \sum_{i=1}^{N} \phi_i/N$, was formed and the standard error of estimate σ was formed from:

$$\sigma = \sqrt{\frac{\Sigma (\phi_i - \overline{\phi})^2}{N}} \qquad (4.4.2\text{-}2)$$

In addition, correlation coefficients and/or the coefficient of multiple determination were obtained. The correlation coefficient r is a measure of explained variation in relation to total variation through:

$$r = \pm \sqrt{\frac{\text{explained variation}}{\text{total variation}}} \qquad (4.4.2\text{-}3)$$

and indicates how well one parameter correlates with another. For perfect correlation r = ± 1, while for no correlation at all r = 0. When a dependent parameter, such as Ka in Equation (4.4.1-1), is a function of more than one independent parameter, then it is necessary to utilize the coefficient of multiple determination to check on the validity of correlation. Using the subscript system Ka = 1, L = 2, G = 3 and T = 4 for Equation (4.4.2-1), then the coefficient of multiple determination[10] $R_{1.234}$ is defined as

$$R_{1.234} = \sqrt{1 - (1-r_{14}^2)\,(1-r_{13.4}^2)\,(1-r_{12.34}^2)} \qquad (4.4.2\text{-}4)$$

where, for example r_{IJ} is defined as:

$$r_{IJ} = \frac{N\Sigma IJ - (\Sigma I)\,(\Sigma J)}{\sqrt{[N\Sigma I^2 - (\Sigma I)^2]\,[N\Sigma J^2 - (\Sigma J)^2]}} \qquad (4.4.\ \text{-}5)$$

and so, for example:

$$r_{14} = \frac{N\Sigma Ka_i T_i - (\Sigma Ka_i)\,(\Sigma T_i)}{\sqrt{[N\Sigma Ka_i^2 - (\Sigma Ka_i)^2]\,[N\Sigma T_i^2 - (\Sigma T_i)^2]}} \qquad (4.4.2\text{-}6)$$

The remaining factors in Equation (4.4.2-4) are defined as:

$$r_{13.4} = \frac{r_{13} - r_{14}\,r_{34}}{\sqrt{(1-r_{14}^2)\,(1-r_{34}^2)}} \qquad (4.4.2\text{-}7)$$

and

$$r_{12.34} = \frac{r_{12.4} - r_{13.4}\, r_{23.4}}{\sqrt{(1-r^2_{13.4})\,(1-r^2_{23.4})}} \qquad (4\text{-}4\text{-}2\text{-}8)$$

The coefficient of multiple determination lies between 0 and 1, and the closer it is to 1.0, the better is the correlation.

4.4.3 Linear Regression

Although the correlation equations for mass transfer coefficient, water loss and heat exchanger air-side heat transfer coefficient are of exponential form, linear regression may be used to determine the unknown correlation parameters simply by taking logarithms of the correlations prior to regression. For example, taking the logarithm of Equation (4.4.1-1) yields:

$$\ell n\, Ka = \ell n\, C_o + a\, \ell n\, L + b\, \ell n\, G + c\, \ell n\, T \qquad (4.4.3\text{-}1)$$

Let Ka_i be the mass transfer coefficient as determined from data reduction for the ith test, in which test parameters L_i, G_i and T_i prevailed, and let Ka_i^* be the value of Ka from Equation (4.4.3-1) when L_i, G_i and T_i are applied. Then the coefficients C_o, a, b and c are determined for least mean square error between Ka_i and Ka_i^* for all N data sets when:

$$\sum_{i=1}^{N} (\ell n\, Ka_i^* - \ell n\, Ka_i)^2 = \text{minimum} \qquad (4.4.3\text{-}2)$$

This will occur when:

$$\frac{\partial}{\partial \ell n\, C_o} \sum_{i=1}^{N} (\ell n\, Ka_i^* - \ell n\, Ka_i)^2 = 0 \qquad (4.4.3\text{-}3)$$

$$\frac{\partial}{\partial a} \sum_{i=1}^{N} (\ell n\ Ka_i^* - \ell n\ Ka_i)^2 = 0 \qquad (4.4.3\text{-}4)$$

$$\frac{\partial}{\partial b} \sum_{i=1}^{N} (\ell n\ Ka_i^* - \ell n\ Ka_i)^2 = 0 \qquad (4.4.3\text{-}5)$$

$$\frac{\partial}{\partial c} \sum_{i=1}^{N} (\ell n\ Ka_i^* - \ell n\ Ka_i)^2 = 0 \qquad (4.4.3\text{-}6)$$

From Equation (4.4.3-1), the factor $(\ell n\ Ka_i^* - \ell n\ Ka_i)^2$ is:

$$(\ell nKa_i^* - \ell nKa_i)^2 = (\ell nC_o + a\ell nL_i + b\ell nG_i + c\ell nT_i - \ell nKa_i)^2 \qquad (4.4.3\text{-}7)$$

or

$$(\ell n\ Ka_i^* - \ell n\ Ka_i)^2 = (D + aW_i + bX_i + cZ_i - Y_i)^2 \qquad (4.4.3\text{-}8)$$

Performing the square of the right-hand side of (4.4.3-8) yields

$$(\ell n\ Ka_i^* - \ell n\ Ka_i)^2 = D^2 + a^2W_i^2 + b^2X_i^2 + c^2Z_i^2 + Y_i^2 +$$

$$2DaW_i + 2DbX_i + 2DcZ_i + 2abW_iX_i + 2acW_iZ_i + 2bcX_iZ_i$$

$$- 2DY_i - 2aW_iY_i - 2bX_iY_i - 2cZ_iY_i \qquad (4.4.3\text{-}9)$$

Performing the differentiations indicated by Equations (4.4.3-3 through 6) on (4.4.3-9) gives four expressions:

$$\frac{\partial}{\partial D} \sum_{i=1}^{N} (\ell nKa_i^* - \ell nKa_i)^2 = \sum_{i=1}^{N} (D + aW_i + bX_i + cZ_i - Y_i) = 0$$

$$\frac{\partial}{\partial a}\sum_{i=1}^{N}(\ell nKa_i^* - \ell nKa_i)^2 = \sum_{i=1}^{N}(DW_i + aW_i^2 + bW_iX_i + cW_iZ_i - W_iY_i) = 0$$

$$\frac{\partial}{\partial b}\sum_{i=1}^{N}(\ell nKa_i^* - \ell nKa_i)^2 = \sum_{i=1}^{N}(DX_i + aW_iX_i + bX_i^2 + cX_iZ_i - X_iY_i) = 0$$

$$\frac{\partial}{\partial c}\sum_{i=1}^{N}(\ell nKa_i^* - \ell nKa_i)^2 = \sum_{i=1}^{N}(DZ_i + aW_iZ_i + bX_iZ_i + cZ_i^2 - Z_iY_i) = 0$$

This leads to four simultaneous equations in D, a, b and c, the coefficients being summations of tower test data:

$$ND + a\sum_{i=1}^{N} W_i + b\sum_{i=1}^{N} X_i + c\sum_{i=1}^{N} Z_i = \sum_{i=1}^{N} Y_i \qquad (4.4.3\text{-}10)$$

$$D\sum_{i=1}^{N} W_i + a\sum_{i=1}^{N} W_i^2 + b\sum_{i=1}^{N} W_iX_i + c\sum_{i=1}^{N} W_iZ_i = \sum_{i=1}^{N} W_iY_i \qquad (4.4.3\text{-}11)$$

$$D\sum_{i=1}^{N} + a\sum_{i=1}^{N} W_iX_i + b\sum_{i=1}^{N} X_i^2 + c\sum_{i=1}^{N} X_iZ_i = \sum_{i=1}^{N} X_iY_i \qquad (4.4.3\text{-}12)$$

$$D\sum_{i=1}^{N} + a\sum_{i=1}^{N} W_iZ_i + b\sum_{i=1}^{N} X_iZ_i + c\sum_{i=1}^{N} Z_i^2 = \sum_{i=1}^{N} Z_iY_i \qquad (4.4.3\text{-}13)$$

For correlations in which no temperature effect is desired, the set of all T_i may be equated to 1.0. Then $\ell n\ T_i = 0$ and Equations (4.4.3-10 through 13) yield $c = 0$. Likewise, when the correlation for dry heat exchanger air-side heat transfer coefficient is sought, Equations (4.4.3-10 through 13) can be used by letting $W_i = \ell n\ Re_i$, $Y_i = \ell n\ j_i$, and $X_i = Z_i = \ell n 1 = 0$. For fan efficiency correlations, a linear form was assumed and no logarithms were necessary. Here Equations (4.4.3-10 and 11) are used where $Y_i = \eta_{f_i}$, $D = C_3$, $a = C_4$, $W_i = Q_i$, and $Y_i = Z_i = 0$.

In order to use the prior four equations to obtain correlations for mass transfer coefficient, water loss, heat transfer coefficient and fan efficiency, a set of four computer codes were written. These correlation programs are listed in Appendix D, which includes necessary explanations of inputs, outputs and some internal logic explanations.

4.5 RESULTS OF CORRELATIONS

The correlations of four cooling tower parameters with their corresponding independent parameters are reported in this section. The great bulk of output data from the correlation programs precludes total inclusion here. Samples of the four correlation detailed outputs are shown in Appendix D. Results are summarized in condensed tables in this section.

4.5.1 Mass Transfer Coefficient Ka

A total of 539 good data sets were obtained in WET fill tests. In addition, a total of 194 WET/DRY tests were run, each containing Ka data, so that a total of 733 data sets for Ka were available. Note, however, that in WET/DRY tests some water was diverted to the dry heat exchangers and so the consequent water loadings L in the wet fill were much less than in pure WET tests. This allows us to analyze the Ka data (a) for all tests, (b) for WET tests only and (c) for low water loadings in WET/DRY tests. This last condition is of some value since data for these conditions (i.e., very low L) are not found in the literature and they are necessary for the design of towers operating wet/dry. In addition to the WET and WET/DRY tests, some WET tests were performed with a fraction of the fill theoretically inactive. This was accomplished by blocking flow nozzles in the top deck of the tower such that the active fill depth was either 14 feet or 10 feet, rather than the full 18 feet. In these cases the water was truly loaded onto the first 14 or 10 feet of fill at the top of the tower, but it was not assured that the water did not spread toward the rear four or eight feet of fill at lower depths of fill. With this uncertainty, these tests were kept separate from "full fill depth" tests and were correlated separately as SHORT tests. There were 147 tests at 14 feet of air travel and 104 tests at 10 feet air travel.

Reference 11 reports data taken in 1974 in a small cooling tower test facility using the same fill elements as in the Cliffside tower and using water loadings L and air loadings G similar to those in the tests reported here. In the prior work a correlation of the form (424 data points):

$$Ka = 1188\, L^{0.599}\, G^{0.438}\, T^{2.04} \qquad (4.5.1\text{-}1)$$

was obtained, where T was water inlet temperature. When temperature was ignored a correlation of the form:

$$Ka = 0.0609\, L^{0.649}\, G^{0.436} \qquad (4.5.1\text{-}2)$$

was obtained. The results were not subjected to statistical analysis.

Strong physical and mathematical arguments were made for the exponent on L to be somewhat less than unity and the exponent on G to be somewhat less than 0.6 (expected from heat transfer data) and about 0.45. The consistency of the exponents in the two correlations and the fact that they fell near predicted values was gratifying. We had hoped that there would be similar results occurring in the analysis of the Cliffside tower tests. Such was not entirely the case.

The results of all attempts to correlate WET, WET/DRY and SHORT test data are presented in Table 4.5.1-1, a total of 39 program runs. Variations were run to determine the effects of:

TABLE 4.5.1-1

MASS TRANSFER COEFFICIENT CORRELATION DATA

	Input	Statistics							Correlation Parameters			
No.	Data File and Correlation Conditions	σ	$\bar{X}$	N	r_{12}	r_{13}	r_{14}	R^2	C_o	a	b	c
1	All WET data; no effect of temperature	.183	1.017	539	.592	.916	-	.926	.00153	.626	.852	0
2	Winter WET data (11xxxx tests); no temperature	.157	1.012	172	.562	.863	-	.906	.00545	.596	.733	0
3	Spring WET data (12xxxx tests); no temperature	.085	1.004	167	.408	.914	-	.973	.00077	.727	.823	0
4	Summer WET data (13xxxx tests) no temperature	.152	1.013	200	.585	.926	-	.923	.00650	.487	.801	0
5	All WET data; inlet water temperature	.152	1.012	539	.592	.916	-.370	.946	1.254	.571	.831	-1.341
6	All WET data; outlet water temperature	.145	1.011	539	.592	.916	-.676	.950	1.639	.700	.689	-1.473
7	All WET data; average water temperature	.148	1.012	539	.592	.916	-.568	.948	1.679	.628	.766	-1.435
8	All WET data; inlet air temperature	.140	1.011	539	.592	.916	-.357	.952	.0260	.598	.824	-.582
9	All WET data; outlet air temperature	.164	1.014	539	.592	.916	-.488	.938	.1815	.679	.776	-1.053
10	All WET data; mean air temperature	.145	1.011	539	.592	.916	-.441	.949	.1234	.637	.793	-.946
11	All WET data; mean fluid temperature	.145	1.011	539	.592	.916	-.510	.949	.5035	.633	.778	-1.216
12	All WET/DRY data; no effect of temperature	.205	1.017	194	.664	.845	-	.916	.0328	.433	.649	0
13	All WET/DRY data; inlet water temperature	.191	1.016	194	.664	.845	.038	.919	.4266	.438	.650	-.586
14	All WET/DRY data; outlet water temperature	.149	1.011	194	.664	.845	-.354	.942	1085.	.711	.291	-2.369
15	All WET/DRY data; average water temperature	.172	1.014	194	.664	.845	-.263	.927	31.60	.520	.549	-1.570
16	All WET/DRY data; inlet air temperature	.205	1.017	194	.664	.845	-.571	.916	.0286	.433	.651	+.0278
17	All WET/DRY data; outlet air temperature	.200	1.017	194	.664	.845	-.266	.917	.1267	.462	.615	-.3094
18	All WET/DRY data; average air temperature	.204	1.017	194	.664	.845	-.452	.916	.0480	.437	.641	-.0826
19	All WET/DRY data; mean fluid temperature	.189	1.016	194	.664	.845	-.379	.920	1.8919	.479	.578	-.9010
20	WET + WET/DRY data; no effect of temperature	.227	1.021	733	.508	.786	-	.913	.00645	.497	.808	0
21	WET + WET/DRY data; no temperature; $L \leq 10{,}000$	.229	1.021	592	.474	.779	-	.909	.00577	.511	.807	0

(Continued)

Table 4.5.1-1 (cont'd)

	Input	Statistics							Correlation Parameters			
No.	Data File and Correlation Conditions	σ	$\bar{X}$	N	r_{12}	r_{13}	r_{14}	R^2	C_o	a	b	c
22	WET + WET/DRY data; no temperature; L ≤ 8,000	.193	1.016	540	.359	.802	-	.909	.01457	.439	.754	0
23	WET + WET/DRY data; no temperature; L ≤ 6,000	.193	1.016	408	.287	.831	-	.910	.01898	.406	.751	0
24	SHORT data (14 and 10 feet travel); no temperature	.124	1.008	251	.269	.914	-	.938	.00222	.582	.881	0
25	SHORT data; 14 feet travel; no temperature	.082	1.004	147	.322	.927	-	.953	.00622	.508	.815	0
26	SHORT data; 10 feet travel; no temperature	.045	1.001	104	-.038	.994	-	.994	.06514	.190	.925	0
27	SHORT data; 14 feet travel; exit water temperature	.081	1.003	147	.322	.927	-.437	.954	.03823	.551	.787	-.4470
28	SHORT data; 10 feet travel; exit water temperature	.045	1.001	104	-.038	.994	-.780	.994	.08893	.194	.920	-.0699
29	WET data; no temperature; L ≤ 10,000	.159	1.013	498	.586	.909	-	.939	.00029	.830	.838	0
30	WET data; no temperature; L ≤ 8,000	.139	1.011	346	.420	.922	-	.931	.00091	.726	.799	0
31	WET data; no temperature; L ≤ 6,000	.118	1.008	214	.227	.940	-	.944	.00014	.914	.839	0
32	WET data; exit water temperature; L ≤ 10,000	.123	1.008	498	.586	.909	-.704	.961	.26145	.875	.683	-1.392
33	WET data; exit water temperature; L ≤ 8,000	.115	1.008	346	.420	.922	-.613	.950	.12724	.855	.680	-1.188
34	WET data; exit water temperature; L ≤ 6,000	.096	1.006	214	.227	.940	-.831	.959	.07605	.852	.703	-1.099
35	WET + WET/DRY; exit water temperature (See #20)	.185	1.016	733	.508	.786	-.235	.933	2.2159	.671	.618	-1.377
36	WET data; no temperature; G ≥ 400	.192	1.019	454	.562	.867	-	.883	.00182	.625	.828	0
37	WET data; no temperature; G ≥ 600	.193	1.019	396	.599	.831	-	.860	.00172	.632	.827	0
38	WET data; no temperature; G ≥ 800	.192	1.018	292	.686	.740	-	.820	.00228	.670	.745	0
39	WET data; no temperature; G ≥ 1,000	.196	1.018	261	.727	.750	-	.814	.00218	.645	.781	0

1. Including or excluding fluid temperature
2. Considering WET and WET/DRY data together and separately
3. Eliminating data with high water loading L
4. Eliminating data with low air loading G
5. Considering seasonal data separately

and combinations of these variations.

Consider runs 1 and 5 through 11 in Table 4.5.1-1 in which the effect of fluid temperature is first ignored and then considered in terms of specific or average water or air temperatures. First it should be noted that in all cases the correlation coefficient between Ka and L (r_{12}) is moderate (0.592) and between Ka and G (r_{13}) is high (0.916). Further, the coefficient of multiple determination R^2 is quite high. Note that R^2 is improved when any fluid temperature is considered and that the standard error of estimate σ is universally reduced when one includes the effect of water temperature. When the correlation is based on fill outlet average water temperaure, run 6, the correlation coefficient between Ka and T is -0.676. Also σ is reduced from 0.183 to 0.145 and R^2 is increased from 0.926 to 0.950. One must conclude that inclusion of the effect of fluid temperature is warranted and fill outlet average water temperature is superior to other fluid temperatures.

Analysis of runs 1 and 5 through 11 with runs 12 through 19 compares corresponding correlations using first WET and then WET/DRY data. Table 4.5.1-1 shows all WET/DRY correlations to be inferior to corresponding correlations using WET data. The standard error of estimate is universally slightly higher in the case of WET/DRY data, r_{12} is slightly higher (0.664 versus 0.592) and r_{13} is slightly lower (0.845 versus 0.916). As for the effect of temperature in the correlation, r_{14} is much lower in all cases and, as a consequence, R^2 suffers slightly. It must be concluded that there is no advantage in using WET/DRY data to the exclusion of WET data.

Comparing run 20 with run 1, we see that when WET and WET/DRY data are correlated together there is degradation in all the statistical parameters.

As a consequence of the above, only the WET data are considered in further attempts to correlate the Ka data.

Comparing run 1 with runs 29 through 31 we see the effect of eliminating from the correlation the data for very high water loadings, values somewhat above those commonly used in crossflow cooling towers. We see that limiting data to $L \leq 10000$ lbm/hr-ft^2 improves σ, only slightly reduces r_{12} , slightly reduces r_{13} and slightly improves R^2. Further, restricting L to values ≤ 8000 and then ≤ 6000 continues to improve σ but has a deleterious effect on r_{12}. All these comparisons are made when no effect of temperature is included. When the effect of exit water temperature is included in the correlation (compare run 1 with runs 32 through 34) we see that σ is improved, r_{12} and r_{13} are as when no temperature is considered and R^2 is improved further. It would appear that restricting data sets to those with $L \leq 10,000$ and including the effect of exit water temperature leads to a fairly good correlation (run 32).

When one systematically removes data sets with low air loading G (runs 1 and 36 through 39) we see that σ is unaffected, r_{12} increases, r_{13} decreases and R^2 is reduced. There is no advantage in restricting the correlation to data sets with higher G only.

There was some concern that the season in which wet fill tests were performed would have an effect on the correlation. The argument ran that winter tests would be superior to spring tests and particularly summer tests since air-water temperature differences would be the greatest in winter. In this case a given error in measuring air or water temperature would produce the least error in temperature difference and, consequently, the least error in deducing Ka. Thus it was reasoned that the scatter in Ka data due to temperature measurement error would be the least in winter tests. Run 1 compared with runs 2 through 4 shows the effect of correlating all WET data with seasonally segregated WET data. The results show a decided improvement in σ (less scatter) but the correlation coefficient r_{12} is reduced somewhat. One might be tempted to elect to use the correlation obtained with spring WET data (lowest σ, greatest R^2) except for the low r_{12} and the fact that only 167 data points were considered.

As for the SHORT data, the correlations (runs 24 through 28) show a very poor correlation coefficient r_{12}. Also, the small number of available data sets (147 for 14 feet air travel and 104 for 10 feet air travel) make any conclusions on these data tenuous at best.

It is recommended that for the wet fill type tested in the Cliffside cooling tower the correlation (run 32):

$$Ka = .2615\, L^{.875}\, G^{.683}\, T^{-1.392} \qquad (4.5.1\text{-}3)$$

be used in design and performance calculations. Note that the temperature in the correlation is average exit water temperature, a quantity not known at the start of calculations. Thus any analysis using the correlation must be iterative. For less precise work, the correlation (run 29):

$$Ka = .00029\, L^{0.830}\, G^{0.838} \qquad (4.5.1\text{-}4)$$

which contains no temperature effect, may be used. As an alternative spring test data (run 3) may be used:

$$Ka = .00077\, L^{.727}\, G^{.823} \qquad (4.5.1\text{-}5)$$

with the warning that it was obtained with limited data and shows a fairly weak correlation coefficient between Ka and L.

4.5.2 Rate of Water Loss Due to Evaporation ($\Delta L/L$)

Again, there were 539 WET test runs and 194 WET/DRY test runs available for analysis, or a total of 733 data sets. Table 4.5.2-1 lists a total of 39 attempts at correlating $\Delta L/L$ with water loading L, air loading G, and water-to-air humidity difference. The column headings in this table are like those in Table 4.5.1-1. We are attempting to correlate water loss with water loading L, air loading G and a humidity difference $\Delta\omega$ (between the air and water in the fill) with an equation of the form:

$$\Delta L/L = C_1 L^d G^e \Delta\omega^f \qquad (4.5.2\text{-}1)$$

As was the case in Ka correlation attempts, the results in Table 4.5.2-1 show that merging of WET and WET/DRY data for the correlation produces a strong degradation in the scatter as predicted by the parameter σ (cf runs 1 and 8, 2 and 9, 3 and 10, etc.), although r_{12} and R^2 are, at the same time, strengthened. The correlation coefficient r_{13} is reduced slightly. Comparing WET data with WET/DRY separately (cf runs 1 and 15, 2 and 16, etc.) we again see more severe scatter in the WET/DRY data, improvement in r_{12}, an anomalous (negative) r_{13} and poor R^2. Note that the WET/DRY correlations show an inverse dependency of $\Delta L/L$ on G, i.e., negative values of the exponent e, which does not stand to reason. We conclude that there must be anomalies in the WET/DRY data and that only the WET data should be used in further correlation attempts.

Comparing run 1 with runs 2 through 7 we see the effect of not applying and then applying various humidity differences (air-to-water) in the water loss correlation. It is apparent that addition of the effects of humidity difference reduces correlation scatter σ and generally improves the coefficient of multiple determination R^2. In all cases, however, the correlation coefficients r_{12}, r_{13} and r_{14} show a rather weak relationship between $\Delta L/L$ and the independent parameters L, G and $\Delta\omega$. The best of the humidity-dependent correlations seems to be the one based on

TABLE 4.5.2-1

WATER LOSS CORRELATION DATA

Input		Statistics							Correlation Parameters			
No.	Data File and Correlation Conditions	σ	$\overline{X}$	N	r_{12}	r_{13}	r_{14}	R^2	C_1	d	e	f
1	All WET data; no effect of humidity difference (Δω)	.271	1.033	539	-.475	.445	0	.646	88.64	-.884	.452	0
2	All WET data; log-mean humidity difference	.175	1.015	539	-.475	.445	.643	.838	152.8	-.561	.437	.720
3	All WET data; Δω between water in & air in	.177	1.015	539	-.475	.445	.530	.842	488.8	-.724	.467	.880
4	All WET data; Δω between water out & air out	.268	1.033	539	-.475	.445	.266	.650	156.9	-.896	.418	.039
5	All WET data; Δω between water in & air out	.179	1.016	539	-.475	.445	.878	.823	31.16	-.326	.204	.419
6	All WET data; Δω between water out & air in	.193	1.017	539	-.475	.445	-.233	.815	1678.	-1.06	.840	.994
7	All WET data; Δω between mean water & air	.190	1.017	539	-.475	.445	.195	.813	524.5	-.798	.607	.847
8	WET + WET/DRY data; no Δω effect	.386	1.058	733	-.848	.339	0	.811	143.8	-.846	.336	0
9	WET + WET/DRY data; log-mean Δω	.365	1.046	733	-.848	.339	.330	.855	1321.	-.807	.354	.587
10	WET + WET/DRY data; Δω between water in & air in	.369	1.047	733	-.848	.339	.025	.857	2176.	-.881	.368	.725
11	WET + WET/DRY data; Δω between water out & air out	.384	1.055	733	-.848	.339	-.220	.823	712.1	-.915	.279	.101
12	WET + WET/DRY data; Δω between water in & air out	.367	1.047	733	-.848	.339	-.760	.851	484.3	-.682	.195	.324
13	WET + WET/DRY data; Δω between water out & air in	.341	1.043	733	-.848	.339	-.615	.864	810.7	-1.16	.750	1.02
14	WET + WET/DRY data; Δω between mean air & water	.359	1.047	733	-.848	.339	-.224	.853	2229.	-.911	-	-
15	WET/DRY data; no effect of humidity difference	.346	1.062	194	-.741	-.276	0	.555	415.5	-.592	-.064	0
16	WET/DRY data; log-mean humidity difference	.335	1.049	194	-.741	-.276	.253	.667	53420.	-.606	-.101	.983
17	WET/DRY data; Δω between water in & air in	.304	1.044	194	-.741	-.276	.268	.700	4438.	-.620	-.110	1.10
18	WET/DRY data; Δω between water out & air out	.344	1.060	194	-.741	-.276	-.197	.579	1228.	-.655	-.066	.089

(Continued)

Table 4.5.2-1 (cont'd)

Input		Statistics							Correlation Parameters			
No.	Data File and Correlation Conditions	σ	X	N	r_{12}	r_{13}	r_{14}	R^2	C_1	d	e	f
19	WET/DRY data; $\Delta\omega$ between water in & air out	.345	1.053	194	-.741	-.276	.353	.645	11.895	-.392	-.354	.611
20	WET/DRY data; $\Delta\omega$ between water out & air in	.323	1.050	194	-.741	-.276	-.198	.654	1.75x10	-1.09	.481	1.35
21	WET/DRY data; $\Delta\omega$ between mean water and air	.311	1.044	194	-.741	-.276	.104	.698	-	-	-	-
22	WET data; $L \leq 10{,}000$; log-mean $\Delta\omega$	.170	1.041	498	-.460	.503	.632	.835	189.9	-.600	.434	.689
23	WET data; $L \leq 8{,}000$; log-mean $\Delta\omega$	.155	1.013	346	-.330	.628	.666	.822	240.6	-.529	.371	.785
24	WET data; $L \leq 6{,}000$; log-mean $\Delta\omega$	.156	1.013	214	-.452	.569	.685	.790	94.68	-.322	.329	.903
25	WET data; $L \leq 10{,}000$; no $\Delta\omega$	.257	1.030	498	-.460	.503	0	.655	205.0	-.979	.451	0
26	WET data; $L \leq 8{,}000$; no $\Delta\omega$	.254	1.032	346	-.330	.628	0	.579	33.62	-.749	.428	0
27	WET data; $L \leq 6{,}000$; no $\Delta\omega$	.263	1.033	214	-.452	.569	0	.517	1122.	-1.09	.333	0
28	SHORT data; no $\Delta\omega$	.181	1.016	251	-.581	.668	0	.741	26.73	-.707	.431	0
29	SHORT data; log-mean $\Delta\omega$	.176	1.015	251	-.581	.668	.472	.761	68.07	-.634	.410	.325
30	SHORT 14-foot data; no $\Delta\omega$	.159	1.012	147	-.628	.639	0	.817	144.32	-.982	.533	0
31	SHORT 14-foot data; log-mean $\Delta\omega$	.121	1.007	147	-.628	.639	.585	.888	1868.	-.903	.447	.613
32	SHORT 10-foot data; no $\Delta\omega$	.141	1.009	104	-.628	.732	0	.836	133.7	-.822	.361	0
33	SHORT 10-foot data; log-mean $\Delta\omega$	.130	1.007	104	-.628	.732	.283	.868	1830.	-.798	.354	.613
34	WET data; winter (11xxxx), no $\Delta\omega$	.129	1.008	172	-.436	.747	0	.9109	3.989	-.766	.705	0
35	WET data; winter (11xxxx), log-mean $\Delta\omega$	.106	1.006	172	-.436	.747	.582	.939	10.62	-.537	.667	.568
36	WET data; spring (12xxxx), no $\Delta\omega$	.136	1.009	167	-.660	.646	0	.888	23.91	-1.01	.462	0
37	WET data; spring (12xxxx), log-mean $\Delta\omega$	.112	1.006	167	-.660	.646	.775	.924	367.8	-.767	.396	.457
38	WET data; summer (13xxxx), no $\Delta\omega$	.241	1.027	200	-.352	.553	0	.671	22.99	-.759	.516	0
39	WET data; summer (13xxxx), log-mean $\Delta\omega$	.195	1.019	200	-.352	.553	.654	.759	167.2	-.596	.417	.633

log-mean humidity difference, run 2, in terms of scatter, R^2 and most important, r_{14}.

Comparing run 2 with run 22 shows the effect of limiting data to tests where $L \leq 10,000$. There is little difference here, as one might expect, since the L discrimination reduces the number of data sets only slightly, from 539 to 498. Further discrimination in L has a mixed effect on correlation coefficients, with no significant improvement.

The best correlations appear to occur when one segregates the WET data into seasonal blocks. Comparing runs 2 (all WET data), 35 (winter WET), 37 (spring WET) and 39 (summer WET) we see an improvement, especially in the winter and spring tests. Direct comparison of all WET data and spring WET data is made in Table 4.5.2-2.

TABLE 4.5.2-2

COMPARISON OF ALL WET AND WINTER WET CORRELATIONS
OF WATER LOSS $\Delta L/L$

Run	σ	r_{12}	r_{13}	r_{14}	R^2	C_1	d	e	f
2	.175	-.475	.445	.643	.838	152.8	-.561	.437	.720
37	.112	-.660	.646	.775	.924	367.8	-.767	.396	.457

The spring WET data correlation is clearly superior to the all WET correlation. Examination of runs 38 and 39 shows that it was probably the summer WET test data that caused the problem in the correlation of all WET data.

The SHORT data correlations show the same trends, i.e., inclusion of humidity difference in the correlation improves correlation coefficients and segregation into 10 foot and 14 foot air travel tests offers further improvement.

Overall we are somewhat disappointed in the scatter (σ) in all correlations. It is recommended that the correlation for spring tests (run 37):

$$\Delta L/L = 367.8\ L^{-.767}\ G^{.396}\ \Delta\omega^{.457} \qquad (4.5.2\text{-}2)$$

(where $\Delta\omega$ is log-mean humidity difference) be used in design or performance calculations. Again these calculations must be iterative because we do not know the humidity of the air at discharge nor the saturation humidity of air at the discharge water temperature at the start of calculations. For a somewhat less accurate prediction of water loss, the correlation based on humidity difference between air at the inlet air state and saturated air at the water inlet temperature, run 3, may be used:

$$\Delta L/L = 488.8\ L^{-.724}\ G^{.467}\ \Delta\omega^{.880} \qquad (4.5.2\text{-}3)$$

All these independent parameters will be known at the start of design or performance calculations.

4.5.3 Dry Heat Exchanger Air-Side Convective Heat Transfer Coefficient H

Based on a wealth of prior experience in the heat transfer literature on heat exchanger surface, correlations of the form:

$$j = C_2\ Re^n \qquad (4.5.3\text{-}1)$$

were used to relate the dry heat exchanger air-side convective heat transfer coefficient H with airflow data. Table 4.5.3-1 presents the limited number of correlation attempts, the number of runs being limited by the simplicity of the correlation. Runs dealt with WET/DRY (194 runs) and DRY (415 runs) test data.

TABLE 4.5.3-1

DRY HEAT EXCHANGER HEAT TRANSFER COEFFICIENT CORRELATION DATA

		Statistics				Correlation Parameters	
No.	Data File and Correlation Conditions	σ	$\overline{X}$	N	r_{12}	C_2	n
1	All DRY data	.264	1.040	415	-.200	.0199	-.1672
2	All WET/DRY data	.338	1.062	194	-.783	.8248	-.6696
3	All DRY + WET/DRY data	.380	1.063	609	-.606	.2852	-.5335
4	DRY data; summer (33xxxx) only	.123	1.006	237	.0288	.0065	-.0117
5	DRY data; spring (32xxxx) only	.332	1.058	176	-.2622	.0215	-.2057

We are extremely disappointed, but not surprised, by the large scatter in these data, as indicated by the standard estimate of error σ, and by the low values of the correlation coefficient between Colburn j factor and Reynolds number, r_{12}. These poor tendencies are expected in light of the conclusions drawn in the analysis of Ka and $\Delta L/L$, where WET/DRY data were not used because of poor statistics. We surmise that one of two problems caused the DRY and WET/DRY data to be poor. First, the method used to measure water flow through the dry exchangers is suspect. A more positive flow-measuring device such as an orifice or venturi would have yielded a more accurate water flow. Water flow is required to determine water-side convective heat transfer coefficient, which is used in conjunction with heat exchanger core heat transfer rate to calculate air-side heat transfer coefficient, and thus j. A second problem in the exchanger core may have arisen because the tubes were vertical, causing the inner tube surfaces to be nonuniformly wetted. The method for determining water-side convective heat transfer coefficient assumed completely wetted water surface in fully developed turbulent flow. In any case, all j-Re correlations are suspect.

Reference 8 shows that for a finned heat exchanger bank similar to the one in the Cliffside tower the Colburn j factor should correlate with Reynolds number by:

$$j = .2130 \ \mathrm{Re}^{-.3840} \qquad (4.5.3\text{-}2)$$

Other circular finned heat exchangers with different tube pitches and tube diameters in Reference 1 show similar exponents but different coefficients.

Examination of Table 4.5.3-1 shows no correlation similar to Equation (4.5.3-2). About the closest would be run 3 which uses all available data and gives:

$$j = .2852 \ \mathrm{Re}^{-.5335} \qquad (4.5.3\text{-}3)$$

Curve 717157A

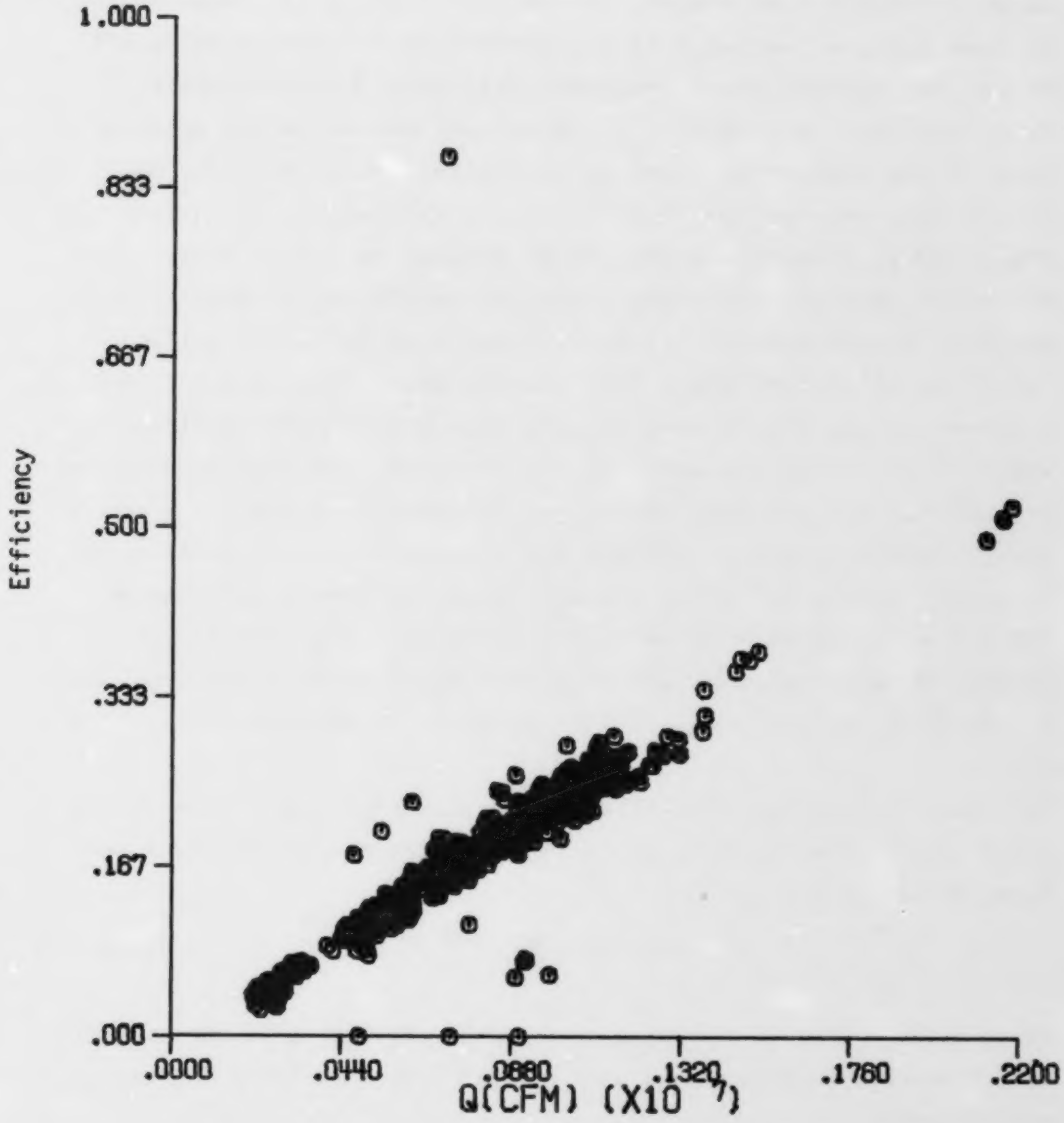

Figure 4.5.4-1. Airflow System Efficiency as a Function of Airflow Rate.

Rather than use Equation (4.5.3-3) or (4.5.3-2), it is recommended that the designer contact the supplier of his finned surface. Suppliers all provide data of this type for their products.

4.5.4 Fan Efficiency

It has been established that in all probability the velocity pressure probes at the fan stack throat did not, for one reason or another, supply good pressure measurements. Consequently, it would be misleading to base the fan efficiency on erroneous airflow rate measurements. Instead, the fan efficiency is based on the airflow rate required to conserve energy. In other words, each fan test was reduced using Equation (4.3-77) to determine airflow rate and the fan efficiency was calculated from,

$$\eta_f = \frac{\alpha Q \Delta P}{E} \qquad (4.5.4\text{-}1)$$

where ΔP is the measured fan inlet-to-stack outlet (atmospheric) pressure difference and E the measured fan-motor energy consumption rate. Note that this efficiency includes the motor and gear box losses as well as any effects associated with the stack. For conciseness, this lumped system efficiency will be referred to as the airflow system efficiency. Figure 4.5.4-1 presents the results of the fan tests. As is evident in the figure, the data are generally very good with only a few obvious exceptions.

Before examining the results in any more detail, it is useful to review the anticipated airflow system efficiency behavior. It is well known that the efficiency of a given fan can be correlated with the specific speed ν, defined as

$$\nu = \frac{\dot{\theta}\, Q^{1/2}}{\Delta P^{3/4}} \qquad (4.6.4\text{-}2)$$

Curve 717158A

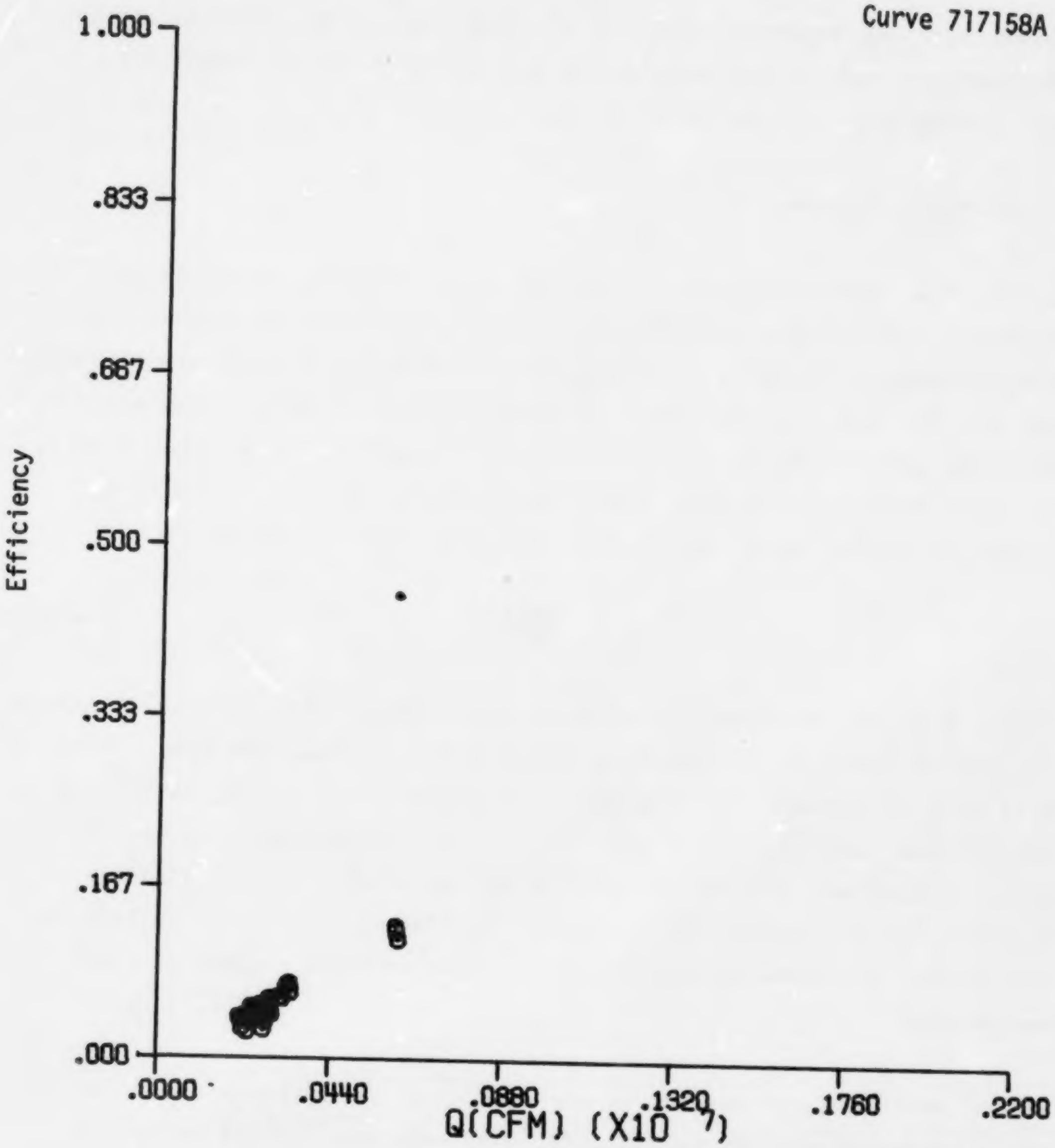

Figure 4.5.4-2. Airflow System Efficiency as a Function of Airflow Rate for a Rotational Speed of 60 RPM.

where $\dot{\theta}$ is the rotational speed, Q the volumetric airflow rate, and ΔP the fan head rise. From the 'fan laws', it is also known that

$$Q = C_a \dot{\theta} \tag{4.5.4-3}$$

$$\Delta P = C_b \dot{\theta}^2 \ . \tag{4.5.4-4}$$

Substitution of (4.5.4-3) and (4.5.4-4) into (4.5.4-2) yields the result:

$$\eta_f = \frac{C_a^{\ 1/2}}{C_b^{\ 3/4}} = \text{constant} \quad . \tag{4.5.4-5}$$

In other words, for any change in angular speed, the specific speed is constant. One would, therefore, expect the fan efficiency to remain constant for changes in angular speed. Clearly, however, Equations (4.5.4-3) and (4.5.4-4) are oversimplified. They do not account for Reynolds number effects--which would tend to increase the efficiency at a constant specific speed--nor do they include the influence of the fan stack, motor, or gear train. Nevertheless, the efficiency should be a weak-to-moderate function of angular speed. Figures 4.5.4-2 through 4.5.4-6, when compared with one another, indicate a rather pronounced influence of rotational speed on the airflow system efficiency. Some of the data which appear in Figure 4.5.4-1 are not present in Figures 4.5.4-2 through 4.5.4-6. The measured angular speed was required to be within ±4 rpm of the plotted speed. Since there was some drifting of the actual speed from the desired test value, several data points were culled for this presentation.

The behavior of the airflow system efficiency to perturbations in blade pitch can also be qualitatively predicted. Figure 4.5.4-7 illustrates the interaction between fan and system. Figure 4.5.4-7a delineates three fan curves, one for each blade pitch; the respective operating

Curve 717159A

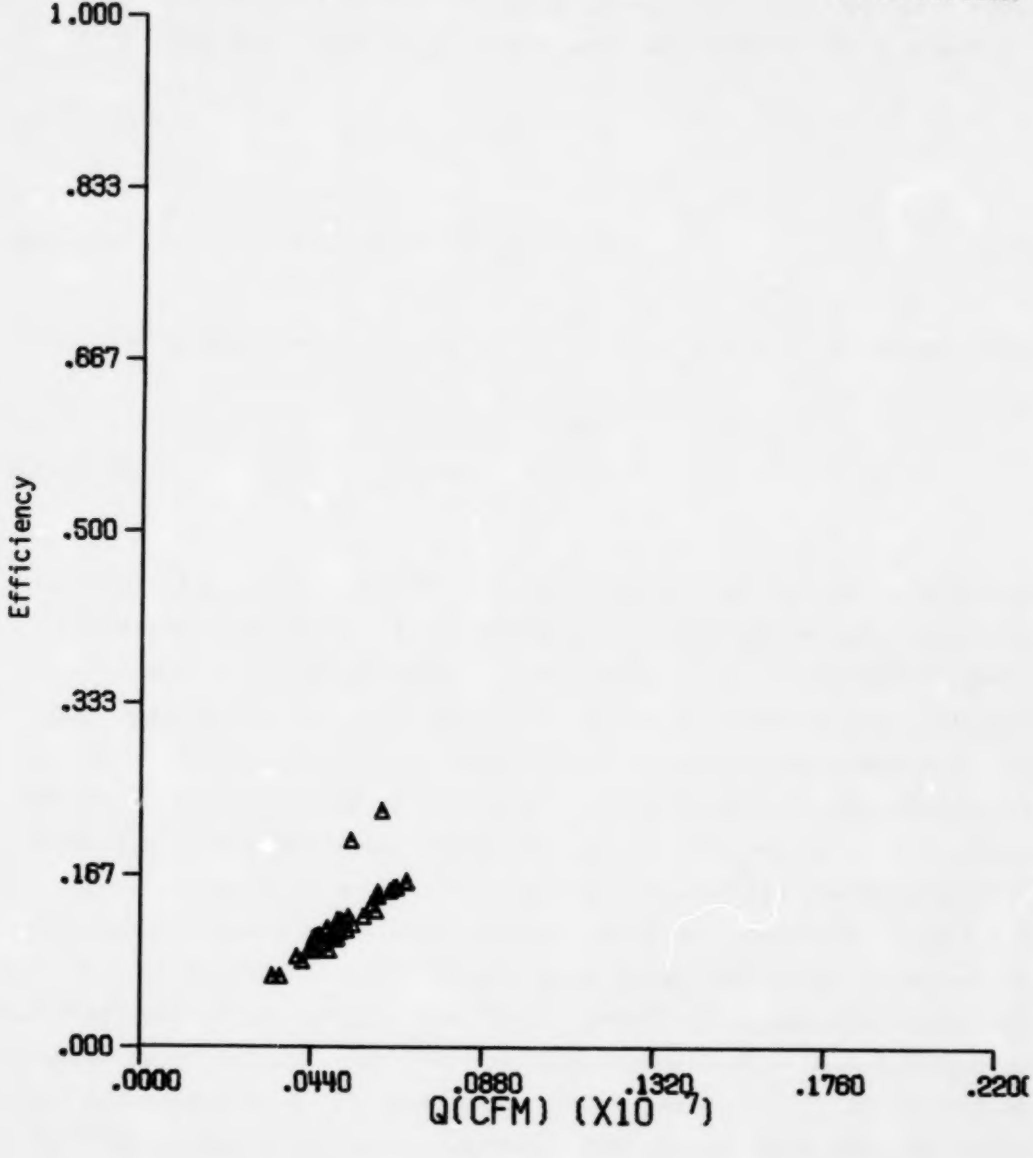

Figure 4.5.4-3. Airflow System Efficiency as a Function of Airflow Rate for a Rotational Speed of 90 RPM.

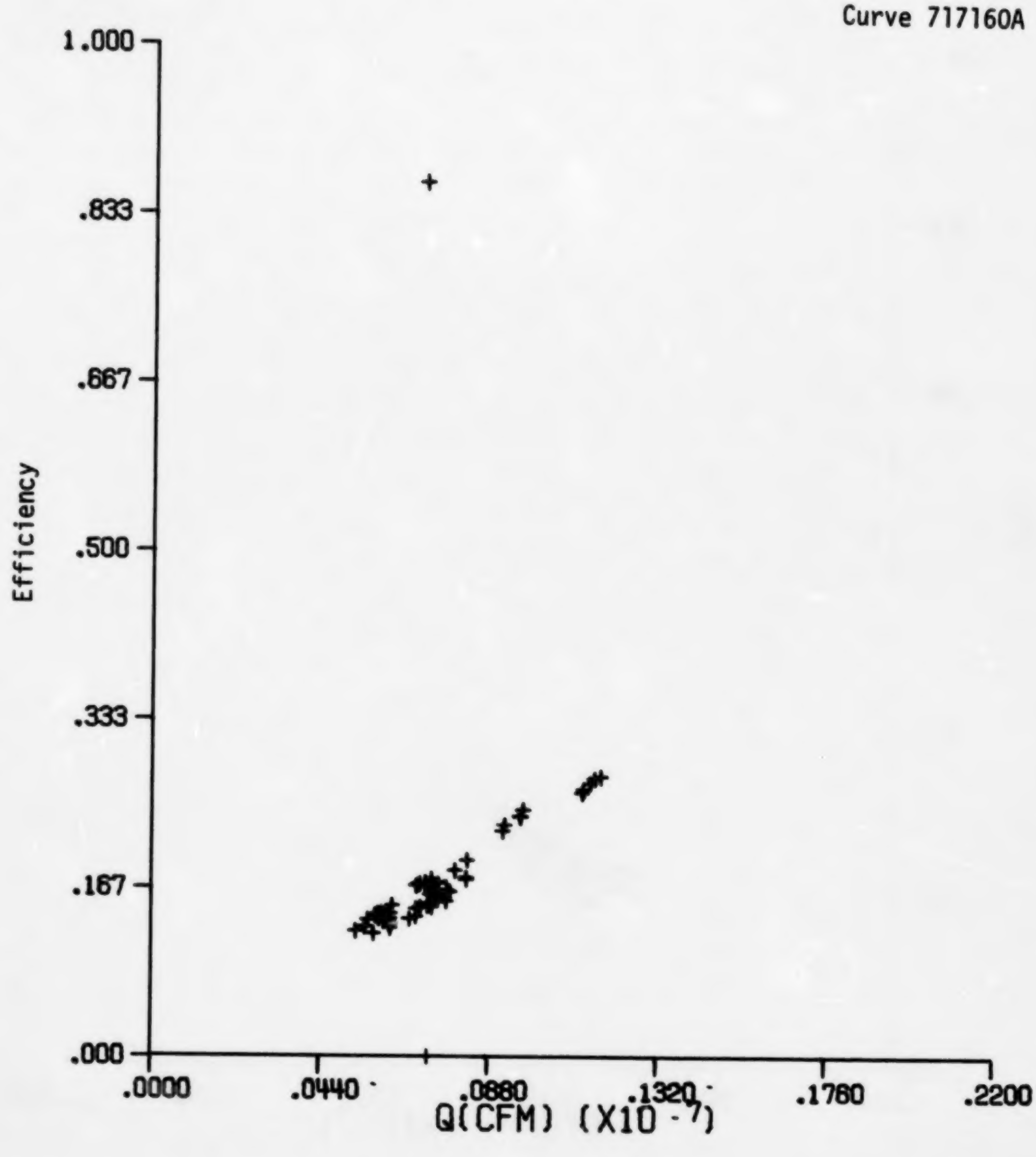

Figure 4.5.4-4. Airflow System Efficiency as a Function of Airflow Rate for a Rotational Speed of 101 RPM.

Curve 717161A

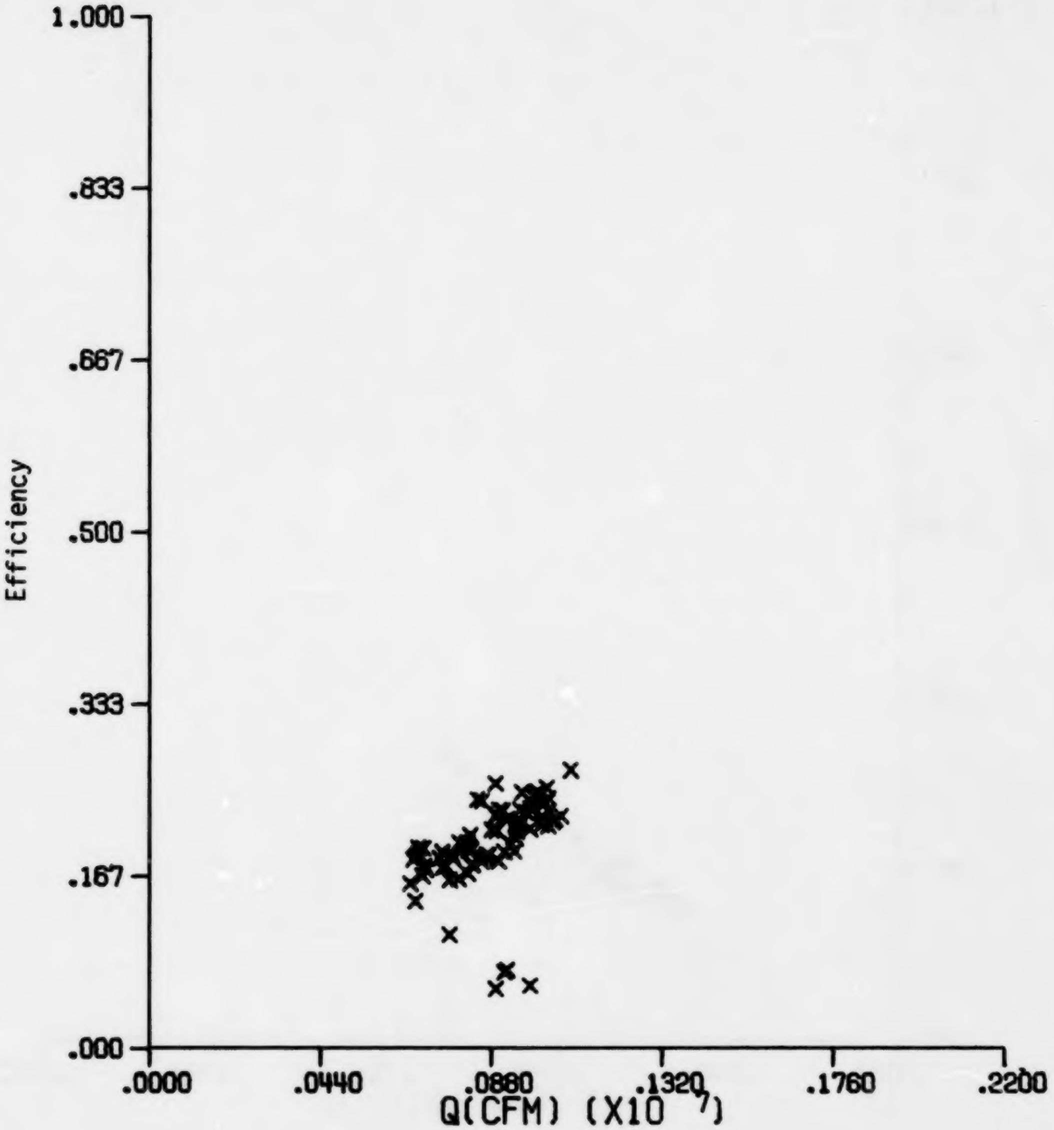

Figure 4.5.4-5. Airflow System Efficiency as a Function of Airflow Rate for a Rotational Speed of 113 RPM.

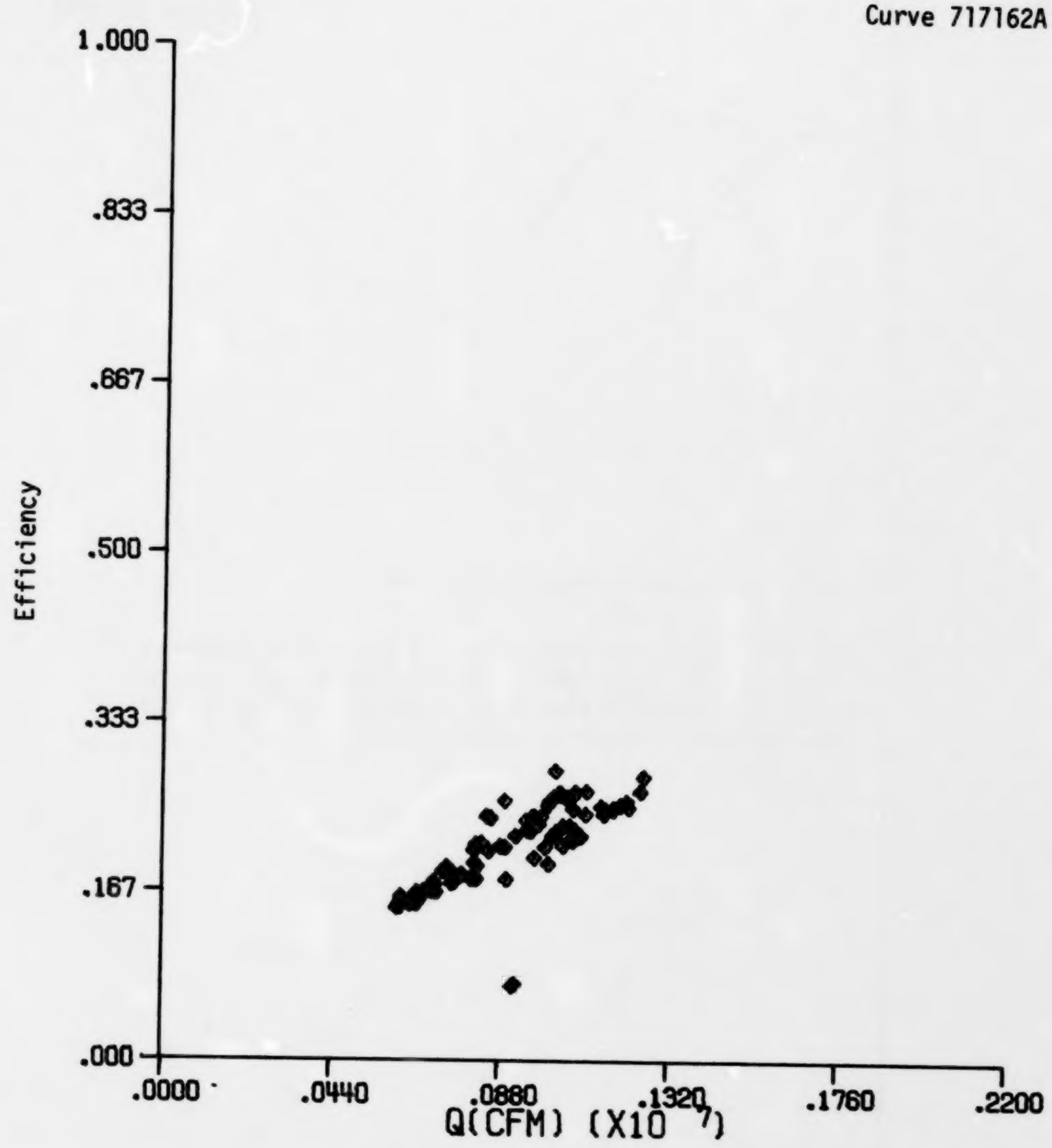

Figure 4.5.4-6. Airflow System Efficiency as a Function of Airflow Rate for a Rotational Speed of 119 RPM.

Curve 717163A

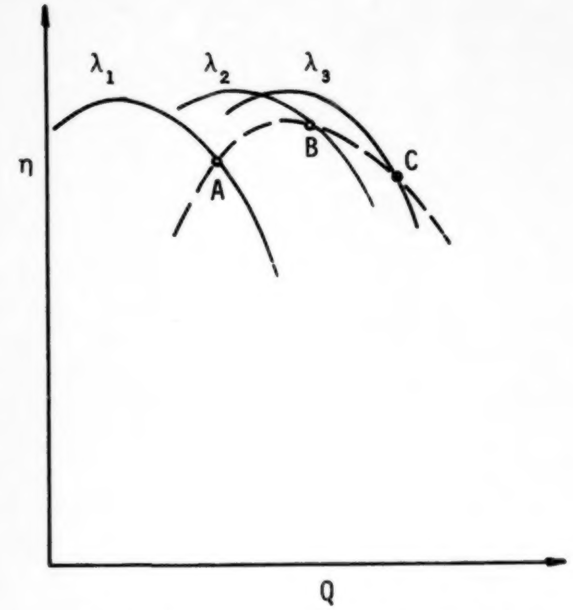

b. Fan Efficiency for Three Blade Angles as a Function of Volumetric Flow Rate. Also Shown is Anticipated Fan Efficiency Behavior While Coupled to the System Characteristic Shown in Figure 6-7a.

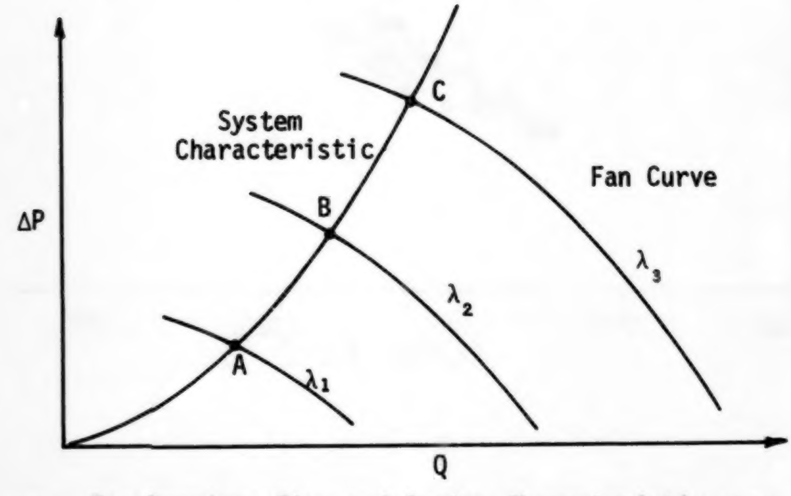

a. Fan Pressure Rise and System Characteristic as a Function of Volumetric Flow Rate. Each Fan Curve Represents a Unique Pitch (λ).

Figure 4.5.4-7. Effect of Pitch on Fan Performance.

points (labeled A, B, and C); and the system characteristic. For each pitch, the fan manifests a unique efficiency versus flow rate performance. Thus, the fan efficiency for a blade angle of λ_1 can be found by noting the flow rate at the operating point A. Using this flow rate in Figure 4.5.4-7b allows the efficiency of the fan with blade pitch λ_1 to be determined. The locus of such points, denoted as the dashed curve in Figure 4.5.4-7b, represents the anticipated influence of pitch on fan performance for a given system characteristic. It is important for the reader to recognize that the dashed curve was synthesized from one system characteristic. A variable system characteristic would hopelessly obfuscate the preceding analysis, making any kind of discussion on the fan-system performance academic. Despite the variable air and water loadings of the fan tests, the system characteristic changed only slightly and is only a second order effect relative to the fan speed and blade pitch. The reader is reminded, however, that the airflow system efficiency is a lumped parameter manifesting the influence of the fan, stack, motor, and gear train.

Figures 4.5.4-8 through 4.5.4-12, when compared to each other, show the observed influence of pitch on the airflow system efficiency—negligible within the limits imposed by the data scattering. The only discernible trend (gradual monotonic increase in efficiency with flow rate) is the previously discussed influence of rotation speed—observable for each blade pitch. One can only conclude that the fan-system efficiency performance for variable pitch conditions (dashed curve in Figure 4.5.4-7b) is very flat over the range of blade angles tested. This result could be a consequence of a very flat family of fan efficiency curves for a fixed pitch (solid curves in Figure 4.5.4-7b) or the tested variations in pitch (±4°) were simply too small to manifest any observable trends. The latter is most likely and is aggravated by the dilution effect attributable to the other (drive train, stack, and motor) system losses. Any small change in fan efficiency could easily be overwhelmed by the remaining system components.

Curve 717164A

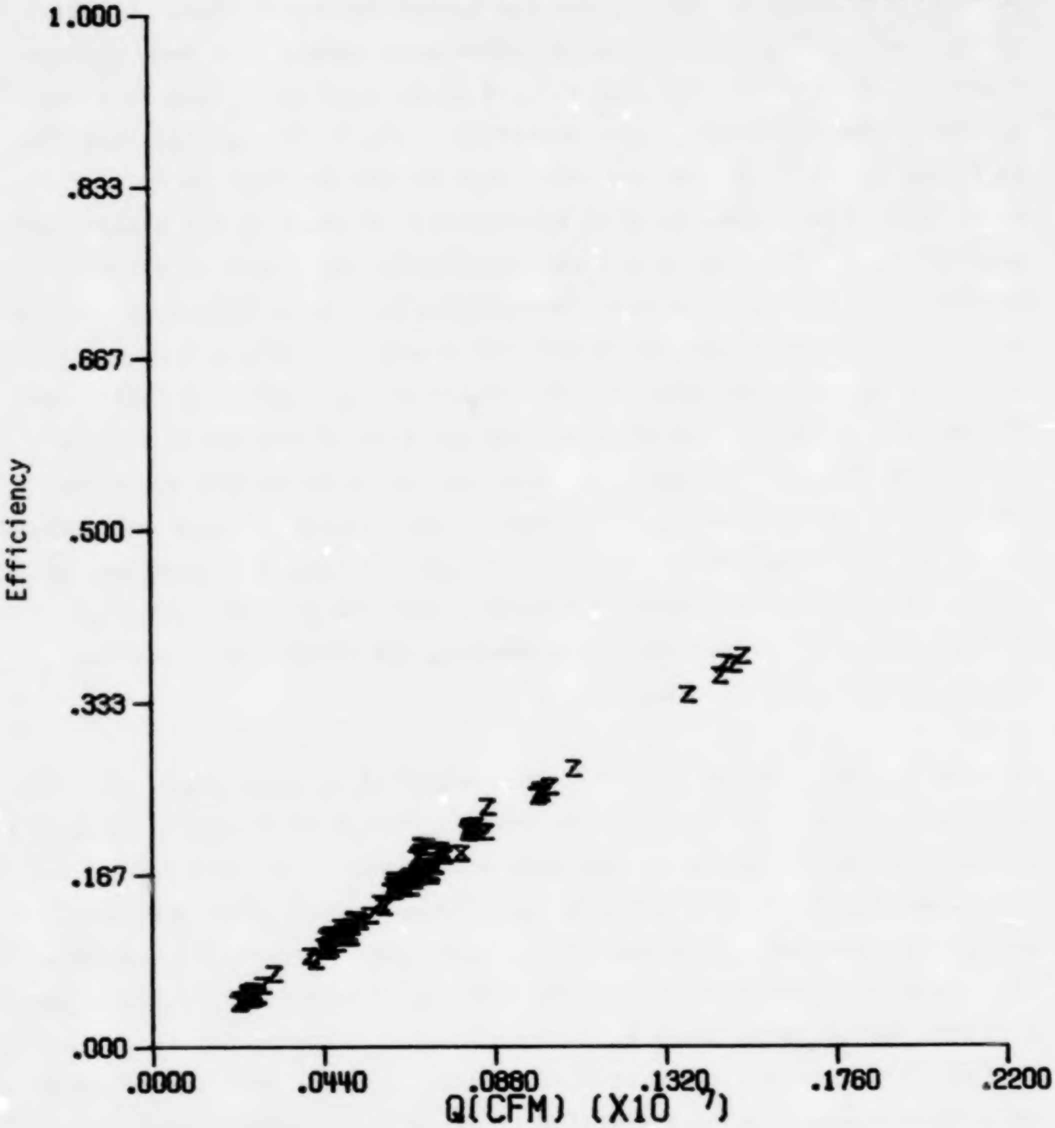

Figure 4.5.4-8. Airflow System Efficiency as a Function of Airflow Rate for an 8-Degree Blade Pitch.

Curve 717165A

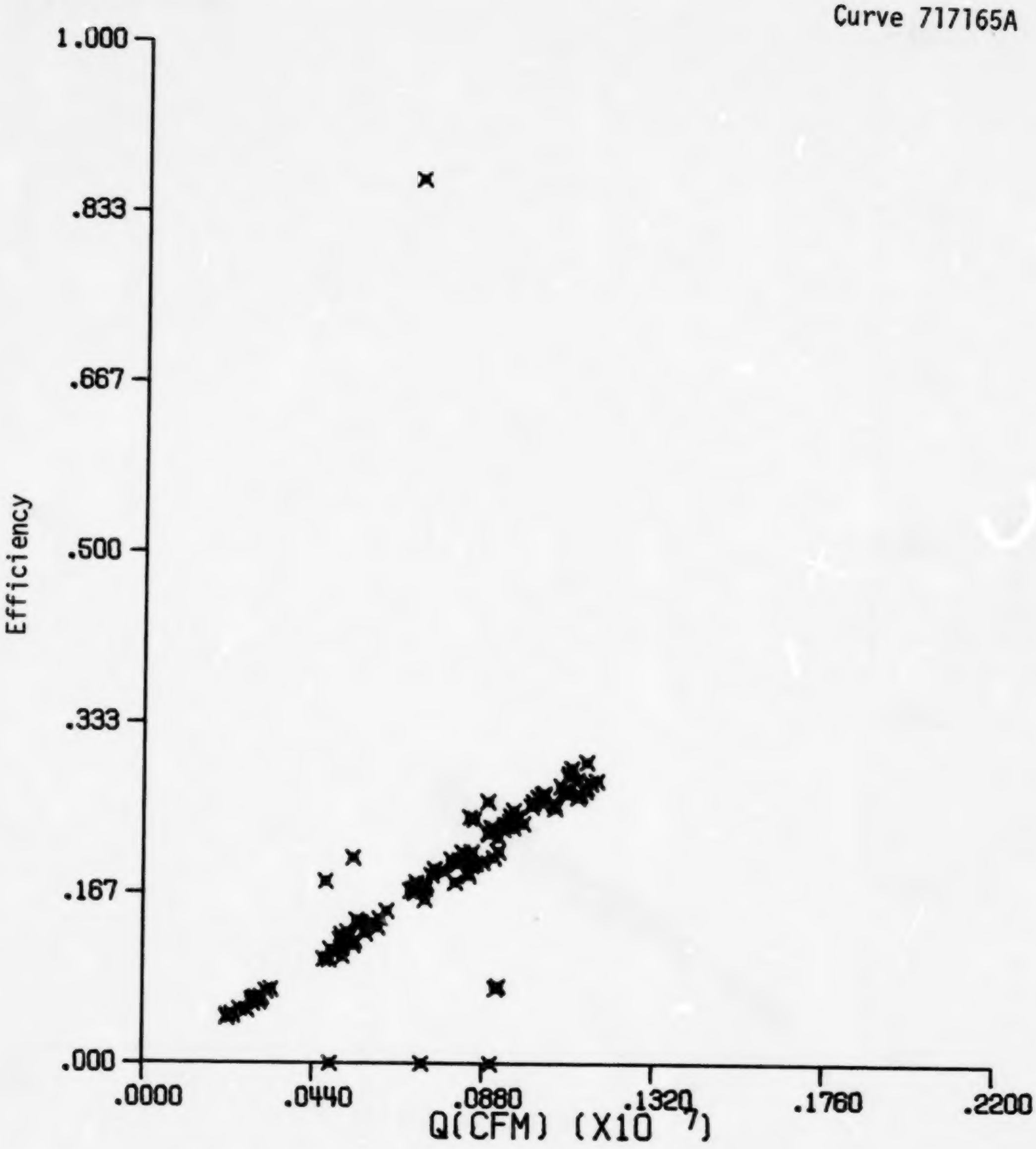

Figure 4.5.4-9. Airflow System Efficiency as a Function of Airflow Rate for a 10-Degree Blade Pitch.

Curve 717166A

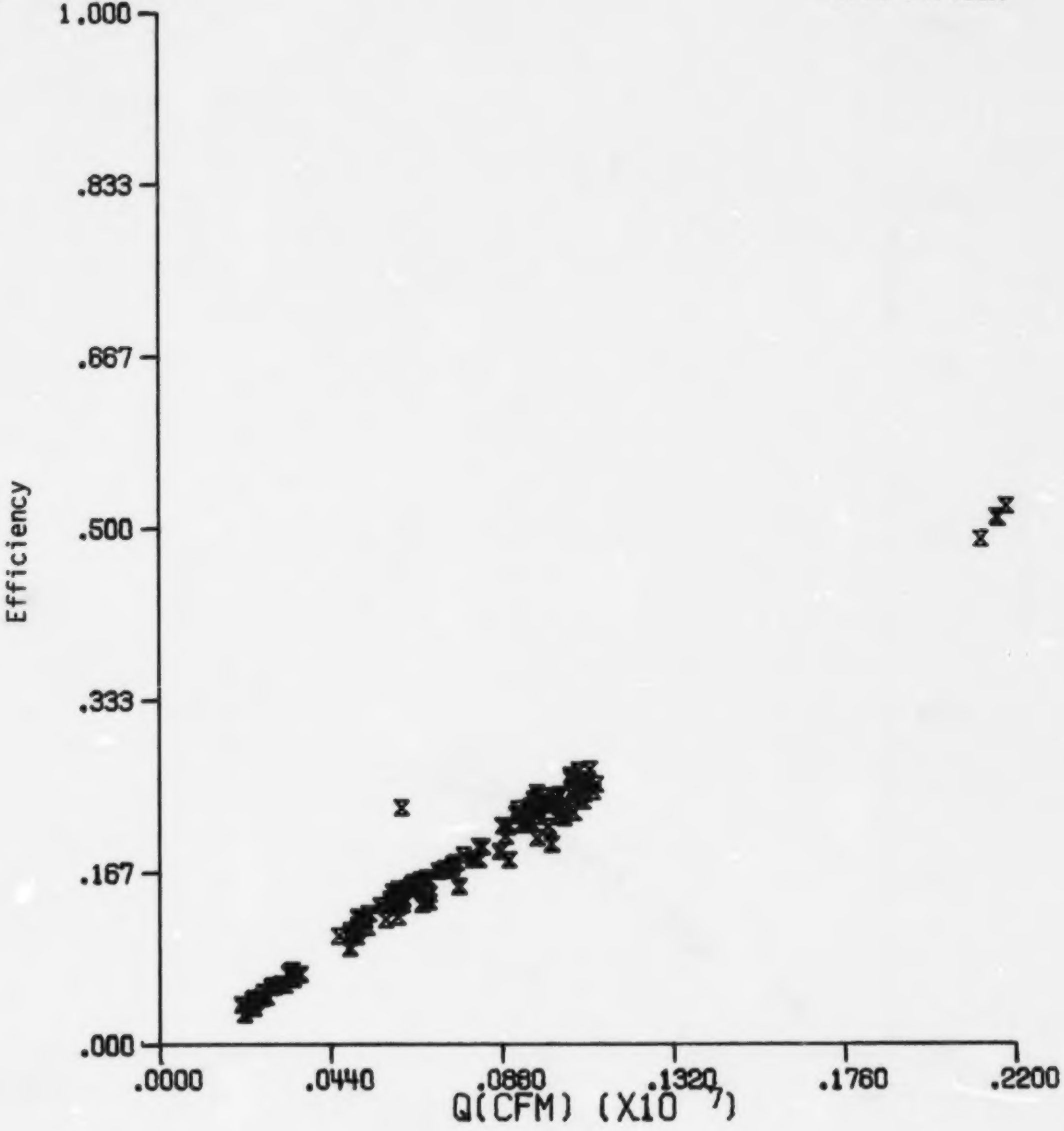

Figure 4.5.4-10. Airflow System Efficiency as a Function of Airflow Rate for a 12-Degree Blade Pitch.

Curve 717167A

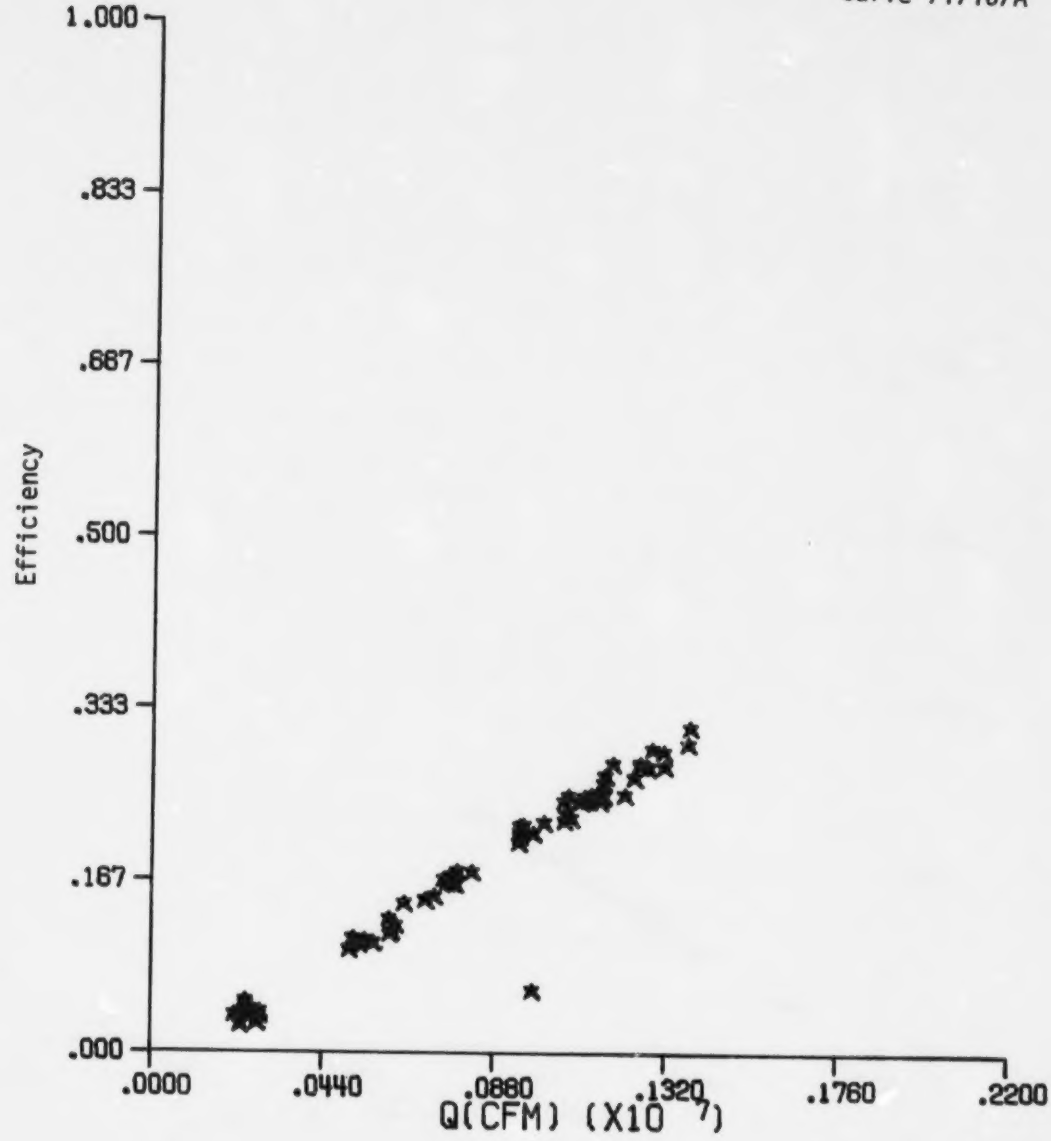

Figure 4.5.4-11. Airflow System Efficiency as a Function of Airflow Rate for a 14-Degree Blade Pitch.

Curve 717168A

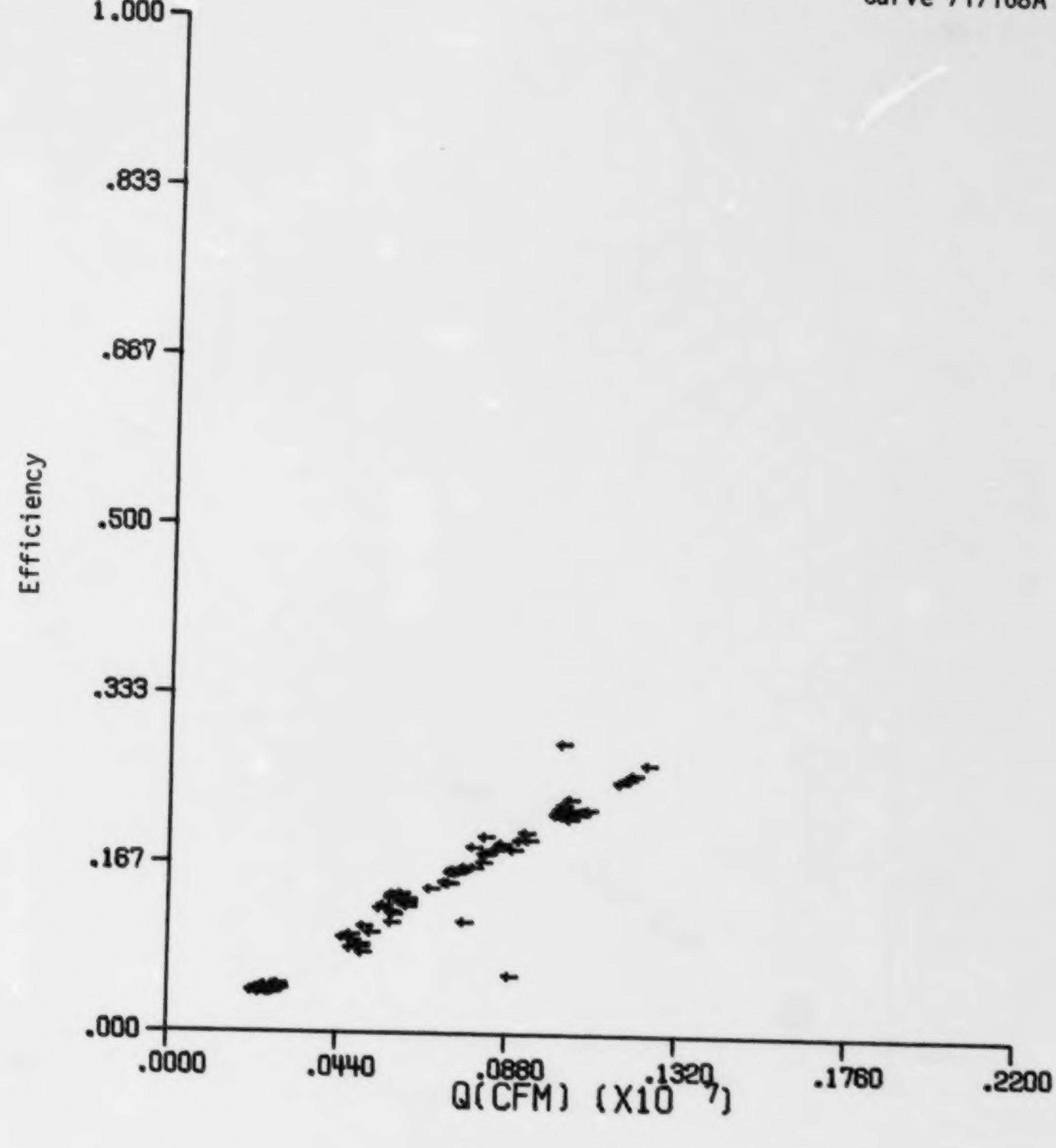

Figure 4.5.4-12. Airflow System Efficiency as a Function of Airflow Rate for a 16-Degree Blade Pitch.

It is clear that the airflow system efficiency is a complex function of several interacting components. The fan efficiency alone is a very complex function of geometry and operating conditions. If just the fan efficiency (no stack, gears, or motors) were available, it still could not be correlated with any confidence in applying the result to a different fan. Fan efficiency, as it is defined and applied here, is simply not a fundamental variable--the measured process is not basic enough to allow confident generalizations or correlations. Consequently, any quantitative relationship derived from the presented data will be valid only for the tested system. Qualitative extrapolation to different systems is less hazardous but should be done with caution. With these warnings firmly established, Figure 4.5.4-13 is presented for the purpose of visual establishment of the quality of the data. Compared is the experimental airflow system efficiency data and a straight line representing the best least squares fit of the data. The line manifests a standard error of estimate of .2495 (refer to the heat and mass transfer analysis for the development of the standard estimate of error) and a correlation coefficient of .8872. The statistical information is presented to indicate the data quality--not the degree of confidence in the generality of the approximating line.

Perhaps the most useful conclusion that can be drawn from this work is the poor utilization of electrical power manifested by the airflow system. Only 25 to 35 percent of the available electrical energy is ever used to move air. Generally, a range of 50 to 70 percent (the latter value would be very good) is reasonable for a fan efficiency. If the former value is assumed reasonable for this application, then the motor and drive train consume from 15 to 25 percent of the total electrical input power.

4.6 NOMENCLATURE

A	Surface area (ft^2).
$\tilde{A}$	Cross-sectional area (ft^2).

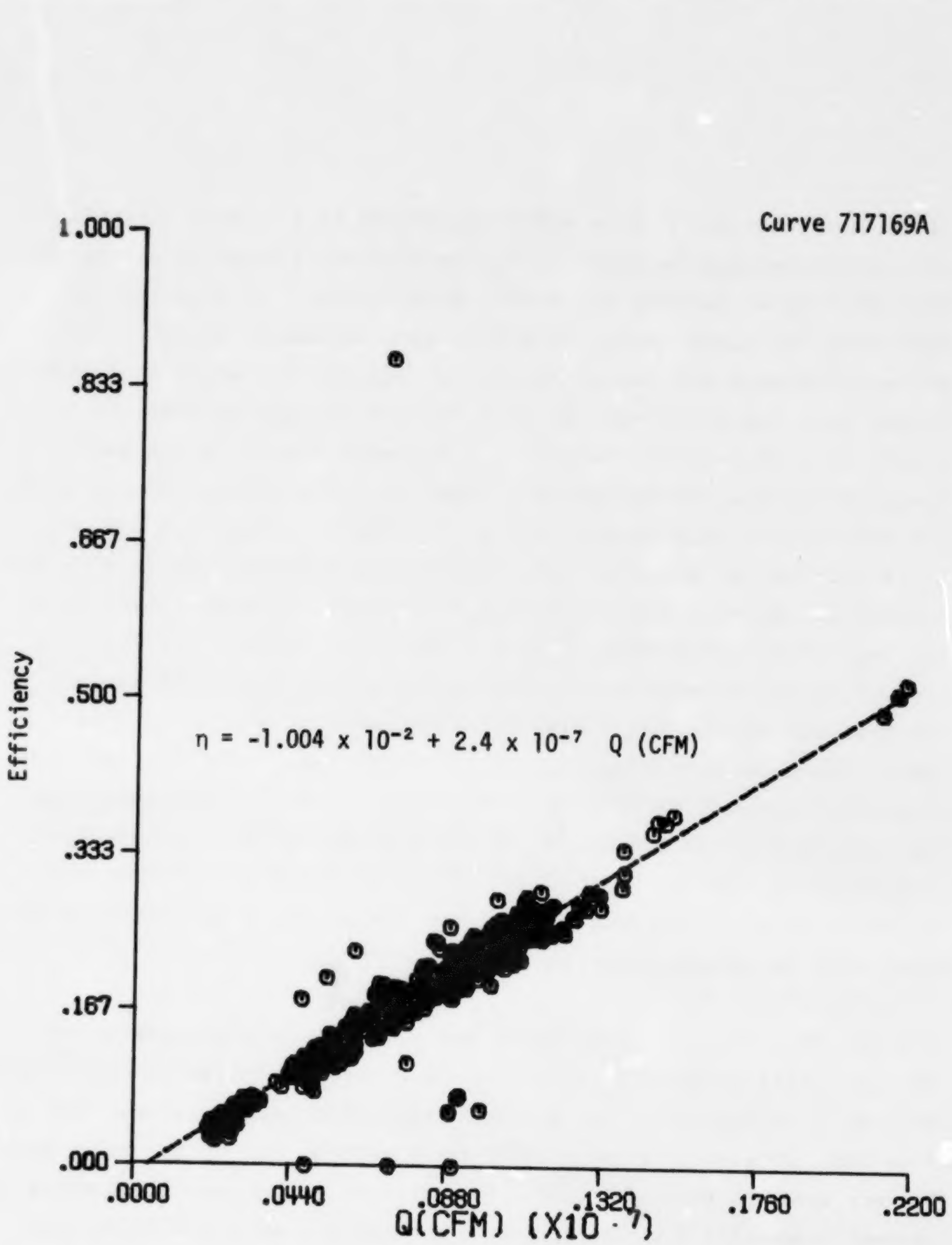

Figure 4.5.4-13. Airflow System Efficiency and Approximating Straight Line as a Function of Volumetric Flow Rate.

a	Water droplet area per unit volume (ft^{-1}).
a	Exponent of water loading L in the mass transfer coefficient correlation (dimensionless).
b	Exponent of air loading G in the mass transfer coefficient correlation (dimensionless).
C	A constant ($gal\text{-}lb_f^{1/2}/in\text{-}min$).
Cp	Specific heat at constant pressure (btu/lbm-°F).
C_o	Coefficient in the correlation of mass transfer coefficient Ka.
C_1	Coefficient in the correlation of water loss $\Delta L/L$.
C_2	Coefficient in the correlation of heat exchanger air-side heat transfer coefficient.
C_3	Coefficient in the correlation of fan system efficiency.
C_4	Coefficient in the correlation of fan system efficiency.
C_a	Proportionality constant, Q with $\dot{\theta}$.
C_b	Proportionality constant, ΔP with $\dot{\theta}^2$.
c	Exponent of temperature T in the mass transfer coefficient correlation (dimensionless).
D	Diameter (ft).
D	Logarithm of C_o in the regression analysis.
d	Tower depth (ft).
d	Exponent of water loading L in the correlation for water loss $\Delta L/L$ (dimensionless).
E	Electrical input to the fan motor (kW).
E	Energy flux (Btu/hr).
e	Exponent of air loading G in the correlation for water loss $\Delta L/L$ (dimensionless).
F	Cross-flow heat exchanger temperature difference correction factor (dimensionless).
f	Exponent of air specific humidity difference $\Delta\omega$ in the correlation for water loss $\Delta L/L$ (dimensionless).
f	A general function.
G	Air loading or mass velocity ($lbm/hr\text{-}ft^2$).
g_c	Gravitational acceleration (ft/sec^2).
H	Heat transfer coefficient ($Btu/hr\text{-}ft^2\text{-}°F$).

h	Specific enthalpy (Btu/lbm).
I_o	Zeroth order modified Bessel function of first kind (dimensioness).
I_1	First order modified Bessel function of first kind (dimensionless).
i	Index (dimensionless).
j	Colburn j factor (Nu/Re Pr) $Pr^{2/3}$ (dimensionless).
K	Mass transfer coefficient ($lbm/hr-ft^2$)
Ka	Mass transfer coefficient per unit volume of tower fill ($lbm/hr-ft^3$).
Ke, Ko	Entrance and exit loss coefficients (dimensionless).
$K\ell$	Stack loss coefficient (dimensionless).
Kg	Sensible heat transfer coefficient ($Btu/hr-ft^2-°F$).
k	Thermal conductivity (Btu/hr-ft-°F).
K_o	Zeroth order modified Bessel function of second kind (dimensionless).
K_1	First order modified Bessel function of second kind (dimensionless).
L	Water loading ($lbm/hr-ft^2$).
Le	Lewis number, Kg/K Cp_{ma} (dimensionless).
$\tilde{L}$	Total tube length (ft).
ℓ	Tower height (ft).
M	Maximum index in a summation.
m	Mass (lbm); index.
$\dot{m}$	Mass flow rate of water (lbm/hr).
N	Maximum index in a summation; number of data sets.
n	Exponent of Reynolds number Re in the correlation of heat exchanger air-side heat transfer coefficient (Colburn j factor) (dimensionless).
N_f	Fin pitch (in^{-1}).
Nu	Nusselt number, HD/k (dimensionless).
NTU	Number of transfer units (dimensionless).
P	Pressure (lbf/ft^2).
P_{fs}	Percent of full scale (dimensionless).
Pr	Prandtl number (dimensionless).
ΔPr	Pressure rise (lbf/ft^2).

p	Defined in Equation (4.3-64) (dimensionless).
Q	Flow rate (ft /sec).
$\tilde{Q}$	Flow rate (gal/min).
q	Heat transfer rate (Btu/hr).
$\tilde{q}$	Defined in Equation (4.3-64) (dimensionless).
q	Defined in Equation (4.3-64) (dimensionless).
R	Thermal resistance (°F-hr/Btu).
R_{ij}	Coefficient of multiple determination between parameters i and j (1=Ka, 2=L, 3=C, 4=T or $\Delta\omega$) (dimensionless).
Re	Reynolds number (dimensionless).
r	Defined in Equation (4.3-63) (dimensionless).
r_{ij}	Correlation coefficient between parameters i and j (1=Ka or $\Delta L/L$, 2=L, 3=G, 4=T or $\Delta\omega$) (dimensionless).
$\bar{r}$	Mean radius, defined in Equation (4.3-82) (ft).
$\tilde{r}$	Radius (ft).
T	Temperature (°F).
t	Time (hr).
$\tilde{t}$	Fin thickness (in).
U	Internal energy (Btu).
U_b	Defined in Equation (4.3-69) (dimensionless).
U_e	Defined in Equation (4.3-70) (dimensionless).
V	Velocity (ft/hr); (ft/sec) in Section 4.3.1.4.
v	Electrical potential (v).
Ɏ	Volume (ft^3).
W_i	Logarithm of L for the i^{th} data set.
X	Fill total depth (ft).
X_i	Logarithm of G for the i^{th} data set.
Xmf	Multiplication factor (dimensionless).
x	Depth to a given point in the fill (ft).
Y	Fill total height (ft).
Y_i	Logarithm of Ka for the i^{th} data set.

y	Distance of vertical water travel in the fill (ft).
Z	Total width of tower fill (ft).
Z_i	Logarithm of T in the i^{th} data set.
z	Distance from one side of the fill to a given point in the fill (ft).

Greek Symbols

α	Diffuser divergence angle (deg).
β	Defined in Equation (4.3-68) (dimensionless).
γ	Differential pressure (lbf/in^2).
$\bar{\gamma}$	Manometer column height (in).
Δ	Finite difference step size (ft).
ε	An error term.
η	Fin efficiency (dimensionless).
η_f	Fan system efficiency (dimensionless).
θ	Fan blade angle (degrees).
$\dot{\theta}$	Fan speed (rpm).
λ	Wall friction coefficient (dimensionless).
μ	Dynamic viscosity (lbm/ft-hr)
ν	Kinematic viscosity (ft^2/hr).
ρ	Density (lbm/ft^3); (slugs/ft^3) in Section 4.3.1.4.
σ	Standard estimate of error (similar to standard deviation) (dimensionless).
ϕ	Ratio of a test parameter from data to its value from a correlation (dimensionless).
$\bar{\phi}$	The mean value of ϕ for a data set.
ω	Specific humidity (dimensionless).
$\tilde{\omega}$	Angular velocity (sec^{-1}).

Subscripts

a	Air; axial.
amb	Ambient.

avg	Average.
ax	Axial.
c	Collar.
cf	Crossflow.
ccf	Counter-current flow.
co	Effective for convection.
d	Diameter.
e	Exit.
f	Fin.
fg	Latent.
fs	Full scale.
htx	Heat exchanger.
hub	Hub.
i	In; inside; index.
in	In.
j	Index
lmtd	Log mean temperature difference.
ma	Moist air.
mf	Manometer fluid.
o	Out; outside.
oc	Tube-to-fin interface.
of	Fin outer edge.
ref	Reference.
s	Swirl.
std	Standard.
t	Tube.
tip	Tip.
v	Velocity; vapor phase.
w	Water.
wv	Water vapor.
wall	Wall.
1,2,3	Specific indices.

Superscripts

'"	Unit volume.
•	Time derivative.
'	Refined value.
*	Value from a correlation.

4.7 REFERENCES

1. Wegstein, J. H., "Accelerating Convergence of Iterative Processes", Communications for Association for Computing Machinery, Vol. I, No. 6, June 1958, pp. 9-13.

2. Hamming, R. W., *Numerical Methods for Scientists and Engineers*, 2nd Ed., McGraw-Hill Book Company, New York NY, 1973.

3. Bowman, R. A., Mueller, A. C. and Nagle, W. M., "Mean Temperature Difference in Design", *Trans. ASME*, May 1940.

4. Gardner, K. A., "Efficiency of Extended Surface", *Trans. ASME*, November 1945, pp. 621-634.

5. Eckels, P. W., "Contact Conductance of Mechanically Expanded Plate Finned Tube Heat Exchangers", ASME Paper 77-HT-24, 1977.

6. Sieder, E. N. and Tate, C. E., "Heat Transfer and Pressure Drop of Liquids in Tubes", *IEC*, Vol. 28, 1936, p. 1429.

7. Idel'Chik, I. E., "Resistance Coefficients of Diffusers", *Handbook of Hydraulic Resistance*, AEC-TR-360, 1966.

8. Kays, W. M. and London, A. L., *Compact Heat Exchangers*, 2nd Ed., McGraw-Hill Book Company, New York NY, 1964.

9. McAdams, W. H., *Heat Transmission*, 3rd Ed., McGraw-Hill Book Co., New York, 1954.

10. Spiegel, M. R., *Statistics*, McGraw-Hill Book Co., New York NY, 1961.

11. Ayers, D. L. and Hogan, M. R., "Mass Transfer Measurements in a Wet Crossflow Cooling Tower Test Facility", Westinghouse Research Report 75-1E9-TOTES-R1, December 2, 1975.

SECTION 5.0

ACOUSTICS TESTS

Measurement of the noise radiated by the TVA test cooling tower, at Duke Power Company's Cliffside Station, was made and corrected for background noise. Data were obtained for 31 combinations of fan speed, fan blade pitch, total water flow rate and water flow through the dry heat exchangers. These combinations were chosen so that a second order central composite experimental design could be fitted to the data. Resulting empirical equations for the octave band, linear and A-weighted sound levels at the top of the fan exhaust stack and in front of the open louvered face of the tower are presented. These equations were used to update an existing computer code for predicting the noise level of such cooling towers as a function of observer location and tower operating parameters. This computer code is presented along with suitable documentation for its use.

5.1 DESCRIPTION OF ACOUSTIC INSTRUMENTATION

All of the data acquisition and analysis equipment utilized were of precision grade and meet all relevant national standards. This equipment is described in the following subsections.

5.1.1 Data Acquisition Equipment

Figure 5.1-1 is a schematic diagram of the noise measurement equipment used for the data acquisition. Table 5.1-1 identifies the equipment by manufacturer and model number.

Dwg. 7697A95

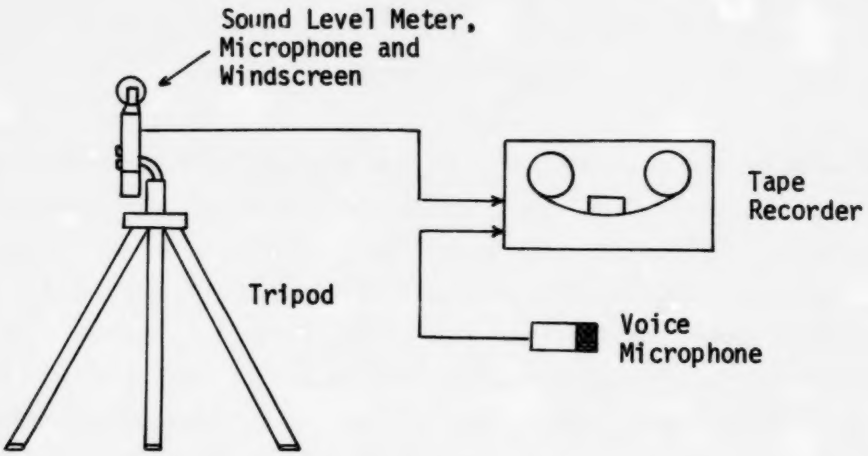
Sound Level Meter,
Microphone and
Windscreen
Tape
Recorder
Tripod
Voice
Microphone

Figure 5.1-1. Data Acquisition Equipment.

TABLE 5.1-1

MEASUREMENT EQUIPMENT MODELS

Bruel and Kjaer (B&K) Type 4145 one inch condenser microphone

B&K Type 2204 sound level meter

Stellavox SP-7 professional tape recorder

B&K Type 4220 pistonphone

Voice microphones

Tripods, cables and miscellaneous items

The B&K 4145 one-inch microphone is a design tailored for use in a free-field environment. This microphone has the frequency response and directivity characteristics illustrated in Figures 5.1-2 and 5.1-3*. Figure 5.1-2 shows, in the upper curve, the free-field response at normal incidence for the microphone with its protective grid. The lower curve is the microphone pressure response. Figure 5.1-3 shows the free-field corrections which must be added to the pressure response curve of Figure 5.1-2 in order to determine the microphone response at other angles of incidence. The windscreen used with the microphone is a B&K UA 0207 polyurethane sponge ball. Its effect on the microphone frequency response is shown in Figure 5.1-4 as a function of the incidence angle. In general, the windscreen produces a slight (0.0 - 0.7 dB) amplification of the noise over frequencies from about 1 to 5 kHz and an attenuation of about 0.6 to 1.4 dB at about 10 kHz. Since the random incidence response of the B&K 4145 microphone is amplified by several dB at frequencies near 10 kHz, the use of the windscreen tends to give the microphone a "flatter" frequency response.

The B&K 2204 sound level meter is a precision grade instrument whose characteristics surpass those of the microphone. Hence, the sound level meter conditions the input microphone signal without adversely affecting the signal frequency or amplitude characteristics. The Stellavox SP-7 is an exceptionally high quality two-channel portable tape recorder. The frequency response of both channels of the recorder, operating at 15 ips, is shown in Figure 5.1-5.

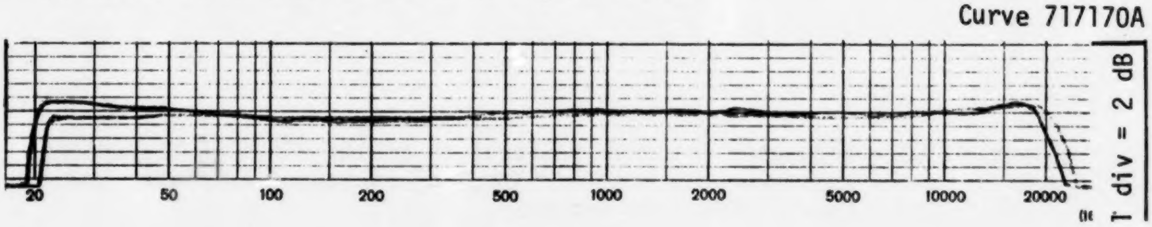

Figure 5.1-5. Measured Frequency Response at 15 ips of the Stellavox SP-7 Recording Channels.

---

*This data is taken from B&K equipment manuals and calibration curves.

Curve 717171A

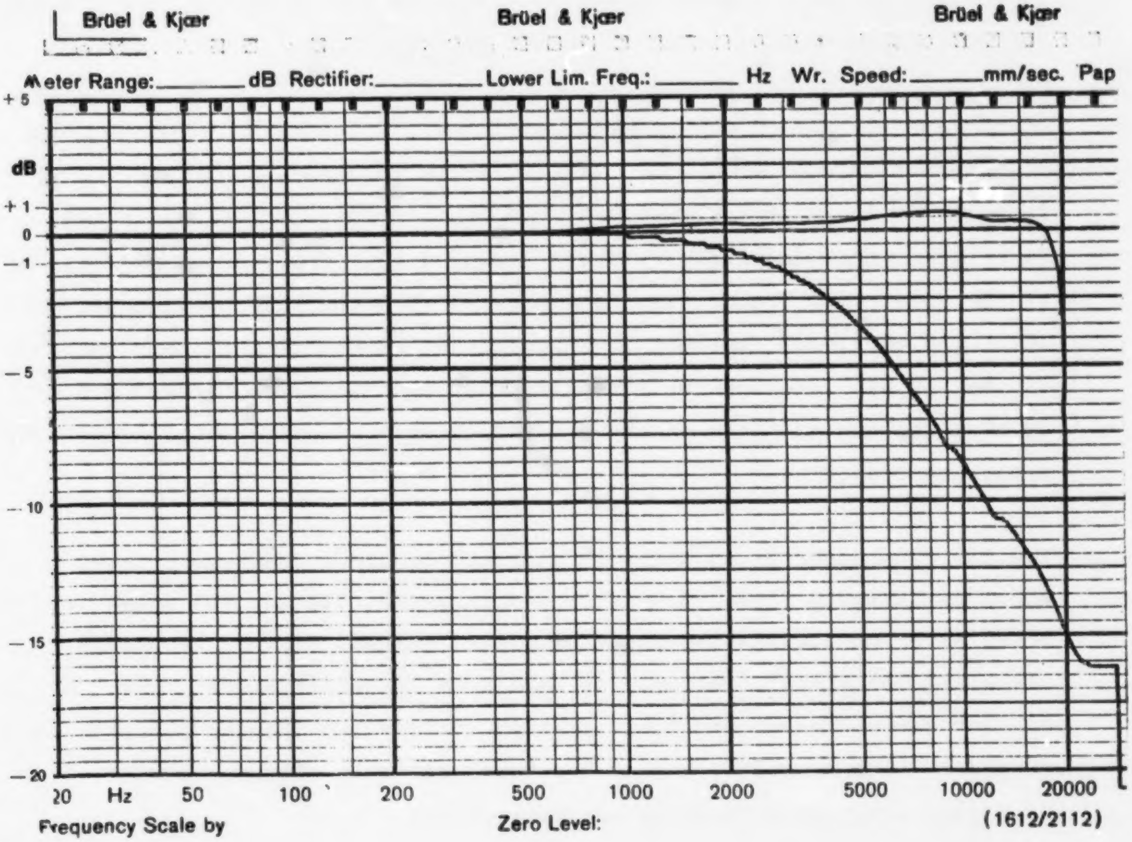

Figure 5.1-2. Frequency Response Calibration of the B&K 4145 Microphone. Upper Curve - Free-Field Normal Incidence Response; Lower Curve - Pressure Response.

Curve 717172A

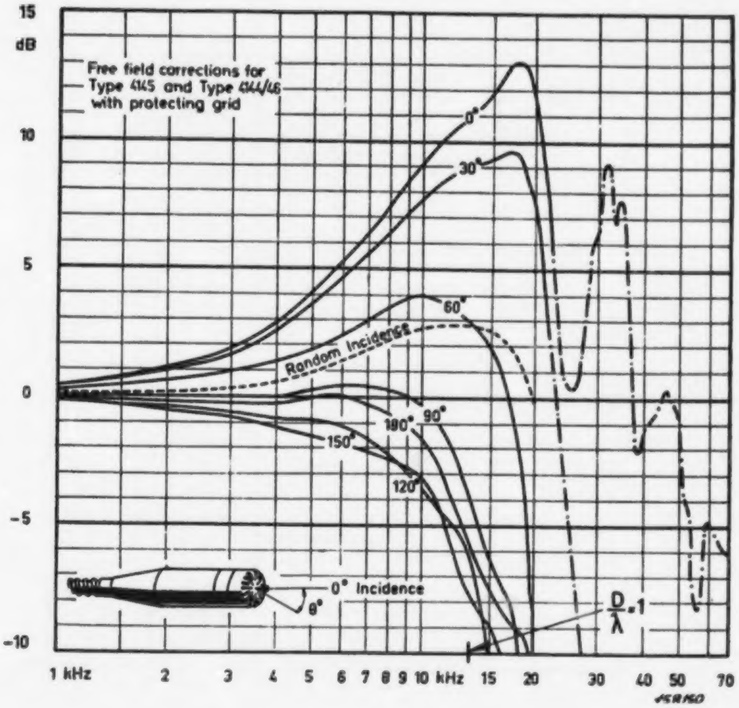

Figure 5.1-3. Free-Field Corrections for the B&K 4145 Microphone with Protective Grid as a Function of Incidence Angle.

Curve 717173A

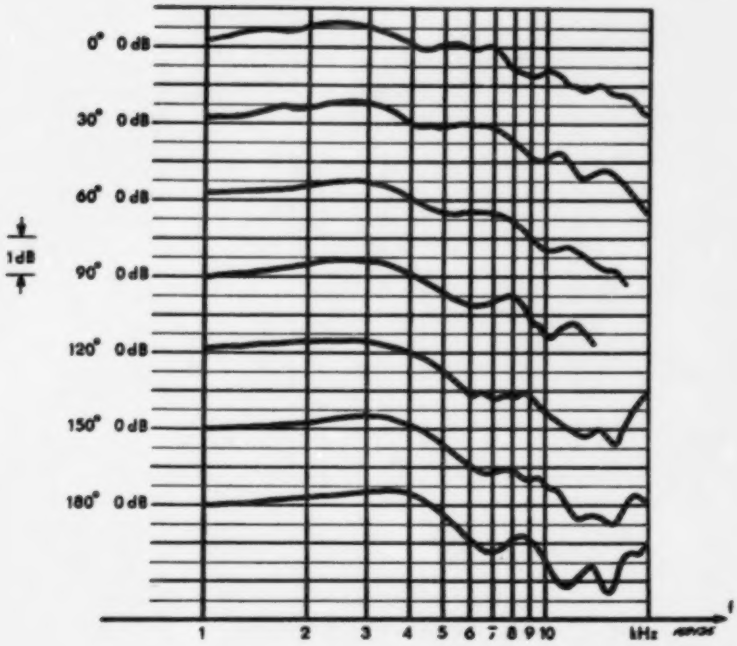

Figure 5.1-4. Free-Field Response Corrections for the B&K 4145 Micro-Phone When Used with the B&K UA 0207 Windscreen

The entire measuring system was calibrated with a B&K 4220 pistonphone. This unit allows proper amplitude calibration of the sound level meter and tape recorder within ±0.2 dB at a frequency of 250 Hz. To ensure proper analysis of the data, the pistonphone calibration signal was recorded on tape to provide a known reference signal level.

All of the recording equipment used is of precision grade and was utilized in a manner consistent with accepted measuring standards and the equipment manufacturer's instructions.

In addition to the equipment listed in Table 5.1-1, a small Dwyer wind speed indicator and a sling psychrometer were used to measure the wind speed and wet and dry bulb temperatures respectively.

5.1.2 Data Analysis Equipment

The data analysis equipment is schematically represented in Figure 5.1-6 and identified in Table 5.1-2. The microphone amplifier and attenuator were used to adjust the tape recorder output signal level to the proper range for input to the real time analyzer. The analyzer consists of a parallel set of octave and third octave filters followed by an rms detector and averager. It allows simultaneous determination of all of the octave and third octave band levels in a given signal. The PDP 11/10 computer is used to control operation of the analyzer and to store the analyzed data in a disc file. The cathode ray tube (CRT) terminal was used to input commands to the computer and to display analysis results. A thermal copier was used to make hard copies of results displayed on the CRT screen.

5.2 ACOUSTIC DATA ACQUISITION TECHNIQUES

Two measuring systems as shown in Figure 5.1-1 were used to acquire the data. One system was located on the top deck of the tower--it was

Dwg. 7697A75

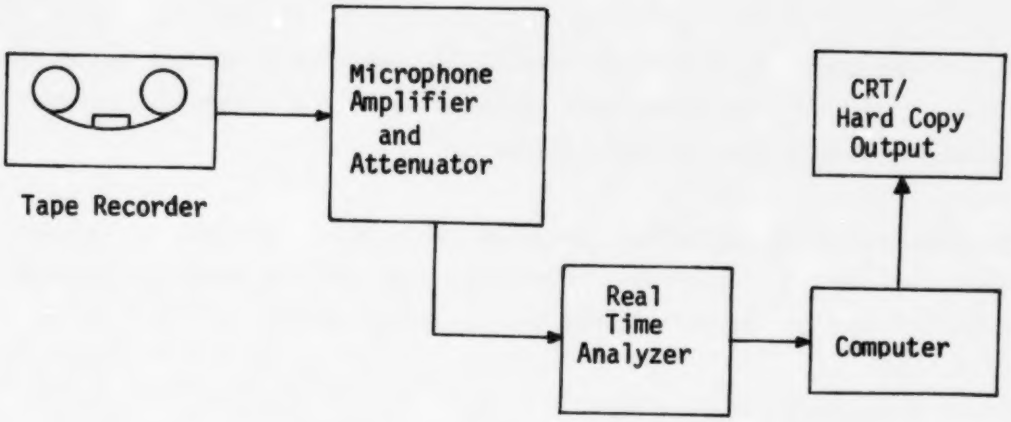
Tape Recorder
Microphone Amplifier and Attenuator
Real Time Analyzer
Computer
CRT/ Hard Copy Output

Figure 5.1-6. Data Reduction Equipment.

TABLE 5.1-2

DATA REDUCTION EQUIPMENT MODELS

General Radio Type 1921 - octave and third octave real-time analyzer

Stellavox SP-7 professional tape recorder

Digital Equipment Corp. PDP 11/10 Minicomputer System

Tektronix 4010-1 CRT Display Terminal

Tektronix 4631 Thermal Copier

B&K 2608 Microphone Amplifier

used to measure the noise level at the top edge of the fan discharge stack. The second system was located at ground level to make measurements around the tower. The use of two systems reduced the time needed to obtain the data.

For each of the planned tests, measurements were made approximately five feet above the ground at the locations shown in Figure 5.2-1 and at the rim of the fan discharge stack. The measurements near ground level were made at distances of 3, 6 and 12 ft from the louvered face of the tower. The location 6 ft from the louvered face of the tower is labelled location #1 and the location at the fan stack discharge is labelled location #2. These locations were well within the near-field of the tower. The louvered face of the tower was about 40 ft wide and about 40 ft high. Measurements were also made near to the enclosed sides of the tower. As had been expected from Ref. 2, the noise levels near the enclosed sides were so low that they could not be distinguished from the background noise levels measured at the same positions. For this reason, these locations are not shown in Figure 5.2-1 and the data are not presented.

The measurements at ground level were intended to document the noise radiated from the louvered faces. The measurement at the fan stack discharge was intended to determine the stack radiated noise level.

Measurements were not made at distances greater than shown in Figure 5.1-1 because previous work at the site (Reference 2) showed that the background noise level is too high for accurate measurements to be made at greater distances. Measurements of the background noise levels were made at all of the measuring locations before the TVA tower was turned on and again after the tower was turned off at the end of a day's testing.

A windscreen was used on the microphone at all times to reduce the effect of wind gusts. A Dwyer wind speed indicator was used to monitor wind speeds. No data were recorded during periods of excessive wind

Dwg. 7697A76

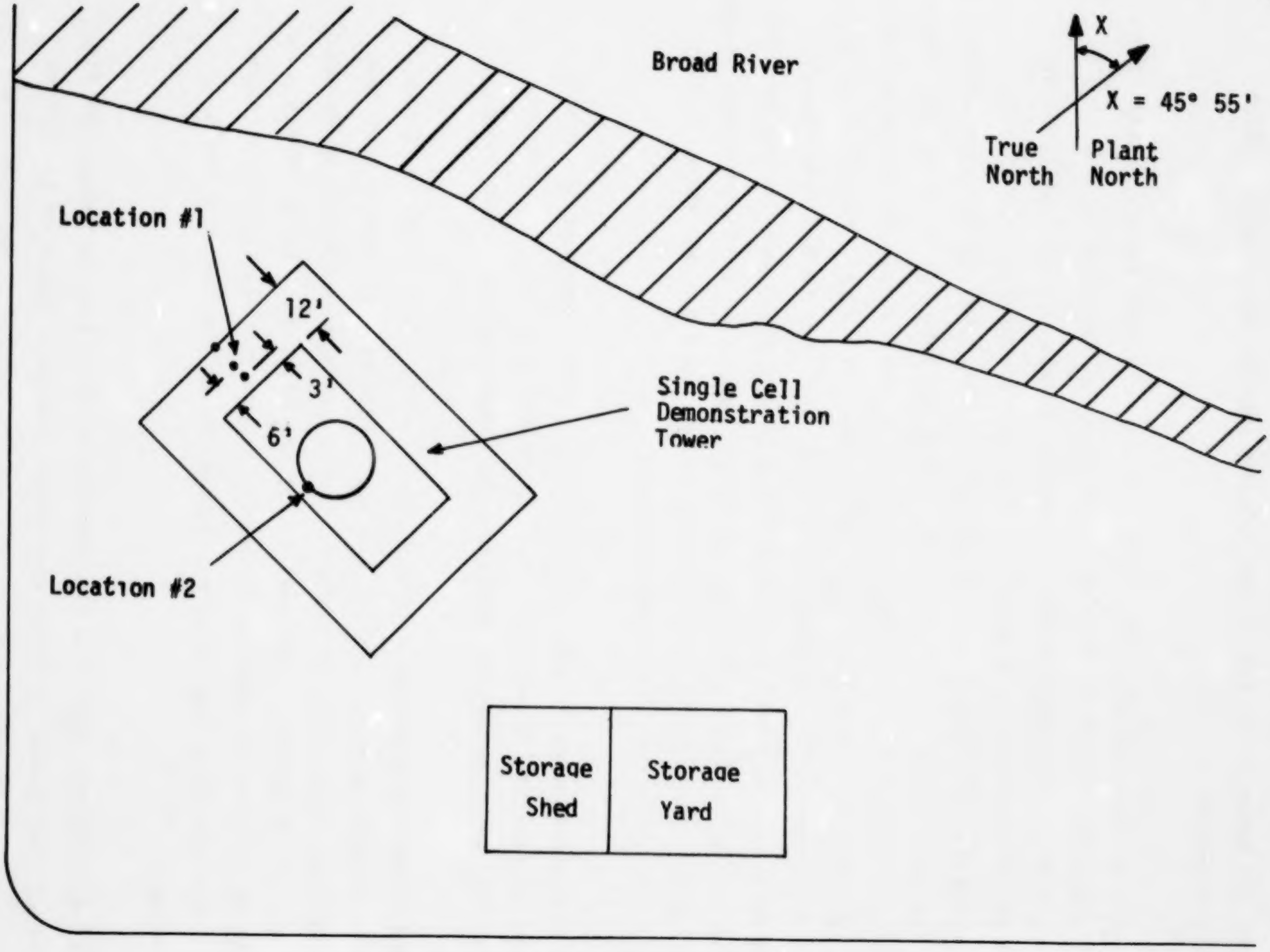
X
X = 45° 55'
True North
Plant North
Broad River
Location #1
12'
3'
6'
Single Cell Demonstration Tower
Location #2
Storage Shed
Storage Yard

Figure 5.2-1. Ground Level Measurement Locations.

speeds. The operator stood to one side and behind the microphone, approximately five to 10 feet away, while data were being recorded. During the recording periods, the sound level was monitored by the operator to ensure that the microphone signal did not overload the sound level meter and/or recorder. A voice microphone was used to record identifying information about each test on the recording tapes. Data were recorded for at least 40 seconds for each of the tests at each of the test locations. A standard calibrator was used to check operation of the sound level meters and to record a calibration signal at the beginning of each reel of tape. This provided a means to accurately reproduce the amplitude of the recorded data.

5.3 ACOUSTIC DATA REDUCTION TECHNIQUES

The field-recorded data were played back into the real-time analyzer illustrated in Figure 5.1-2. The recorded calibration signal was used to adjust the analyzer input gain to the proper value. Each of the input data records was averaged for 32 seconds. The octave band, A-weighted and linear sound pressure level values were then outputted to the minicomputer. When the data analysis was complete, a data reduction program was run on the minicomputer. This program formatted the analyzed data, corrected the data for the effects of background noise and printed out the results on a CRT terminal. The data from the real time analyzer for the 31 tests and the background noise levels are listed in Appendix E. The analyzed data corrected for the background noise were used as input for the regression analysis to fit a model to the data (see Section 5.4).

5.4 ANALYSIS OF DATA

This section describes the statistical models formulated from the experimental data and the procedures utilized in their formulation.

TABLE 5.4-1

INDEPENDENT VARIABLES AND CORRECTED NOISE LEVELS

Test		Physical Variables				Coded Variables				Octave Band Noise Levels* (dB) and Locations							
ID No.	Seq No.	FS (%)	WFR (gpm)	DF (%)	BP (°)	x_1	x_2	x_3	x_4	63 Hz		125 Hz		250 Hz		500 Hz	
										1	2	1	2	1	2	1	2
1	9	50	14000	40	-2	-1.0	-1	-1	-1	70.1	80.2	0.0	79.7	70.4	79.0	71.3	78.7
2	10	100	14000	40	-2	1.0	-1	-1	-1	83.2	94.7	89.1	96.5	83.4	95.5	76.1	91.2
3	11	50	22000	40	-2	-1.0	1	-1	-1	67.9	79.6	0.0	78.3	72.6	79.6	72.1	78.7
4	12	100	22000	40	-2	1.0	1	-1	-1	82.1	94.7	88.0	96.2	83.4	95.0	75.3	91.0
5	13	50	14000	80	-2	-1.0	-1	1	-1	71.7	78.1	66.6	80.0	72.0	79.3	72.4	78.4
6	14	100	14000	80	-2	1.0	-1	1	-1	84.0	95.0	90.1	96.7	84.9	95.5	76.3	91.0
7	15	50	22000	80	-2	-1.0	1	1	-1	71.2	77.1	63.9	77.9	74.4	78.5	72.1	77.4
8	16	100	22000	80	-2	1.0	1	1	-1	82.7	95.5	89.8	96.5	83.7	95.2	75.8	90.5
9	18	50	14000	40	2	-1.0	-1	-1	1	70.1	78.4	0.0	76.7	70.7	77.4	70.7	75.3
10	19	100	14000	40	2	1.0	-1	-1	1	83.7	97.5	89.3	98.0	83.4	96.5	77.1	92.5
11	20	50	22000	40	2	-1.0	1	-1	1	67.0	77.5	0.0	77.1	72.0	78.2	71.8	76.6
12	21	100	22000	40	2	1.0	1	-1	1	84.3	97.2	89.3	97.2	84.9	96.0	76.9	92.0
13	22	50	14000	80	2	-1.0	-1	1	1	70.1	77.8	0.0	80.0	71.0	78.2	71.5	76.3
14	23	100	14000	80	2	1.0	-1	1	1	84.5	96.5	89.6	98.2	83.9	96.3	79.9	92.8
15	24	50	22000	80	2	-1.0	1	1	1	71.2	78.1	63.9	79.3	73.5	77.7	73.2	75.8
16	25	100	22000	80	2	1.0	1	1	1	84.3	96.5	90.1	97.2	84.7	96.0	77.9	92.3
17	1	50	18000	60	0	-1.0	0	0	0	65.9	77.8	63.9	79.7	71.7	79.0	72.6	78.4
18	3	105	18000	60	0	1.2	0	0	0	83.2	96.5	89.1	97.7	83.9	95.5	77.4	93.0
19	5	75	10000	60	0	0.0	-2	0	0	76.2	87.9	79.0	87.0	75.8	84.9	72.4	82.5
20	7	75	26000	60	0	0.0	2	0	0	76.5	87.4	79.0	85.9	76.6	84.9	73.7	82.5
21	28	75	18000	20	0	0.0	0	-2	0	74.7	86.6	75.8	85.1	73.8	83.7	72.4	80.4
22	30	75	18000	100	0	0.0	0	2	0	75.5	86.3	78.3	86.7	75.8	84.9	72.1	81.2
23	17	75	18000	60	-4	0.0	0	0	-2	76.2	87.1	80.3	87.8	76.9	87.5	72.9	83.2
24	26	75	18000	60	4	0.0	0	0	2	72.7	85.3	72.3	85.1	72.0	83.7	70.1	80.7
25	2	75	18000	60	0	0.0	0	0	0	75.8	87.6	78.3	87.0	75.5	84.4	72.6	82.5
26	4	75	18000	60	0	0.0	0	0	0	75.5	87.6	78.6	86.7	75.5	84.4	72.4	82.7
27	6	75	18000	60	0	0.0	0	0	0	75.5	87.1	77.9	86.4	75.0	84.9	72.4	83.2
28	8	75	18000	60	0	0.0	0	0	0	75.8	87.6	78.3	86.7	75.3	85.2	72.9	83.0
29	29	75	18000	60	0	0.0	0	0	0	74.0	86.9	75.8	85.9	73.8	83.9	70.7	80.2
30	27	75	18000	60	0	0.0	0	0	0	74.3	87.1	76.7	86.2	73.8	84.2	71.0	81.4
31	31	75	18000	60	0	0.0	0	0	0	74.3	86.3	76.2	85.6	73.5	84.4	71.3	80.9

---

[*] dB re 20 $\mu N/m^2$

(Continued)

5.4.1 Experimental Design

A central composite experimental design in four independent variables was selected to guide the data acquisition. The four physical independent variables are the fan speed (FS), percent, total water flow rate (WFR), gpm, blade pitch (BP), degrees, and dry flow percentage (DF)[1]. For convenience in the analysis, the physical variables are expressed in a standardized or coded form defined as follows:

$$\begin{aligned} x_1 &= (FS - 75)/25 \\ x_2 &= (WFR - 18000)/4000 \\ x_3 &= (DF - 60)/20 \\ x_4 &= BP/2 \end{aligned} \qquad (5.4\text{-}1)$$

Table 5.4-1 lists the 31 tests required for this design, the corresponding values of the physical and coded variables and the sequence in which the tests were performed.

Column 1 gives the test number, which follows a standardized or "experimental design" pattern that is evident in the coded variables of columns 7-10. Column 2 lists the actual prespecified order in which the tests were conducted; e.g., Test 17 was run first, Test 25 second, etc. The experimental design consists of three kinds of combinations of the coded independent variables. Tests 1-16 are all combinations of a 2^4 factorial design, where $(x_1,x_2,x_3,x_4) = (\pm1,\pm1,\pm1,\pm1)$. Tests 17-24 are eight so-called axial combinations, where one x_i assumes extreme values while the other three x_i's assume the center value zero. Tests 25-31 are repeat runs of the design's center point (0,0,0,0). Such

---

[1] The percent of the total water flow rate passing through the heat exchangers.

Table 5.4-1 (cont'd)

Test		Physical Variables				Coded Variables				Octave Band Noise Levels (dB) and Locations							
ID No.	Seq No.	FS (%)	WFR (gpm)	DF (%)	BP (°)	x_1	x_2	x_3	x_4	1000 Hz		2000 Hz		4000 Hz		8000 Hz	
										1	2	1	2	1	2	1	2
1	9	50	14000	40	-2	-1.0	-1	-1	-1	70.6	75.6	66.9	70.3	63.4	69.6	61.2	66.7
2	10	100	14000	40	-2	1.0	-1	-1	-1	75.6	90.8	70.1	88.3	62.5	78.0	58.8	73.0
3	11	50	22000	40	-2	-1.0	1	-1	-1	71.4	75.4	68.7	71.6	65.6	70.4	63.6	69.5
4	12	100	22000	40	-2	1.0	1	-1	-1	74.3	90.0	69.5	87.5	64.3	78.2	61.2	74.0
5	13	50	14000	80	-2	-1.0	-1	1	-1	71.7	75.6	67.1	70.8	62.8	69.3	59.9	66.9
6	14	100	14000	80	-2	1.0	-1	1	-1	75.6	90.5	70.3	88.5	61.9	79.0	57.7	73.2
7	15	50	22000	80	-2	-1.0	1	1	-1	72.0	74.3	67.7	71.6	64.5	70.4	62.3	69.5
8	16	100	22000	80	-2	1.0	1	1	-1	73.8	89.8	69.5	87.3	63.4	79.2	60.2	74.2
9	18	50	14000	40	2	-1.0	-1	-1	1	70.9	73.6	67.1	68.7	63.7	66.4	60.7	65.4
10	19	100	14000	40	2	1.0	-1	-1	1	75.4	90.0	68.7	87.5	62.5	80.7	57.4	75.2
11	20	50	22000	40	2	-1.0	1	-1	1	71.2	73.3	67.9	70.8	64.5	70.4	61.8	70.5
12	21	100	22000	40	2	1.0	1	-1	1	75.9	89.5	68.5	86.5	62.2	80.7	58.2	76.0
13	22	50	14000	80	2	-1.0	-1	1	1	69.5	73.6	66.6	70.3	62.2	68.8	58.2	66.9
14	23	100	14000	80	2	1.0	-1	1	1	82.0	90.5	68.2	87.5	60.4	80.5	55.0	74.5
15	24	50	22000	80	2	-1.0	1	1	1	72.0	73.8	68.7	71.6	63.7	70.1	60.7	69.5
16	25	100	22000	80	2	1.0	1	1	1	77.2	89.5	68.7	87.3	61.9	80.7	57.1	75.5
17	1	50	18000	60	0	-1.0	0	0	0	71.2	73.8	67.4	68.2	63.4	63.7	60.7	56.5
18	3	105	18000	60	0	1.2	0	0	0	74.9	90.0	69.5	86.8	62.2	74.7	58.5	65.1
19	5	75	10000	60	0	0.0	-2	0	0	71.7	82.5	67.1	74.9	61.9	66.2	57.9	57.9
20	7	75	26000	60	0	0.0	2	0	0	72.8	82.0	68.5	73.9	64.5	67.2	60.4	59.9
21	28	75	18000	20	0	0.0	0	-2	0	70.9	81.2	67.7	75.7	64.3	71.9	62.3	70.2
22	30	75	18000	100	0	0.0	0	2	0	70.9	83.5	64.9	75.7	57.9	68.8	52.2	62.8
23	17	75	18000	60	-4	0.0	0	0	-2	73.0	86.5	68.2	76.7	63.7	71.9	61.5	69.5
24	26	75	18000	60	4	0.0	0	0	2	69.8	80.0	66.6	75.2	63.4	71.7	60.7	69.5
25	2	75	18000	60	0	0.0	0	0	0	72.5	82.5	67.9	74.7	63.4	66.4	60.4	58.8
26	4	75	18000	60	0	0.0	0	0	0	72.3	82.5	67.7	74.4	63.4	66.7	61.0	58.8
27	6	75	18000	60	0	0.0	0	0	0	72.3	82.5	68.5	74.4	63.4	67.0	61.5	60.4
28	8	75	18000	60	0	0.0	0	0	0	72.5	82.0	68.2	74.2	64.5	67.2	61.8	58.5
29	29	75	18000	60	0	0.0	0	0	0	70.1	82.0	66.9	75.9	62.5	71.9	60.4	69.5
30	27	75	18000	60	0	0.0	0	0	0	69.8	82.0	66.6	76.2	62.8	72.4	61.0	68.9
31	31	75	18000	60	0	0.0	0	0	0	70.6	81.2	66.9	75.4	62.8	71.4	61.0	68.9

an experimental design yields a good estimate of a full second-order statistical model in the x_i's, as described in Section 5.4-3.

5.4.2 Observed Noise Levels

An initial examination of the data obtained at the three measuring locations near the ground showed that (1) the data at 3 and 6 ft. were virtually identical and (2) the data at 12 ft. were more affected by the background noise levels than that at 3 and 6 ft. Consequently the data obtained at 6 ft. (Location #1) were chosen for use in the regression analysis along with the data obtained at the fan stack discharge (Location #2).

Table 5.4-1 lists the measured noise levels corrected for the background noise (the dependent variables) for these two locations. The data consist of octave band sound levels for the bands from 63 Hz to 8 kHz. The background noise data and the uncorrected data are presented in Appendix E.

Several of the corrected data values in Table 5.4-1 for the 125 Hz octave band at Location 1 are listed as zero. These are test conditions for which the tower noise was less than 3 dB above the background. In these cases no conclusion can be drawn about the true value of the tower noise level and, hence, zero values are listed. These values were not included in the regression analysis.

5.4.3 Statistical Model

The general form of the statistical model, relating the dependent variable, y, to the four independent variables, is

$$y = \beta_o + \sum_{i=1}^{4} \beta_i x_i + \sum_{i=1}^{4} \beta_{ii} x_i^2 + \sum_{\substack{ij \\ i<j}}\sum \beta_{ij} x_i x_j \qquad (5.4\text{-}2)$$

TABLE 5.4-2

FITTED COEFFICIENTS FOR SURVIVING MODEL TERMS

Model Term	Octave Band Coefficients 63 Hz 1	 2	 125 Hz 1	 2	 250 Hz 1	 2	 500 Hz 1	 2
Constant	74.87	87.03	77.14	86.36	74.65	84.58	72.10	82.10
1	6.92	8.76	12.48	9.05	5.85	8.41	2.41	7.10
2	¯0.25		¯0.10	¯0.34	0.46		0.10	
3	0.53			0.40	0.47			
4		0.04	¯1.11	¯0.14	¯0.43	¯0.37	0.09	¯0.35
11	1.03		¯0.98	1.41	2.80	2.07	2.27	2.53
22	0.53		0.53		0.47			
33								¯0.29
44						0.32		
12					¯0.47		¯0.43	
13								
14		0.69	0.84	0.47		0.52	0.55	0.93

Model Term	Octave Band Coefficients 1000 Hz 1	 2	 2000 Hz 1	 2	 4000 Hz 1	 2	 8000 Hz 1	 2
Constant	71.56	81.97	67.54	74.75	63.42	68.18	60.83	61.84
1	2.35	7.76	0.79	8.29	¯0.69	4.95	¯1.38	3.09
2	¯0.06		0.29	0.01	0.66		0.88	
3			¯0.25	0.15	¯0.85	¯0.11	¯1.33	¯0.62
4	0.10	¯0.89	¯0.36	¯0.36	¯0.33	0.16	¯0.72	0.27
11	1.94		1.07	3.21		3.66		4.34
22							¯0.39	
33			¯0.28	0.40	¯0.49	0.86	¯0.87	1.67
44		0.30		0.46		1.21		2.41
12	¯0.70		¯0.40	¯0.55				
13								
14	0.82		¯0.33					

The β_o and β_i terms denote the unknown model coefficients to be estimated by the method of least squares. This model has the obvious capability of estimating the (x_1,x_2,x_3,x_4) combination associated with minimal (or maximal) y, should the experimental region contain such a combination.

Since there is no theoretical model for relating the noise, y, to the x_i terms, we use the above second-order model and assume that it is of the correct form, with the unknown β's to be estimated by least squares. If the assumed form is a poor approximation to the correct form for one or more of the y's, the quality of interpolative y-predictions (i.e., predictions of y at x-combinations between ones actually included in the experimental design) will diminish somewhat and that of extrapolative y-predictions even more. To fit and assess a more complex model would require a much larger experiment.

In practice, most of the potential terms will be dropped from the model. When we initially fit the full model to a particular y we generally find several b's (least square estimates of the β's) do not differ significantly from zero, as judged by an estimate of experimental error obtained from the differences between observed y's and fitted $\hat{y}$'s calculated from the fitted model. A process of iteration thus begins, since dropping the β's corresponding to the least significant b's from the model will (1) always change and often decrease the estimated experimental error, and (2) may alter the relative importance of the remaining β's, although such alterations will be small in the case of our symmetrical experimental design. We proceed in this way until all surviving second-order b's are significant at the 10% level. There is little basis for dropping any insignificant first-order term, say $\beta_i x_i$, as long as x_i is still present in at least one surviving second-order term.

Table 5.4-2 lists the fitted coefficients corresponding to all surviving model terms. These coefficients may be used to predict noise level

TABLE 5.4-3

COMPARISON OF MEASURED (y) AND PREDICTED ($\hat{y}$) NOISE LEVELS* WITH STANDARD ERROR (s)

63 Hz Octave Band								125 Hz Octave Band							
Location 1				Location 2				Location 1				Location 2			
y	$\hat{y}$	e	s(y)	y	$\hat{y}$	e	s(y)	y	$\hat{y}$	e	s(y)	y	$\hat{y}$	e	s(y)
70.1	69.2	0.8	0.57	80.2	78.9	1.2	0.34	89.1	89.5	-0.5	0.71	79.7	79.3	0.4	0.46
83.2	83.1	0.1	0.55	94.7	95.1	-0.3	0.34	88.0	89.3	-1.3	0.69	96.5	96.4		0.45
67.9	68.7	-0.8	0.57	79.6	78.9	0.7	0.34	66.6	66.3	0.3	0.90	78.3	78.6	-0.3	0.46
82.1	82.6	-0.4	0.55	94.7	95.1	-0.3	0.34	90.1	89.5	0.6	0.71	96.2	95.7	0.5	0.45
71.7	70.3	1.4	0.57	78.1	78.9	-0.8	0.34	63.9	66.1	-2.1	0.89	80.0	80.1	-0.1	0.46
84.0	84.1	-0.1	0.55	95.0	95.1	-0.1	0.34	89.8	89.3	0.5	0.69	96.7	97.2	-0.5	0.45
71.2	69.8	1.4	0.57	77.1	78.9	-1.8	0.34	89.3	89.0	0.4	0.69	77.9	79.4	-1.5	0.46
82.7	83.6	-1.0	0.55	95.5	95.1	0.4	0.34	89.3	88.8	0.5	0.71	96.5	96.5	-0.1	0.45
70.1	69.2	0.8	0.57	78.4	77.6	0.8	0.34	89.6	89.0	0.6	0.69	76.7	78.1	-1.4	0.46
83.7	83.1	0.7	0.55	97.5	96.5	1.0	0.34	63.9	62.2	1.8	1.06	98.0	97.1	0.9	0.45
67.0	68.7	-1.7	0.57	77.5	77.6	-0.2	0.34	90.1	88.8	1.3	0.71	77.1	77.4	-0.3	0.46
84.3	82.6	1.7	0.55	97.2	96.5	0.7	0.34	63.9	63.7	0.2	0.72	97.2	96.4	0.8	0.45
70.1	70.3	-0.2	0.57	77.8	77.6	0.2	0.34	89.1	90.7	-1.6	0.63	80.0	78.8	1.2	0.46
84.5	84.1	0.4	0.55	96.5	96.5		0.34	79.0	79.4	-0.5	1.12	98.2	97.9	0.3	0.45
71.2	69.8	1.4	0.57	78.1	77.6	0.5	0.34	79.0	79.1	-0.1	1.11	79.3	78.2	1.2	0.46
84.3	83.6	0.6	0.55	96.5	96.5		0.34	75.8	77.1	-1.4	0.41	97.2	97.2		0.45
65.9	69.0	-3.1	0.47	77.8	78.3	-0.5	0.23	78.3	77.1	1.1	0.41	79.7	78.7	1.0	0.28
83.2	84.7	-1.5	0.60	96.5	97.5	-1.1	0.26	80.3	79.4	1.0	0.79	97.7	99.2	-1.5	0.36
76.2	77.5	-1.3	1.02	87.9	87.0	0.9	0.14	72.3	74.9	-2.6	0.79	87.0	87.0	-0.1	0.41
76.5	76.5		1.02	87.4	87.0	0.3	0.14	78.3	77.1	1.1	0.41	85.9	85.7	0.2	0.41
74.7	73.8	0.9	0.65	86.6	87.0	-0.4	0.14	78.6	77.1	1.5	0.41	85.1	85.6	-0.5	0.41
75.5	75.9	-0.5	0.65	86.3	87.0	-0.7	0.14	77.9	77.1	0.7	0.41	86.7	87.2	-0.5	0.41
76.2	74.9	1.3	0.39	87.1	87.0	0.2	0.35	78.3	77.1	1.1	0.41	87.8	86.6	1.1	0.41
72.7	74.9	-2.2	0.39	85.3	87.1	-1.8	0.35	75.8	77.1	-1.4	0.41	85.1	86.1	-1.0	0.41
75.8	74.9	0.9	0.39	87.6	87.0	0.6	0.14	76.7	77.1	-0.5	0.41	87.0	86.4	0.6	0.23
75.5	74.9	0.6	0.39	87.6	87.0	0.6	0.14	76.2	77.1	-0.9	0.41	86.7	86.4	0.3	0.23
75.5	74.9	0.6	0.39	87.1	87.0	0.1	0.14					86.4	86.4	0.1	0.23
75.8	74.9	0.9	0.39	87.6	87.0	0.6	0.14					86.7	86.4	0.3	0.23
74.0	74.9	-0.9	0.39	86.9	87.0	-0.2	0.14					85.9	86.4	-0.5	0.23
74.3	74.9	-0.5	0.39	87.1	87.0	0.1	0.14					86.2	86.4	-0.2	0.23
74.3	74.9	-0.5	0.39	86.3	87.0	-0.7	0.14					85.6	86.4	-0.7	0.23

(Continued)

---

* dB re 20 $\mu N/m^2$

at any combination of interest provided that the variables are properly coded. An example follows:

Predict the 63 Hz octave band noise level at the fan stack discharge

Fan Speed = 70% — $x_1 = -0.2$

Water Flow Rate = immaterial
Dry Flow % = immaterial
} Terms did not survive

Blade Pitch = +1 degree — $x_4 = +0.5$

Substitute $x_1 = -0.2$ and $x_4 = +0.5$ into

$$\hat{y} = 87.03 + 8.76x_1 + 0.04x_4 + 0.69x_1x_4$$

$$\hat{y} \simeq 85 \text{ dB}$$

5.4.4 Examination of Model Fit

Table 5.4-3 lists the observed sound levels y, the corresponding fitted sound levels $\hat{y}$, the differences or residuals $e = y - \hat{y}$, and the standard errors $s(y)$ of the fitted $\hat{y}$'s. Clearly, the residuals must necessarily exhibit whatever lack of fit there is between model and observed data; hence, examination of model fit implies careful study of the residuals. We find no evidence that the assumed second-order model fails to adequately represent the effects of the four independent variables. Also, we find no significant trends in the residuals (trends which would indicate drift in the measurement process) with respect to the order of measurement, although occasionally residuals of very large absolute magnitude occur for which we have no explanation.

The most striking example of large absolute residuals occurs for Test ID 28, 30 and 31 at Location 2 for the 8000 Hz octave band; Table 5.4-3 shows residuals of 7.6, 7.1, and 7.1 for these tests, respectively. It is interesting to note that the noise levels for these tests (Table 5.4-1) are relatively low. It is possible that fluctuations in the background noise were sufficiently large so that the average background noise correction applied to the measured data was not adequate.

Table 5.4-3 (cont'd)

250 Hz Octave Band								500 Hz Octave Band							
Location 1				Location 2				Location 1				Location 2			
y	$\hat{y}$	e	s(y)	y	$\hat{y}$	e	s(y)	y	$\hat{y}$	e	s(y)	y	$\hat{y}$	e	s(y)
70.4	71.1	-0.7	0.53	79.0	79.5	-0.4	0.35	71.3	71.9	-0.6	0.57	78.7	78.5	0.2	0.40
83.4	83.7	-0.3	0.53	95.5	95.2	0.3	0.35	76.1	76.5	-0.4	0.56	91.2	90.9	0.4	0.40
72.6	73.0	-0.3	0.53	79.6	79.5	0.1	0.35	72.1	73.0	-0.9	0.57	78.7	78.5	0.2	0.40
83.4	83.7	-0.3	0.53	95.0	95.2	-0.2	0.35	75.3	75.8	-0.5	0.56	91.0	90.9	0.1	0.40
72.0	72.0		0.53	79.3	79.5	-0.2	0.35	72.4	71.9	0.5	0.57	78.4	78.5	-0.1	0.40
84.9	84.7	0.3	0.53	95.5	95.2	0.3	0.35	76.3	76.5	-0.1	0.56	91.0	90.9	0.1	0.40
74.4	73.9	0.5	0.53	78.5	79.5	-0.9	0.35	72.1	73.0	-0.9	0.57	77.4	78.5	-1.1	0.40
83.7	84.7	-1.0	0.53	95.2	95.2		0.35	75.8	75.8		0.56	90.[illegible]	90.9	-0.4	0.40
70.7	70.2	0.5	0.53	77.4	77.7	-0.2	0.35	70.7	71.0	-0.3	0.57	75.3	76.0	-0.7	0.40
83.4	82.9	0.6	0.53	96.5	95.5	1.0	0.35	77.1	77.7	-0.6	0.56	92.5	92.0	0.5	0.40
72.0	72.1	-0.1	0.53	78.2	77.7	0.6	0.35	71.8	72.0	-0.2	0.57	76.6	76.0	0.6	0.40
84.9	82.9	2.1	0.53	96.0	95.5	0.5	0.35	76.9	77.1	-0.2	0.56	92.0	92.0		0.40
71.0	71.2	-0.1	0.53	78.2	77.7	0.6	0.35	71.5	71.0	0.6	0.57	76.3	76.0	0.4	0.40
83.9	83.8	0.1	0.53	96.3	95.5	0.7	0.35	79.9	77.7	2.2	0.56	92.8	92.0	0.7	0.40
73.5	73.0	0.5	0.53	77.7	77.7		0.35	73.2	72.0	1.2	0.57	75.8	76.0	-0.1	0.40
84.7	83.8	0.9	0.53	96.0	95.5	0.5	0.35	77.9	77.1	0.8	0.56	92.3	92.0	0.2	0.40
71.7	71.6	0.1	0.36	79.0	78.2	0.8	0.28	72.6	72.0	0.7	0.33	78.4	77.5	0.9	0.29
83.9	85.7	-1.8	0.46	95.5	97.7	-2.2	0.36	77.4	78.3	-0.9	0.44	93.0	94.3	-1.3	0.37
75.8	75.6	0.2	0.77	84.9	84.6	0.4	0.23	72.4	71.9	0.5	0.49	82.5	82.1	0.4	0.24
76.6	77.5	-0.8	0.77	84.9	84.6	0.4	0.23	73.7	72.3	1.4	0.49	82.5	82.1	0.4	0.24
73.8	73.7	0.1	0.49	83.7	84.6	-0.9	0.23	72.4	72.1	0.3	0.28	80.4	80.9	-0.5	0.63
75.8	75.6	0.2	0.49	84.9	84.6	0.4	0.23	72.1	72.1		0.28	81.2	80.9	0.3	0.63
76.9	75.5	1.4	0.49	87.5	86.6	0.9	0.60	72.9	71.9	1.0	0.49	83.2	82.8	0.4	0.40
72.0	73.8	-1.8	0.49	83.7	85.1	-1.5	0.60	70.1	72.3	-2.1	0.49	80.7	81.4	-0.7	0.40
75.5	74.6	0.9	0.29	84.4	84.6	-0.1	0.23	72.6	72.1	0.5	0.28	82.5	82.1	0.4	0.24
75.5	74.6	0.9	0.29	84.4	84.6	-0.1	0.23	72.4	72.1	0.3	0.28	82.7	82.1	0.6	0.24
75.0	74.6	0.3	0.29	84.9	84.6	0.4	0.23	72.4	72.1	0.3	0.28	83.2	82.1	1.1	0.24
75.3	74.6	0.6	0.29	85.2	84.6	0.6	0.23	72.9	72.1	0.8	0.28	83.0	82.1	0.9	0.24
73.8	74.6	-0.8	0.29	83.9	84.6	-0.7	0.23	70.7	72.1	-1.4	0.28	80.2	82.1	-1.9	0.24
73.8	74.6	-0.8	0.29	84.2	84.6	-0.4	0.23	71.0	72.1	-1.1	0.28	81.4	82.1	-0.6	0.24
73.5	74.6	-1.1	0.29	84.4	84.6	-0.1	0.23	71.3	72.1	-0.8	0.28	80.9	82.1	-1.1	0.24

(Continued)

Table 5.4-3 (cont'd)

1000 Hz Octave Band								2000 Hz Octave Band							
Location 1				Location 2				Location 1				Location 2			
y	$\hat{y}$	e	s(y)	y	$\hat{y}$	e	s(y)	y	$\hat{y}$	e	s(y)	y	$\hat{y}$	e	s(y)
70.6	71.2	-0.6	0.84	75.6	75.4	0.2	0.29	66.9	67.1	-0.3	0.36	70.3	70.2	0.1	0.52
75.6	75.7	-0.1	0.83	90.8	90.9	-0.2	0.29	70.1	70.2	-0.1	0.36	88.3	87.9	0.4	0.51
71.4	72.5	-1.1	0.84	75.4	75.4		0.29	68.7	68.5	0.2	0.36	71.6	71.3	0.3	0.52
74.3	74.2	0.2	0.83	90.0	90.9	-0.9	0.29	69.5	70.0	-0.4	0.36	87.5	86.8	0.7	0.51
71.7	71.2	0.5	0.84	75.6	75.4	0.2	0.29	67.1	66.6	0.5	0.36	70.8	70.5	0.4	0.52
75.6	75.7	-0.1	0.83	90.5	90.9	-0.4	0.29	70.3	69.7	0.7	0.36	88.5	88.2	0.3	0.51
72.0	72.5	-0.5	0.84	74.3	75.4	-1.1	0.29	67.7	68.0	-0.3	0.36	71.6	71.6		0.52
73.8	74.2	-0.3	0.83	89.8	90.9	-1.2	0.29	69.5	69.4	0.1	0.36	87.3	87.1	0.2	0.51
70.9	69.8	1.1	0.84	73.6	73.6	-0.1	0.29	67.1	67.1	0.1	0.36	68.7	69.5	-0.7	0.52
75.4	77.5	-2.1	0.83	90.0	89.1	0.9	0.29	68.7	68.8	-0.1	0.36	87.5	87.1	0.4	0.51
71.2	71.1	0.1	0.84	73.3	73.6	-0.3	0.29	67.9	68.5	-0.5	0.36	70.8	70.6	0.3	0.52
75.9	76.0	-0.1	0.83	89.5	89.1	0.4	0.29	68.5	68.6	-0.1	0.36	86.5	86.1	0.4	0.51
69.5	69.8	-0.2	0.84	73.6	73.6	-0.1	0.29	66.6	66.6		0.36	70.3	69.8	0.6	0.52
82.0	77.5	4.4	0.83	90.5	89.1	1.4	0.29	68.2	68.3	-0.1	0.36	87.5	87.4	0.1	0.51
72.0	71.1	0.9	0.84	73.8	73.6	0.2	0.29	68.7	68.0	0.8	0.36	71.6	70.9	0.8	0.52
77.2	76.0	1.2	0.83	89.5	89.1	0.4	0.29	68.7	68.1	0.7	0.36	87.3	86.4	0.9	0.51
71.2	71.1		0.50	73.8	74.2	-0.4	0.26	67.4	67.8	-0.4	0.22	68.2	69.7	-1.4	0.39
74.9	77.2	-2.3	0.65	90.0	91.3	-1.3	0.29	69.5	70.0	-0.5	0.28	86.8	89.3	-2.6	0.48
71.7	71.7		0.73	82.5	82.0	0.5	0.18	67.1	67.0	0.2	0.31	74.9	74.7	0.2	0.49
72.8	71.4	1.3	0.73	82.0	82.0		0.18	68.5	68.1	0.3	0.31	73.9	74.8	-0.8	0.49
70.9	71.6	-0.6	0.41	81.2	82.0	-0.7	0.18	67.7	66.9	0.7	0.48	75.7	76.0	-0.3	0.75
70.9	71.6	-0.6	0.41	83.5	82.0	1.5	0.18	64.9	65.9	-1.0	0.48	75.7	76.6	-0.9	0.75
73.0	71.4	1.7	0.73	86.5	84.9	1.6	0.60	68.2	68.3		0.31	76.7	77.3	-0.6	0.75
69.8	71.8	-1.9	0.73	80.0	81.4	-1.4	0.60	66.6	66.8	-0.2	0.31	75.2	75.9	-0.7	0.75
72.5	71.6	1.0	0.41	82.5	82.0	0.5	0.18	67.9	67.5	0.4	0.18	74.7	74.7	-0.1	0.31
72.3	71.6	0.7	0.41	82.5	82.0	0.5	0.18	67.7	67.5	0.1	0.18	74.4	74.7	-0.3	0.31
72.3	71.6	0.7	0.41	82.5	82.0	0.5	0.18	68.5	67.5	0.9	0.18	74.4	74.7	-0.3	0.31
72.5	71.6	1.0	0.41	82.0	82.0		0.18	68.2	67.5	0.7	0.18	74.2	74.7	-0.6	0.31
70.1	71.6	-1.5	0.41	82.0	82.0		0.18	66.9	67.5	-0.7	0.18	75.9	74.7	1.2	0.31
69.8	71.6	-1.7	0.41	82.0	82.0		0.18	66.6	67.5	-1.0	0.18	76.2	74.7	1.5	0.31
70.6	71.6	-0.9	0.41	81.2	82.0	-0.7	0.18	66.9	67.5	-0.7	0.18	75.4	74.7	0.7	0.31

(Continued)

Table 5.4-3 (cont'd)

4000 Hz Octave Band								8000 Hz Octave Band							
Location 1				Location 2				Location 1				Location 2			
y	$\hat{y}$	e	s(y)	y	$\hat{y}$	e	s(y)	y	$\hat{y}$	e	s(y)	y	$\hat{y}$	e	s(y)
63.4	64.1	-0.7	0.35	69.6	68.9	0.7	1.01	61.2	62.1	-0.9	0.51	66.7	67.5	-0.8	1.75
62.5	62.8	-0.2	0.35	78.0	78.8	-0.8	0.99	58.8	59.4	-0.6	0.51	73.0	73.7	-0.7	1.72
65.6	65.5	0.2	0.35	70.4	68.9	1.5	1.01	63.6	63.9	-0.3	0.51	69.5	67.5	1.9	1.75
64.3	64.1	0.2	0.35	78.2	78.8	-0.6	0.99	61.2	61.1	0.1	0.51	74.0	73.7	0.3	1.72
62.8	62.4	0.4	0.35	69.3	68.7	0.6	1.01	59.9	59.5	0.4	0.51	66.9	66.3	0.6	1.75
61.9	61.1	0.9	0.35	79.0	78.6	0.4	0.99	57.7	56.7	1.0	0.51	73.2	72.5	0.8	1.72
64.5	63.8	0.8	0.35	70.4	68.7	1.7	1.01	62.3	61.2	1.1	0.51	69.5	66.3	3.2	1.75
63.4	62.4	1.0	0.35	79.2	78.6	0.6	0.99	60.2	58.5	1.7	0.51	74.2	72.5	1.8	1.72
63.7	63.5	0.2	0.35	66.4	69.2	-2.8	1.01	60.7	60.7		0.51	65.4	68.1	-2.7	1.75
62.5	62.1	0.4	0.35	80.7	79.1	1.6	0.99	57.4	57.9	-0.5	0.51	75.2	74.2	1.0	1.72
64.5	64.8	-0.3	0.35	70.4	69.2	1.1	1.01	61.8	62.4	-0.7	0.51	70.5	68.1	2.4	1.75
62.2	63.4	-1.2	0.35	80.7	79.1	1.6	0.99	58.2	59.7	-1.4	0.51	76.0	74.2	1.7	1.72
62.2	61.8	0.5	0.35	68.8	69.0	-0.2	1.01	58.2	58.0	0.2	0.51	66.9	66.8	0.1	1.75
60.4	60.4		0.35	80.5	78.9	1.6	0.99	55.0	55.3	-0.3	0.51	74.5	73.0	1.5	1.72
63.7	63.1	0.6	0.35	70.1	69.0	1.1	1.01	60.7	59.8	0.9	0.51	69.5	66.8	2.6	1.75
61.9	61.7	0.2	0.35	80.7	78.9	1.8	0.99	57.1	57.0	0.1	0.51	75.5	73.0	2.5	1.72
63.4	64.1	-0.7	0.25	63.7	66.9	-3.2	0.94	60.7	62.2	-1.5	0.40	56.5	63.1	-6.6	1.64
62.2	62.6	-0.4	0.27	74.7	79.4	-4.7	1.16	58.5	59.2	-0.6	0.43	65.1	71.8	-6.7	2.01
61.9	62.1	-0.2	0.35	66.2	68.2	-2.0	0.75	57.9	57.5	0.4	0.82	57.9	61.8	-3.9	1.30
64.5	64.7	-0.2	0.35	67.2	68.2	-0.9	0.75	60.4	61.0	-0.6	0.82	59.9	61.8	-2.0	1.30
64.3	63.2	1.1	0.56	71.9	71.8	0.1	1.82	62.3	60.0	2.3	0.82	70.2	69.8	0.5	3.16
57.9	59.8	-1.8	0.56	68.8	71.4	-2.6	1.82	52.2	54.7	-2.5	0.82	62.8	67.3	-4.5	3.16
63.7	64.1	-0.4	0.35	71.9	72.7	-0.8	1.82	61.5	62.3	-0.8	0.54	69.5	70.9	-1.5	3.16
63.4	62.8	0.6	0.35	71.7	73.4	-1.7	1.82	60.7	59.4	1.3	0.54	69.5	72.0	-2.6	3.16
63.4	63.4		0.17	66.4	68.2	-1.7	0.75	60.4	60.8	-0.4	0.30	58.8	61.8	-3.0	1.30
63.4	63.4		0.17	66.7	68.2	-1.5	0.75	61.0	60.8	0.1	0.30	58.8	61.8	-3.0	1.30
63.4	63.4		0.17	67.0	68.2	-1.2	0.75	61.5	60.8	0.7	0.30	60.4	61.8	-1.4	1.30
64.5	63.4	1.1	0.17	67.2	68.2	-0.9	0.75	61.8	60.8	0.9	0.30	58.5	61.8	-3.3	1.30
62.5	63.4	-0.9	0.17	71.9	68.2	3.7	0.75	60.4	60.8	-0.4	0.30	69.5	61.8	7.6	1.30
62.8	63.4	-0.6	0.17	72.4	68.2	4.2	0.75	61.0	60.8	0.1	0.30	68.9	61.8	7.1	1.30
62.8	63.4	-0.6	0.17	71.4	68.2	3.2	0.75	61.0	60.8	0.1	0.30	68.9	61.8	7.1	1.30

Estimates of σ, the standard deviations due to experimental error, can be obtained from the residuals and are listed in Table 5.4-4. The quantity σ is the standard deviation among sound level measurements taken under fixed experimental conditions. Based on the estimate of σ, the form of the experimental design and the final form of the fitted model, the standard error $s(\hat{y})$ of each $\hat{y}$ can be obtained; see Table 5.4-3. This quantity is the standard error of the estimated average sound level at the particular experimental conditions. The standard error , $s(\hat{y})$, is obviously small if σ is small and if $\hat{y}$ is a prediction corresponding to experimental conditions near the center of the experimental design. As we depart from the experimental region $s(\hat{y})$ increases sharply, a consequence of extrapolation. If we recall the six relatively remote axial combinations (Tests 19-24 of Table 5.4-1), we note that these $s(\hat{y})$'s are higher whenever the term $\beta_{kk}x_k^2$ is in the fitted model, where x_k denotes the variable that assumes the extreme values ± 2 in the axial combination.

5.5 NOISE PREDICTION COMPUTER CODE

The original prediction code is based on the material in Reference 7. This code was developed to predict the linear and A-weighted noise levels radiated from the cooling tower without the dry flow heat exchangers.

5.5.1 Program Code Modifications

In the form described in Reference 7, the code did not include corrections for either atmospheric absorption or ground attenuation. Thus the major modifications that were made to this code were (1) incorporating the regression equations from Section 5.4 to account for the effect of the heat exchangers, (2) adding code to calculate the total atmosphere absorption for any conditions, (3) adding code to calculate the absorption of the ground surface between the tower and the receiver and (4) rewriting much of the mainline code to accommodate

TABLE 5.4-4

ESTIMATES OF STANDARD DEVIATION

Octave Band Center Frequency	Estimate of σ, dB	
	Location 1	Location 2
63 Hz	1.3	0.8
125 Hz	1.4	0.8
250 Hz	1.0	0.8
500 Hz	1.0	0.8
1000 Hz	1.5	0.8
2000 Hz	0.6	0.9
4000 Hz	0.8	2.3
8000 Hz	1.1	4.0

calculations on an octave band rather than an overall frequency basis. This last step was necessary because the atmospheric and ground attenuations are frequency-dependent and, hence, cannot be applied directly to the linear and A-weighted sound levels.

5.5.1.1 Atmospheric Absorption

Correcting noise propagation over ground terrain has been a very difficult task because of the need to know the complex acoustic impedance over the ground between the source and receiver. In the last few years, considerable success has been achieved in modeling the ground surface with the acoustic properties of fibrous absorbent materials. Delany and Bazley[6] determined expressions for the complex acoustic impedance of the fibrous materials as a function of frequency and the flow resistance of the material. Chessel[4,5] was the first to show that use of these impedance expressions along with either Rudnick's[7] or Ingard's[8] theory of sound reflection from a finite impedance produced results for ground absorption which agree very well with experimental data.

The geometry of the ground propagation problem is as shown in Figure 5.5-1.

Dwg. 7697A77

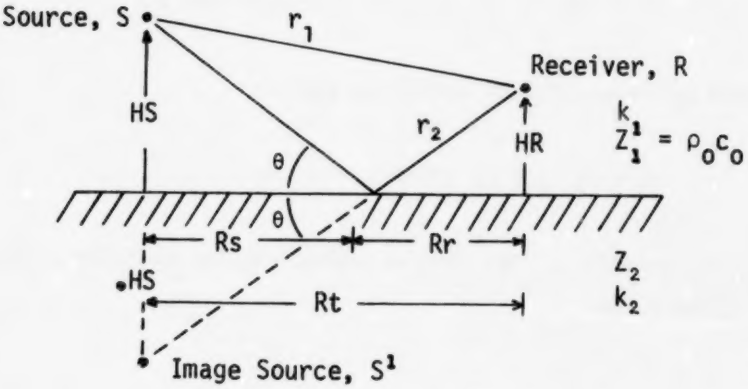

Figure 5.5-1. Source-Receiver Geometry.

Delaney and Bazley have shown that the impedance ratio, Z_2/Z_1 can be written as

$$Z_2/Z_1 = 1 + 9.08(f/\alpha)^{-0.75} - 11.9i(f/\alpha)^{-0.73} \qquad (5.5\text{-}1)$$

and that the propagation coefficient ratio, k_2/k_1, can be written as

$$k_2/k_1 = 10.3(f/\alpha)^{-0.59} + i(1 + 10.8(f/\alpha)^{-0.70}) \qquad (5.5\text{-}2)$$

Rudnick's[7] expressions for the plane wave reflection coefficient, RP, and the 'so-called' numerical distance, w, have been used rather than Ingard's simpler expressions. Ingard's formulations are strictly valid only for small grazing angles (small values of θ) which may not exist if noise levels are calculated close to the cooling tower. The spherical wave reflection coefficient is found from

$$RP = (\sin\theta - \delta Z_1/Z_2)/(\sin\theta + \delta Z_1/Z_2) \qquad (5.5\text{-}3)$$

where $\delta = (1 - k_1^2/k_2^2 \cos^2\theta)^{\frac{1}{2}}$

and the numerical distance from

$$w = 2ik\ r\ (Z_1/Z_2)^2\delta^2/[(1\text{-}RP)\cos\theta] \qquad (5.5\text{-}4)$$

The image source strength can be expressed as

$$Q = RP + F(w)\ (1\text{-}RP) \qquad (5.5\text{-}5)$$

where F(w) is a boundary loss factor which can be evaluated from the following expressions.

$$F(w) = \begin{cases} 1 + i\left[\exp(-w)\right](\pi w)^{\frac{1}{2}} \quad -2\left[\exp(-w)\right] \sum\limits_{n=1}^{\infty} \dfrac{w^n}{(n-1)!(2n-1)} & \\ \qquad\qquad\qquad\qquad\qquad\qquad\qquad\qquad \text{for } |w| < 10 & \\ -\sum\limits_{n=1}^{\infty} \dfrac{(2n)!}{2^n n!(2w)^n} \quad \text{for } |w| > 10 & \end{cases} \tag{5.5-6}$$

Considering spherical spreading, the velocity potential at the source can be given as

$$\phi = \frac{\exp(ikr_1)}{r_1}\left[1 + (r_1/r_2)Q \exp(ik\Delta r]\right) \tag{5.5-7}$$

The excess attenuation caused by the boundary surface alone is

$$A_e(\text{dB}) = 20 \log_{10} \left|1 + (r_1/r_2)Q \exp(ik\Delta r)\right| \tag{5.5-8}$$

On expressing Q as $|Q|\exp(i\beta)$ and modifying the equation to account for finite bandwidths, A_e can be written as

$$A_e(\text{dB}) = 10 \log_{10} \left[1 + (1/r^2)^2 |Q_i|^2 + (2/r^1)|Q_i| \frac{\sin(u\Delta r/\lambda_i)\cos(\eta\Delta r/\lambda_i + \beta_i)}{(u\Delta r/\lambda_i)}\right] \tag{5.5-9}$$

where $u = 2\pi\Delta f/2f_i$

$\eta = 2\pi[1 + (\Delta f/2f_i)^2]^{\frac{1}{2}}$

$\Delta r = r_2 - r_1$

$\lambda_i = c_o/f_i$

$\beta_i = \tan^{-1}[\text{Re}(Q_i)/\text{Im}(Q_i)]$

$r^1 = r_2/r_1$

The Q_i, λ_i and β_i are values corresponding to the respective octave band center frequencies.

For large values of θ ($\theta > 30°$) the effects of the boundary loss factor, F(w), become very small. In this case significant computational economics occur because Equation (5.5-5) reduces to

$$Q = RP \tag{5.5-10}$$

and Ingard's expression for RP

$$RP = (\sin\theta - Z_1/Z_2)/(\sin\theta + Z_1/Z_2) \tag{5.5-11}$$

can be used instead of Equation (5.5-3).

The equations presented here constitute the basis of subroutine GRND with one exception. Oncley[10] points out that the sign of the reactive component of the ground impedance, Equation (5.5-1), is an arbitrary choice. In acoustics this is conventionally taken to be negative. However, for this problem, an examination of the vector relationships of the terms comprising the velocity potential, Equations (5.5-7) and (5.5-5), indicate that the reactive impedance component must be positive for the calculation of the attenuation to be valid. This has been done in subroutine GRND.

5.5.2 Program Code Operation

In terms of calculation, the program treats the noise radiated from the fan stack and the louvered open faces of the tower separately. The first step in the program is to calculate the octave band source sound levels for the specified tower operating conditions from the fitted regression equations. The atmospheric absorption is then calculated in dB/ft for the given atmospheric conditions. Then, for each distance from the tower at which the receiver noise level is desired, the program calculates the spherical spreading attenuation and the ground attenuation for each of the two sources. The octave band noise levels at the receiver from each source is determined by adding the atmospheric absorption attenuation, the respective spherical spreading attenuation and the ground attenuation to the calculated source levels. A directivity correction factor is also applied to the fan stack source noise level. The "total" noise level at the receiver is then found by summing, on a mean square pressure basis, the octave band noise level at the receiver produced by each of the two sources. The overall linear and A-weighted noise levels at the receiver location are determined by summing (again, on a mean square pressure basis) the corrected octave band levels.

The program assumes that the receiver is always located perpendicular to one of the louvered faces of the tower, equidistant from either side. The decrease in the louvered face noise level at the receiver location from that six feet away from the tower is found from

$$\Delta L_1 \,(\mathrm{dB}) = 10 \log_{10} \left[\pi/(2 \tan^{-1}(h/d) \tan^{-1}(t/2d))\right] \qquad (5.5\text{-}12)$$

where

h = tower height, m
t = tower width, m
d = distance from tower base to receiver, m

This equation accounts for spreading 'losses'. It is discussed in more detail in Reference 7. This reference also discusses how this equation changes if the receiver is located either (a) perpendicular to the louvered face of the tower at one of the tower edges, or (b) at an angle γ away from a perpendicular line to the louvered face at one of the tower edges.

The decrease in the fan stack discharge noise level from the stack to the receiver is calculated from Equation (5.5-13)

$$\Delta L_2(\mathrm{dB}) = 10 \log_{10} [S/11.2\pi r^2] \qquad (5.5\text{-}13)$$

where

S = area of the fan stack discharge, m^2
r = distance from fan stack to receiver, m

This equation basically accounts for spherical spreading losses from the finite sized fan stack discharge and is valid regardless of the position of the receiver (as long as r is several times larger than the fan stack diameter).

5.6 DISCUSSION OF RESULTS

The project results can be separated into three categories for purposes of discussion. These three categories are (1) the experimental data and its acquisition, (2) regression analysis and (3) the noise prediction computer model. Each of these are discussed below.

5.6.1 Experimental Data

No apparent problems occurred during the data acquisition at the TVA tower site. Weather conditions were good: temperatures of 60-70°F, sunny-overcast skies with no rain and wind speeds less than 10 miles/hr. As shown in Figure 5.1-3 and noted in Section 5.1, the ground level measurements were made at perpendicular distances of 3, 6 and 12 ft. from the louvered face of the tower oriented away from the main plant.

All of the data from these locations were analyzed and corrected for the effects of background noise. All of the data were louder than the background except for some of the 125 Hz octave band data. When the time-averaged background noise exceeds the time-averaged tower noise, as in this case, no information about the true tower noise level for these conditions can be determined. Hence, for these cases a zero is listed in the tables of corrected tower noise levels. (See Table 5.4-1 for 125 Hz data at Location 1, for example.)

Ten of the 31 noise levels measured at 12 ft. from the tower were indeterminate because of the high average background noise levels. Five of the 31 measured noise levels at 3 and 6 ft. from the tower were similarly indeterminate. The measured noise levels at 3 and 6 ft. for the other 26 tests were virtually identical. From this information, the data obtained at 6 ft. from the tower was chosen as being most representative, and this measuring location was designated 'Location 1'. No further use was made of the data at the other two distances.

The high 125 Hz octave band background noise levels were most likely produced by several sources including (1) nearby multi-cell Marley cooling towers, (2) main plant power transfer and (3) the main plant turbine hall. An examination of the data in Table 5.4-1 at Locations 1 and 2 for those tests where the background noise exceeded the noise level at Location 1 (zero entries in Location 1 data column) indicates that this occurred when the tower fan speed was 50 percent, the lowest value tested. The corresponding data in the Location 2 column indicates that for 50 percent fan speed, the tower produces the lowest 125 Hz octave band fan noise levels. Hence, the zeros in the Location 1 column are explainable in terms of reduced 125 Hz band fan noise coupled with a relatively high 125 Hz band background noise.

5.6.2 Regression Analysis

The regression analysis was a rather straightforward process for this project because it was possible to choose tests optimally to fit the desired experimental design. The only deviation from the optimal was the occurrence of the zero values in the 125 Hz octave band noise levels at Location 1. The regression analysis for this case was performed using the 26 valid test noise levels. The missing five test values did not significantly affect the analysis because not all the terms of the model [Equation (5.4-2)] appeared in the final fitted equation. Hence, less than the 31 test noise levels were needed to successfully fit the data.

Several interesting features of the fitted model coefficients in Table 5.4-2 are in agreement with our understanding of operation of the tower. For example, the noise levels at the fan stack discharge (Location 2) are dominated by the fan noise and this is apparent from the dominance of the x_1 and x_{11} terms in the Location 2 models. The size of the x_1 term diminishes at the higher frequencies (4 kHz and 8 kHz) because the fan noise level is diminishing at these frequencies.

5.6.3 Noise Prediction Code

Operation of the prediction code is straightforward. However, there are some cautions that must be exercised to ensure accuracy of the predicted results. These cautions apply in two areas; one is proper characterization of the ground characteristics and the second is the effect of variations in atmospheric turbulence.

5.6.3.1 Ground Absorption

The ground absorption model incorporated into the code assumes that the ground characteristics are the same over the entire area between the tower and the receiver. In addition the terrain has been assumed to be flat. Inclusion of means to account for uneven terrain is beyond the current state of the art. Significant variations from either of these assumptions can be expected to alter the calculated ground absorption.

The ground absorption model is based on the flow resistance ground impedance model formulated by Chessel from the impedance results of Delany and Bazley. This model relies on an empirical curve fitting of the model impedance equations to field measurements. The fitting parameter is the flow resistance, α. Values of α between 150 and 300 cgs units have been found to fit existing data, acquired by other investigations, for propagation over grass. The data indicate that $\alpha = 150$ is characteristic of shorter grass (15-25 mm) and $\alpha = 300$ is characteristic of taller grass. The prediction code uses $\alpha = 200$ cgs units, and hence, implicitly assumes grass covered ground.

The computer code calculates the ground absorption assuming that the noise sources are concentrated at individual points (at the fan stack discharge nearest the receiver and at the center of the louvered tower face). This assumption is reasonable for the fan stack noise, but open to some question for the noise radiated from the louvered face. This question arises because the predicted A-weighted noise levels as a function of distance from the tower exhibit greater amplitude variations than seen in some experimental data reported in the literature. Because the louvered tower face is relatively large (40 ft x 40 ft), the actual path length of the ground reflected wave reaching the receiver varies depending on the source point selected on the louvered face. This difference in path lengths has the same effect on the received noise level as changes in phase of the arriving waves. These changes in phase will probably reduce the amplitude of the "peaks and valleys" in the ground attenuation vs frequency curves.

The ground absorption calculations should be repeated for several source points on the louvered face and the results averaged. A comparison of the average absorption values with the point source values currently used would indicate how important this effect is. This has not been done for this report because of project time and cost constraints.

5.6.3.2 Wind and Temperature Fluctuations

The real world atmospheric conditions include random fluctuations of wind and temperature which cause fluctuations in the amplitude and phase of the tower noise at the receiver. These fluctuations, if included in the model, are expected to reduce the ground attenuation from the values calculated for a quiet atmosphere. However, the theory required to incorporate these effects is still in its infancy and is not adequate for predictive purposes. Hence, the prediction model is restricted in application to conditions with minimal wind over the region between the tower and the receiver.

5.7 ACKNOWLEDGEMENTS

Our thanks to L. J. Harper and R. P. Martin for acquiring and analyzing the experimental data and for providing many suggestions which contributed to the successful completion of this project.

5.8 ACOUSTICS REFERENCES

1. TVA Cooling Tower Test Grid, November 28, 1977.
2. Hribar, A. E., "Noise Levels Generated by the PCSD Demonstration Cooling Tower--West Configuration", Westinghouse Research Report 74-1E9-TOWNO-R1, Westinghouse Research Laboratories, October 1974.
3. "Standard Values of Atmospheric Absorption as a Function of Temperature and Humidity", ARP 866A, Society of Automotive Engineers, Inc., March 1975.
4. Chessel, C. I., "Propagation of Noise Along a Finite Impedance Boundary", J. Acoust. Soc. Am., Vol. 62, No. 4, October 1977, pp. 825-834.
5. Chessel, C. I., "Meteorological and Ground Effects on the Propagation of Aircraft Noise Close to the Earth's Surface", J. Sound Vib., Vol. 60, No., September 22, 1978, pp. 251-266.
6. Delany, M. E. and Bazley, E. N., "Acoustical Properties of Fibrous Absorbent Materials", Applied Acoustics, Vol. 3, 1970, pp. 105-116.

7. Hribar, A. E., "A Noise Level Prediction Procedure for Multi-Cell Induced Draft Cooling Towers", Westinghouse Scientific Paper 75-1E9-TOWNO-P1, Westinghouse Research Laboratories, May 12, 1975.

8. Rudnick, I., "The Propagation of an Acoustic Wave Along a Boundary", J. Acoust. Soc. Am., Vol. 19, 1947, pp. 348-356.

9. Ingard, U., "On the Reflection of a Spherical Sound Wave from an Infinite Plane", J. Acoust. Soc. Am., Vol. 23, 1951, pp. 329-335.

10. Oncley, P. B., "Propagation of Jet Noise Near a Porous Surface", J. Sound Vib., Vol. 13, No. 1, 1970, pp. 27-35.

5.9 ACOUSTICS NOMENCLATURE

A_e	Excess attenuation, dB.
BP	Tower fan blade pitch, degrees.
c_o	Speed of sound in air, m/sec.
d	Ground distance between tower and receiver, m.
DF	Percent of total tower water flow passing through the dry heat exchangers, percent.
e	Residual value = $y-\hat{y}$, dB
f	Frequency, Hz.
FS	Tower fan speed, percent of maximum.
h	Cooling tower height, m.
i	$\sqrt{-1}$
$k_{1,2}$	Propagation coefficients in air, ground = $2\pi f/c$, m^{-1}
n	Numerical index for summations, dimensionless.
Q	Image source strength.
$r_{1,2}$	Direct and reflected path length between source and receiver, m.
r^1	Ratio r_2/r_1.
R	Receiver location.
Rr	Ground distance defined in Figure 5.5-1.
Rs	Ground distance defined in Figure 5.5-1.
Rt	Ground distance = Rr + Rs, m.

RP	Spherical wave ground reflection coefficient, dimensionless.
$s(\hat{y})$	Standard error of fitted values, dB.
S	Source location (also area of fan stack exhaust for Equation [5.5-13] only, m^2).
s^1	Source image location.
w	Complex numerical distance defined by Equation (5.5-4), m.
WFR	Total tower water flow rate, gpm.
$x_1,...x_4$	Coded form of the tower independent variables, dimensionless.
y	Observed tower dependent variable (sound level), dB.
$\hat{y}$	Fitted tower dependent variable (sound level), dB.
$Z_{1,2}$	Air and ground impedance, mks rayls.

Greek Symbols

α	Material flow resistance
β_i	Unknown model coefficients, $i = 0,1,...,4$
Δf	Octave band frequency bandwidth, Hz.
Δr	Path length difference, $r_2 - r_1$, m.
η	Frequency parameter defined in Equation (5.5-9).
θ	Angle of incidence (to ground) of reflected ray from source, deg.
λ	Wavelength of sound in air = c_o/f, m.
ρ_o	Density of air, kg/m^3.
σ	Standard deviation of fitted variables, dB.
ϕ	Velocity potential of the source.

SECTION 6.0

PLUME TESTS

The prediction of the spread and dissipation of cooling tower plumes is a continuing matter of interest in the electric power industry. This interest has engendered numerous methods for predicting plume behavior using a small number of surface-based meteorological measurements and cooling tower parameters. Of course, these analyses must be verified with experimental data. This verification requires the use of a cooling tower.

The wet/dry cooling tower at the Cliffside Power Station at Cliffside, North Carolina, is a unique facility for collecting such data, because of the available wide range of control of the state of the air leaving the cooling tower.

During the period March 18, 1978, to May 18, 1978, 60 measurements of plume properties were made at Cliffside, mostly in the morning under stable atmospheric conditions. These tests covered the following range of parameters: stack exit relative humidity - 84.42 percent to 100 percent; plume length - 0 to 235 feet; plume height - 0 to 257.2 feet. The results of this investigation are described in this section.

6.1 PLUME INSTRUMENTATION

Study of the growth and dissipation of cooling tower plumes requires both micro-meteorological measurements (in the vicinity of the plume) and measurements of the plume dimensions.

Dwg. 7697A78

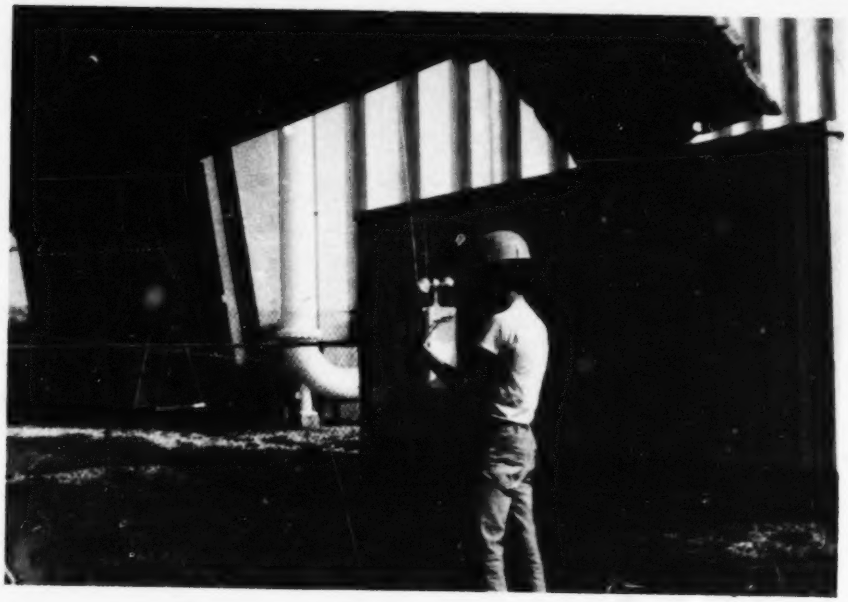

Figure 6.1-1a. Tethersonde Instrument Package.

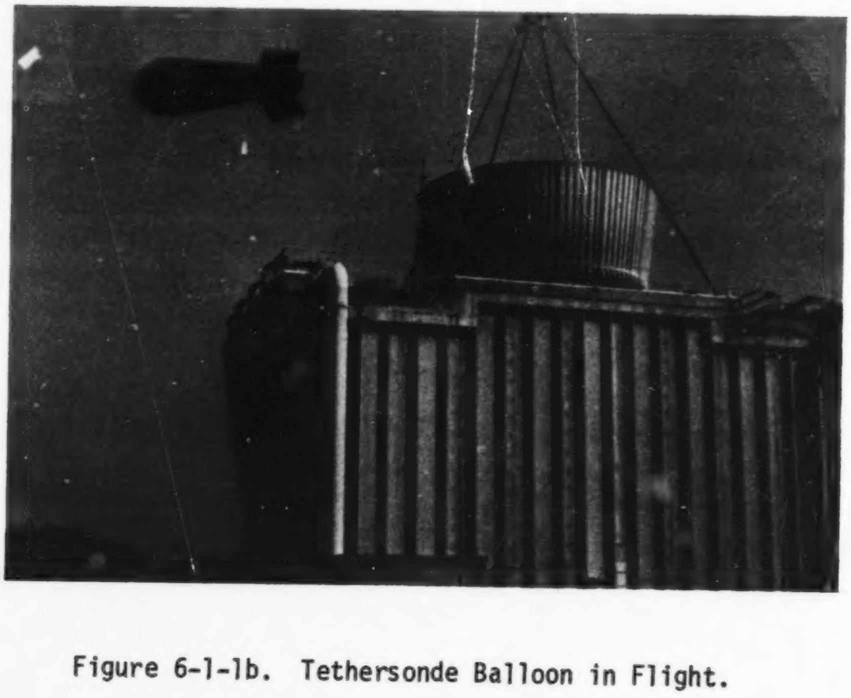

Figure 6-1-1b. Tethersonde Balloon in Flight.

The originally proposed meteorological instrumentation was to be an anemometer and an automatic psychrometer on a meteorological tower. Several problems, however, made the use of a tower undesirable and forced us to consider other alternatives:

1. The plant manager did not want to have a tower which might, conceivably, fall onto some transmission lines near the cooling tower.

2. Since the spread and dissipation of the plume would be expected to be affected most by air temperature and wind velocities at the level of the top of the cooling tower and above, a meteorological tower would have to be much higher than the cooling tower. Such a tower would be very expensive.

3. Because the spread and dissipation of the plume depends on the structure of the atmospheric boundary layer, data on this structure up to the height of the top of the plume (200-300 feet) would be desirable. Since a meteorological tower of practical cost would normally be less than 100 feet high, we can again see that a meteorological tower would have been the wrong instrument platform for the job.

Because of the foregoing considerations, a tethered balloon-mounted meteorological sensor package was used instead of a meteorological tower. This system (see Figure 6.1-1), comprising a balloon and winch, an airborne sensor package, and a ground receiver package, was produced by the Atmospheric Instrumentation Research Company of Boulder, Colorado, under the name of Tethersonde. The sensor package contained a wet and a dry bulb thermometer (mechanically aspirated), an anemometer, a wind direction indicator, and a differential barometric pressure transducer. (This latter was an instrument which read the pressure difference--in millibars--between the surface and the instantaneous balloon altitude.)

While the differential barometer itself had a potential resolution equivalent to an altitude change of 21 feet, pressure fluctuations equivalent to altitude changes of about 100 feet appeared on the Tethersonde output in the stronger winds, when no equivalent change of altitude was apparent from watching the balloon. These fluctuations may have been caused by the effect of the dynamic pressure of the wind on the static pressure port of the Tethersonde.

The sensor package also contained a small UHF telemetry transmitter which transmitted the data to the receiver on the ground as five channels of time-multiplexed data.

The plume program as furnished by Rubin[1] (see Appendix I) contained a prediction of visibility in the densest part of the plume, which was intended to be correlated with subjective evaluations of plume density.

Earlier tests had apparently validated the significance of this predicted visibility as a measure of the perceived density of the plume[1]. In the present tests, an attempt was made to check the quantitative accuracy of this portion of the analysis by mounting a small transmittometer in the exhaust plume one stack radius above the cooling tower outlet. (The transmittometer is manufactured by Meteorology Research, Inc. [MRI] of Altadena, California, as the model 1580 Fog Visiometer.) In order to bring the range of the instrument more in line with the anticipated observations, the range was changed from a span of 256 to 25,600 feet to a range of 25.6 to 2560 feet by changing the reference calibration voltage on the Visiometer from 1.1 volts to 0.11 volts, in accordance with the instructions on pages 4-10 and 4-11 of MRI Instruction Manual IM-142. A tenfold reduction of the range is more than normally recommended by the manufacturer, but MRI verified that such a reduction in range could be done if the reference calibration was set with a sufficiently accurate voltmeter.

Due to the turbulence in the jet leaving the cooling tower, a meaningful measurement of visibility would most accurately be taken along a baseline of length comparable to the visibility to average--in space--the turbulent fluctuations of the scattering coefficient in the plume.

Since the turbulence in a free jet can be considered to be ergodic, an average over a lengthy period of time would be equivalent to an average over a long baseline. Scattering coefficients (or the proportionate voltage output of the Visiometer) were averaged, rather than visibilities, since scattering would be cumulative along a long light path, whereas visibility would not be.

Examination of the plume photographs taken during the tests showed that the Visiometer was always immersed in the plume. While there are severe discrepancies between the calculated and measured visibilities, the measured visibilities are always lower than the calculated (except in test 511071 and 511072), so that the discrepancy could not be explained as a result of the plume missing the Visiometer.

Plume height and length were measured by elementary surveying techniques. Four observing points, designated as A, B, C, and D, were chosen, located on generally perpendicular axes intersecting at the cooling tower. One of these axes was parallel to the prevailing winds at Cliffside. The distances of the observing points from the cooling tower were as follows: point A, 545 feet; point B, 750 feet; point C, 390 feet; point D, 455 feet. The observing point chosen for any given run was always one for which the line of sight from the observing point to the plume was most nearly perpendicular to the axis of the plume, to assure the greatest accuracy of the plume height and length measurements. Obviously, locating an observing point for each run to give a line of sight rigorously perpendicular to the axis of the plume would have given a more accurate measurement, but at the cost of an unaffordable increase in the time required per run. Further, it would be difficult to define a unique plume direction if there were a significant shift of wind direction over the height of the plume, such as might exist under inversion conditions. Once the direction of the axis of the plume had been determined, the proper sighting point was chosen and the elevation and length of the plume determined by sighting with a transit (see Figure 6.1-2).

Dwg. 7697A79

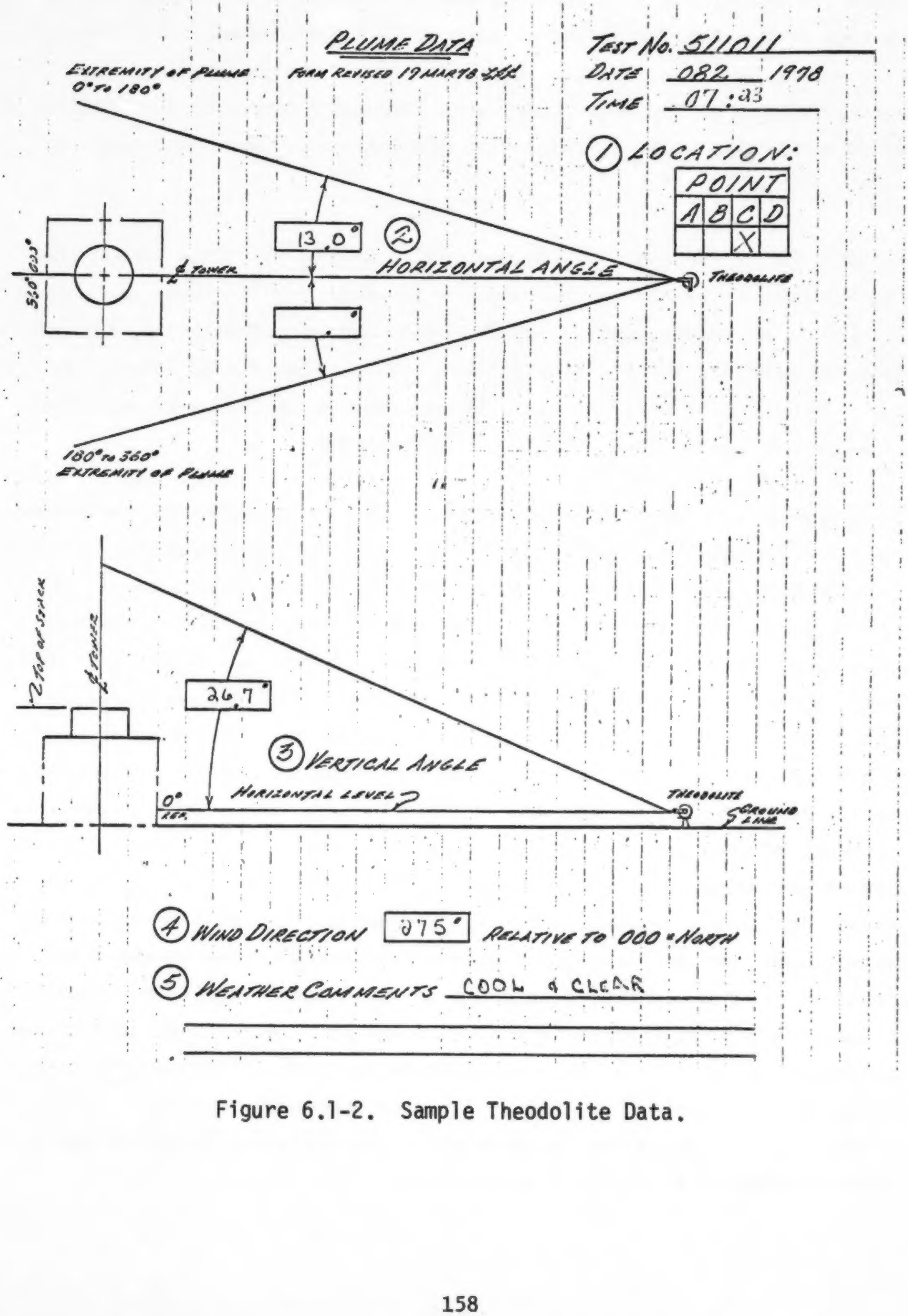
PLUME DATA
FORM REVISED 19 MAR 78
EXTREMITY OF PLUME 0° TO 180°
180° TO 360° EXTREMITY OF PLUME
℄ TOWER
② HORIZONTAL ANGLE
THEODOLITE
TOP OF STACK
℄ TOWER
③ VERTICAL ANGLE
HORIZONTAL LEVEL
0° REF.
THEODOLITE
GROUND LINE

TEST No. 511011
DATE 082 1978
TIME 07:23

① LOCATION:

POINT			
A	B	C	D
		X	

② HORIZONTAL ANGLE 13.0°

③ VERTICAL ANGLE 26.7°

④ WIND DIRECTION 075° RELATIVE TO 000 = NORTH

⑤ WEATHER COMMENTS COOL & CLEAR

Figure 6.1-2. Sample Theodolite Data.

The temperature, velocity, and humidity of the efflux from the cooling tower were measured by the cooling tower instrumentation (see Section 4.0).

A complete study of plume spread and dissipation further requires that the cloud cover be described for each test, and that the shape of the plume be described. This was achieved, during these tests, by photographing the plume with Polacolor ^{R} type 108 film from the observing point. (Polacolor is a trademarked name for a color film produced by the Polaroid Company of Cambridge, Massachusetts.) Earlier studies had shown that color photographs, much more than black and white photographs, were capable of depicting the subtle differences between a plume and an overcast background, and some trial runs at the start of these tests verified this.

6.2 PLUME DATA ACQUISITION TECHNIQUE AT THE CLIFFSIDE SITE

In order to actually acquire the data, a combination of manual and automatic methods were used. Plume tests were run only on days when a plume was observed by the on-site personnel arriving in the morning, about sunrise. (Obviously, plumes cannot be observed in the dark.)

Data were acquired and recorded on three different media:

a) punched paper tapes containing cooling tower, Visiometer, and Tethersonde data

b) written sheets containing transit readings of plume angular height and length

c) photographs of the plume.

The Tethersonde receiver package contained a microprocessor which automatically synchronized the receiver with the airborne unit, decoded the signal, and presented the data on a strip chart recorder. The five variables were also formatted in 7-bit ASCII code for output on a male

EIA-RS-232 connector. Further, one selected channel of data was also routed to the second channel of the strip chart recorder mentioned earlier and recorded continuously.

In order to record data from both a Fluke 2240-B data logger and from the Tethersonde, the outputs of the Tethersonde and of the data logger were connected to a teletype equipped with a paper tape punch. Thus, during operation, data could be routed to the paper tape punch from the TTY keyboard, from the Fluke data logger, or from the Tethersonde receiver unit.

At the start of any given run, cooling tower data were scanned by the Fluke datalogger and automatically punched onto paper tape. Fifty readings of the Visiometer were then punched manually onto the tape.

Following this, Tethersonde data were entered on the tape, as follows. A pseudo-channel number was punched onto the tape through the TTY keyboard, after which four lines of Tethersonde data were punched onto the paper tape (together with additional incomplete first and last lines). The Tethersonde data were taken at several levels, each level being indicated by a different pseudo-channel number, as follows:

Channel 200 - 30 feet above ground level (AGL)

Channel 201 - 75 feet AGL

Channel 202 - 125 feet AGL

Channel 203 - 175 feet AGL

Channel 204 - Top of plume

On days when the wind was too high to fly the balloon, the instrument package was mounted on a pole near the trailer, and this situation was identified by the pseudo-channel number 300.

Concurrently with this, the observer with the transit was positioned at the appropriate observing point. Typically, five to eight measurements were made of the height and length of the plume while a set of cooling tower and Tethersonde measurements were being taken. These measurements were written down.

The observer photographed the plume using a Polaroid ^{R} Automatic 250 Land Camera, taking one photograph at the start of a set of data and one at the end. Both the photographs and the transit data sheets were mailed directly to the Westinghouse R&D Center, Pittsburgh, Pennsylvania.

6.2.1 Data Handling at Westinghouse Fluid Systems Laboratory

The contents of the punched paper tapes so produced were transmitted via commercial telephone circuits to the Westinghouse Fluid Systems Laboratory, where the cooling tower data were extracted to perform cooling tower calculations, and the Visiometer and Tethersonde data were combined with the results of the cooling tower data to produce input cards formatted for Rubin's plume analysis program. A sample is in Table 6.2.1-1.

6.2.2 Data Handling at Westinghouse R&D Center

These cards were sent to the Westinghouse R&D Center where they were loaded onto magnetic disc. A series of text processing programs then extracted the input cards for Rubin's program and sorted them by test number. Identifying headers were then attached to the data for each test run. The card images were then used as input for Rubin's program.

The transit data (see Figure 6.1-2) were also analyzed (by elementary triganometric formulae) to produce a tabulation of plume heights and lengths.

Cloud cover was estimated from the plume photographs, using the terminology of the National Weather Service "Manual of Surface Weather Observations", where "overcast" means a cloud cover of more than 90 percent,

TABLE 6.2.1-1

SAMPLE DATA, AS RECEIVED

```
100
110   : RUNID 511021   MAR 23, 1978
120    2.945   2.945   2.945   2.947   2.949   2.949   2.947   2.946   2.945
130    2.943   2.941   2.938   2.937   2.936   2.935   2.936   2.937   2.938
140    2.934   2.934   2.932   2.931   2.931   2.932   2.935   2.938   2.941
150    2.945   2.948   2.947   2.945   2.948   2.950   2.950   2.949   2.950
160    2.951   2.951   2.951   2.949   2.946   2.945   2.941   2.937   2.932
170    2.930   2.928   2.923   2.920   2.918   2.917   2.914
180  200
190  109.240   9.870  39.000   3.190  84.870   7.950  35.610    .350 317.400
200  109.450   9.950  39.310   3.190  84.660   6.660  33.010    .590 341.300
210  109.670   9.970  39.300   3.240  84.820   6.300  27.210    .590 341.800
220  109.980  10.140  39.700   3.180  84.980   7.590  37.840    .300 345.200
230  201
240  111.170  10.210  39.700   3.230  84.910   8.830  41.300   1.120  19.800
250  111.390  10.110  40.330   3.220  84.850  10.170  42.380   1.280  25.600
260  111.600   9.990  39.710   3.230  84.790  10.000  36.200   1.320  15.800
270  111.820  10.030  39.500   3.160  84.710   9.330  33.700    .970 359.400
280  202
290  113.330  10.020  39.940   3.140  84.730  11.750  44.820    .680 331.700
300  113.540  10.150  39.820   3.190  84.850  11.660  46.670   1.080 342.600
310  113.760   9.900  40.290   3.230  84.840  11.010  44.560    .720 334.700
320  113.970  10.160  40.340   3.190  84.540  11.000  43.420    .700 355.700
330  204
340  114.830  10.370  41.290   3.480  84.720  13.270  58.550    .020 358.200
350  115.050  10.460  41.600   3.630  84.810  12.710  54.510   1.110  28.500
360  115.260  10.480  41.670   3.400  84.820  14.060  56.110   1.220 326.900
370  115.480  10.420  41.350   3.550  84.790  12.510  60.440   1.250  40.600
380   : RUNID 511022   MAR 23, 1978
390    1.953   1.953   1.954   1.955   1.957   1.961   1.966   1.971   1.975
400    1.977   1.976   1.974   1.972   1.971   1.972   1.971   1.968   1.966
410    1.965   1.965   1.965   1.966   1.959   1.952   1.949   1.947   1.945
420    1.945   1.945   1.943   1.940   1.937   1.936   1.937   1.938   1.939
430    1.930   1.918   1.910   1.908   1.907   1.907   1.907   1.908   1.908
440    1.909   1.911   1.909   1.906   1.904   1.902   1.900
450  200
460  126.460  11.590  46.610   3.880  84.640  10.070  37.580    .850 341.900
470  126.680  11.900  47.380   4.070  84.780   9.900  39.420    .560  22.200
480  126.890  11.930  46.980   4.090  84.810   9.690  44.510    .250  18.100
490  127.110  12.020  47.210   4.070  84.900  11.110  43.260    .330  13.100
500  201
510  128.400  11.780  46.540   3.830  84.680  11.240  47.790    .880 356.900
520  128.620  11.750  46.740   3.980  84.810  13.900  48.400    .700  16.000
530  128.830  11.830  47.040   3.930  84.690  11.420  44.930    .900 339.800
540  129.050  11.670  46.610   3.960  84.800  10.950  53.090    .610 334.000
550  204
```

RAW DATA

(Continued)

Table 6.2.1-1 (cont'd)

```
560  130.130  12.910  50.820   4.740  84.660  13.940  59.260   1.600  48.600
570  130.350  12.490  49.800   4.530  84.680  14.220  62.920    .880  45.500
580  130.560  12.950  51.410   4.940  84.750  15.610  57.210    .360  60.400
590  130.780  13.330  52.870   5.080  84.820  14.610  55.160    .490  40.600
600   : RUNID 511023   MAR 23, 1978
610    1.458   1.457   1.456   1.455   1.456   1.459   1.462   1.465   1.467
620    1.470   1.471   1.471   1.472   1.473   1.476   1.481   1.479   1.476
630    1.477   1.480   1.484   1.489   1.493   1.492   1.491   1.491   1.493
640    1.496   1.497   1.498   1.498   1.494   1.488   1.484   1.483   1.484
650    1.483   1.482   1.481   1.476   1.471   1.468   1.461   1.452   1.448
660    1.448   1.449   1.448   1.447   1.447   1.448   1.444
670  200
680  141.140  12.660  50.640   4.380  84.790  10.680  38.780    .680 284.300
690  141.360  12.990  51.450   4.600  84.970  11.190  44.530   1.000 280.400
700  141.570  12.850  51.420   4.550  84.920  11.840  43.290   1.300 303.100
710  141.790  12.880  51.520   4.440  84.840   9.710  38.240   1.100 282.000
720  201
730  142.870  13.490  53.690   5.230  85.010  10.890  43.250    .120 150.500
740  143.080  14.450  56.940   5.660  84.860  11.610  44.760    .900 129.100
750  143.300  14.100  56.320   5.580  84.870  11.530  50.590   1.310 116.400
760  143.520  14.330  57.100   5.750  84.890  11.590  45.810   1.320 109.500
770 PLUME DATAPLUME DATAPLUME DATAPLUME DATAPLUME DATAPLUME DATAPLUME DATA
780  511021
790       36.4      63.5      71.0      11.8     100.01.2273E+046.0658E+07
800       50.2      82.9      3.8       75.0 2.939E+00
810 PLUME DATAPLUME DATAPLUME DATAPLUME DATAPLUME DATAPLUME DATAPLUME DATA
820  511022
830       36.4      63.5      71.3      12.3     100.01.2769E+045.9784E+07
840       53.3      81.4      2.5       75.0 1.942E+00
850
860   : RUNID 511061   MAR 28, 1978
870    2.147   2.148   2.152   2.159   2.160   2.157   2.157   2.157   2.159
880    2.161   2.163   2.157   2.151   2.147   2.148   2.152   2.157   2.163
890    2.165   2.165   2.155   2.151   2.147   2.147   2.145   2.142   2.137
900    2.127   2.121   2.122   2.125   2.129   2.133   2.131   2.132   2.136
910    2.146   2.151   2.156   2.158   2.159   2.161   2.163   2.162   2.150
920    2.144   2.139   2.135   2.134   2.137   2.137   2.132
930  200
940   48.680   -.230 100.240   -.090  84.360       0  28.460   1.850 287.400
950   48.900   -.090 100.320   -.050  84.370       0  26.020   1.770 287.300
960   49.110   -.230  99.980   -.090  84.250       0  28.480   2.010 288.700
970   49.330   -.040 100.190   -.050  84.360       0  29.320   1.750 281.300
980  201
990   50.410    .770   2.340    .110  84.490  -9.570  33.090   1.970 279.800
1000  50.630    .740   2.370    .160  84.420       0  29.300   2.100 281.400
```

RAW DATA

PROCESSED DATA FOR RUBIN'S PROGRAM

"broken" is 60 to 90 percent coverage, "scattered" is 10 to 50 percent coverage, and "clear" is less than 10 percent coverage. A "thin" layer is one through which the sun, moon, stars, or part of the celestial dome can be seen.

The plume data are tabulated in three appendices as follows: Appendix H contains the raw data from the Visiometer and Tethersonde. Appendix I contains reduced data from the Visiometer and Tethersonde as well as stack exit air conditions, all formatted for input to the Rubin plume model, which is also included in this appendix. Appendix J tabulates plume height and length, comparing actual values with those predicted by Rubin's model. Also included in the tabulation are cloud cover and vertical temperature gradient. In most cases, the vertical temperature gradients were obtained between the temperature on pseudo-channel 200 (30 ft AGL) and the top of the plume (channel 204). In some cases, when the wind was too strong to permit flying the balloon to the top of the plume, the temperature gradient over a lesser range of heights was used.

6.3 PLUME MODELING

The Rubin plume program[1], listed in Appendix I, was used to generate the predicted values given in Appendix J. The program uses Briggs'[2] formula to calculate plume rise for five different vertical temperature gradients, from -0.004 to +0.004°F/ft. A Gausian dispersion model[3] is used to calculate plume length for both stable and unstable air. No intermediate stability categories were considered. No attempt was made to modify the program to consider the actual temperature gradient or stability category.

Actual temperature gradients were often an order of magnitude greater than those considered by Rubin's program. The highest gradient considered by Rubin's program was 0.004°F/ft. If the actual gradient exceeded this value, the 0.004 figure was used in the analysis.

To determine the stability category for calculating plume length, stable conditions were assumed whenever the vertical temperature gradient was greater than -0.0055°F/ft (1°c/100 m). This is the "dry adiabatic lapse rate", the temperature drop a parcel of air would experience due to expansion (or contraction) if raised (or lowered) with no heat loss or gain.

6.4 ANALYSIS OF PLUME DATA

A least-squares fit of the measured plume rise to the forecast plume rise for a correlation of the form

$$(\text{observed rise}) = m \times (\text{computed rise}) + b$$

yielded

$$m = 0.1248$$

$$b = 92.34$$

and a coefficient of correlation of 0.5616 indicating a poor correlation.

The large intercept shows that when the computed plume rise was nearly zero, the actual plume rise averaged 92 feet. This systematic error is probably attributable to the use of the Briggs plume rise model, which is based solely on plume buoyancy and neglects its initial momentum. The initial momentum of the plume from a mechanical draft cooling tower is relatively large and results in significant plume rise even for non-buoyant plumes.

The small slope, $m = 0.1248$, shows that for large predicted plume heights, actual heights were significantly smaller than predicted. This systematic error can be explained by two factors. First, the prediction ignores the internal turbulence of the plume, which significantly enhances dispersion and reduces buoyancy. Second, the computer program assumed a vertical temperature gradient of 0.004°F/ft whenever the actual gradient was greater than this value. Since actual gradients were often much greater than 0.004, this factor alone would produce large errors in predicted plume heights.

A similar calculation of predicted and observed plume lengths yielded a coefficient of correlation = -0.0164 and the correlation between observed and forecast plume scattering coefficients was 0.191. These correlations indicate such a weak relation that it is meaningless to cite the slope or intercept of the regression lines.

This poor correlation can also be explained by two factors. Again the prediction ignores the internal turbulence of the plume in enhancing dispersion. During the early stage of plume growth the dilution of the plume is dominated by this internal turbulence. It is probable that many of these plumes were so short that they did not go beyond this stage. Also, Rubin's model considers only two atmospheric stability classes, stable and unstable. Because predictions for these two classes are generally separated by one or more orders of magnitude, common practice is to use six stability classes[4].

6.5 DISCUSSION OF RESULTS

The results of this study may be considered under three separate headings:

a) The validation of the Ruben model

b) The compilation of plume data

c) Suggestions for further work.

6.5.1 Validation of the Rubin Model

It can be fairly stated that Rubin's program has been shown to accurately predict neither plume height, length, nor visibility under the conditions encountered in this study.

Although the Rubin model could certainly be improved by merely considering more categories of stability and by using the actual vertical temperature gradients, this was not done since many models already exist which are vastly superior to the Rubin model. It is hoped that data from this work can be used by others to help verify or calibrate these models.

6.5.2 Compilation of Plume Data

The plume data have been compiled in the appendices to this report, with the exception of the plume photographs. Copies of these photos on transparency film, as well as the numerical data in machine readable form, will be available from the Division of Energy Demonstrations and Technology, Tennessee Valley Authority, Cattanooga, Tennessee 37401.

6.5.3 Recommendations for Further Research

The authors are not prepared to comment on future developments in plume modeling except to recognize that the state of the art has advanced greatly since the Rubin model was developed.

In planning further field studies of cooling tower plumes, it would be desirable to seek a wider range of atmospheric conditions than were available during this study, which is limited to mostly stable, early morning hours in the spring. Also, in planning plume studies for wet/dry cooling towers, a program should be set up to study the conditions necessary to eliminate the plume, and this study should be independent of the plume trajectory study.

6.6 REFERENCES

1. Rubin and Klanian, "Visible Plume Abatement with the Wet/Dry Cooling Tower", Power Engineering, March 1975, pp. 54-57.

2. Briggs, G. A., Plume Rise, AEC Critical Review Series TID-25075, November 1969.

3. Somers, E. V., "Dispersion of Pollutants Emitted into the Atmosphere", Air Pollution Control, Part 1, Edited by W. Strauss, John Wiley & Sons, New York, pp. 1-33, 1971.

4. Slade, David H., Editor, Meteorology and Atomic Energy, U. S. Atomic Energy Commission, July 1968. Available from NTIS as TID-24190.

SECTION 7.0

ACKNOWLEDGEMENTS

Beside the listed authors of this report there were several individuals in Westinghouse who contributed materially to the successful execution of this program, and their splendid efforts are hereby acknowledged:

1. K. A. Oleson of the Steam Turbine Division acted as an initial liaison with TVA and served as a source of historical information on the test facility.
2. K. A. Katzor and D. E. Gonya of Power Generation Services Division took care of contract administrative details. Mr. Gonya performed yeoman service as liaison between the test facility and the Fluid Systems Laboratory.
3. L. H. Keeler of Power Generation Services Division did an excellent job in reactivating the test facility and conducting the tests. He was ably assisted by D. Hauser, D. Scruggs, and M. Jolley at the test site.
4. Last, but definitely not least, we are indebted to M. R. Sorton and K. H. Lee of the Fluid Systems Laboratory who labored long and hard at data transfer and reduction. Mr. Sorton also contributed materially to the restoration and expansion of instrumentation and data acquisition equipment at the test site when the program was initiated.